Photon upconversion for thin film solar cells

ISBN 978-90-393-5828-3

Photon upconversion for thin film solar cells

Foton upconversie voor dunne film zonnecellen

(met samenvatting in het Nederlands)

Proefschrift

ter verkrijging van de graad doctor aan de Universiteit Utrecht
op gezag van rector magnificus, prof.dr. G.J. van der Zwaan,
ingevolge het besluit van het college voor promoties in het
openbaar de verdedigen op maandag 17 september 2012 des
middags te 2.30 uur

door

Jessica de Wild

geboren op 15 september 1982 te Spijkenisse

Promotoren	Prof.dr. R.E.I. Schropp
	Prof.dr. A. Meijerink
Co-promotoren	Dr. J.K. Rath
	Dr. W.G.J.H.M. van Sark

The work described in this thesis was financially supported by NL Agency (Agentschap NL) of the Ministry of Economic Affairs, Agriculture and Innovation of The Netherlands: program EOS: LT NEO (New Energy Research).

Contents

Chapter 1

Introduction and theory

1.1 Energy losses in solar cells

The ever growing energy demand combined with the decreasing resources of fossil fuels makes it evident that there is a need for a transition towards renewable energy supply technologies. Solar cells are projected to make a significant contribution to the future of renewable energy. Solar energy can provide sufficient energy to fill the gap left by fossil fuels using only a limited fraction of the earth surface area [1]. The relatively high efficiency and flexibility allowing for small scale application in rural areas and on roof tops as well as for large grid connected solar energy farms contributes to the rapidly growing solar energy market. To sustain the present market growth, the cost of solar electricity has to decrease further. Cost reduction can be achieved by combining low-cost production technologies, cheaper materials, and increased efficiency of the solar cells. The maximum efficiency of solar cells is largely determined by the band gap of the semiconductor material. Single junction solar cells suffer from intrinsic efficiency losses, see figure **1.1**. Among other losses, the inability to absorb photons with an energy lower than the band gap (1) and relaxation losses of excess energy of absorbed high energy photons (2) make up at least ~65% of the total energy loss in single junction solar cells [2]. These spectral mismatch losses are called transmission and thermalization losses. Since the sun is a polychromatic light source there is a trade off between these losses, resulting in a fundamentally determined maximum efficiency as a function of band gap energy. This maximum energy efficiency of single junction solar cells was already determined by Shockley and Queisser in the 1960's and is now referred to as Shockley-Queisser (SQ) limit. The highest efficiencies reported for single junction solar cells such as c-Si and GaAs are presently approaching the maximum efficiency set by the SQ limit, which is 33% [3]. Further improvement of these high efficiencies becomes increasingly complicated. Expensive techniques are required for incremental efficiency improvements. Clearly, fundamentally different concepts are necessary to increase the efficiency beyond the SQ limit. Different options are

being explored, which can be divided in concepts based on adapting the solar cell and concepts aimed at adapting the solar spectrum. In both cases multiple energy levels are utilized to reduce transmission and thermalization losses [4, 5]. The most common and proven method to overcome the SQ limit is realized in multi-junction solar cells, consisting of a stack of solar cells with different band gaps. Each type of solar cell converts a part of the solar spectrum with high efficiencies, resulting in record energy efficiencies above 40%, theoretically even higher [3]. Because these cells are normally electrically connected in series, the solar cell with the lowest current is limiting the efficiency. This makes these types of solar cells sensitive to spectral changes, which are due to seasonal changes, daily changes, and sky conditions (clear/cloudy) [6]. Another device structure which is investigated to reach higher efficiency by reducing the transmission losses is the intermediate band solar cell [7, 8]. With an intermediate band, sub band gap photons are absorbed to and from the intermediate band. The photons are absorbed parallel to the operating cell, decreasing the spectral selectivity and increasing the photogenerated current. Device structures reducing the thermalization losses are based on hot carrier extraction and multiple carrier generation. Hot carrier extraction aims at collection of the photogenerated carriers before they thermalize. Hereby the voltage of the cell is increased [9]. With multiple exciton generation, high energy photons undergo impact ionization and multiple carriers are generated, increasing the photogenerated current is increased. Multiple carrier generation mainly occurs in quantum dots [10, 11]. The latter concepts are still under development at the materials level and the efficiency for some of the effects is controversial [12, 13].

1.2 Spectral conversion

An alternative approach is spectral conversion aimed at modification of the solar spectrum to achieve a better match with the wavelength dependent conversion efficiency of the solar cell. The advantage of spectral conversion is that this can be applied to existing solar cells and that optimization of the solar cell and spectral converter can be done separately. Different types of spectral conversion can be distinguished: two low energy (sub band gap) photons are combined to one high energy photon (upconversion) or one high energy photon is transformed into one (downshifting) or two (downconversion or quantum cutting) lower energy photons, see figure 1.2. Downshifting can give a marginal efficiency increase by shifting photons to a spectral region where the solar cell has a higher efficiency. Up- and downconversion however can raise the efficiency above the SQ limit. Research on spectral conversion is focused on organic dyes and quantum dots for downshifting and lanthanide ions and transition metal ion for up- and downconversion [15, 16, 17]. Especially upconversion attracts a lot of attention recently, because it involves low energy photons that are not absorbed by the solar cells: the transmitted photons. An upconversion layer can be placed at the back of the solar cells and by converting part of the transmitted photons to wavelengths that can

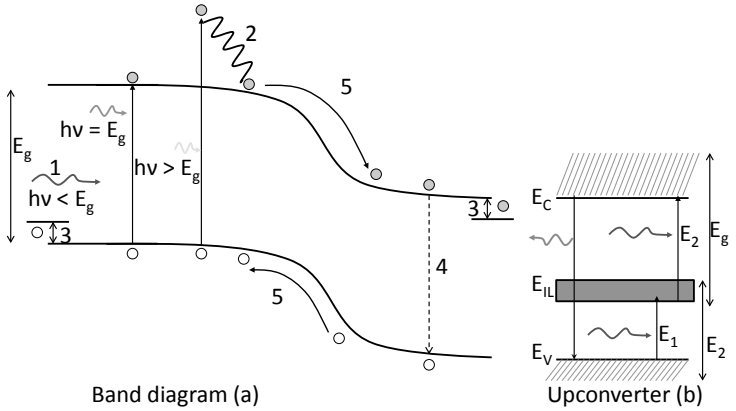

Figure 1.1: Losses in single junction solar cells (a). The thermalization and transmission losses are represented by 1 and 2. Other losses are contact losses (3), recombination losses (4) and junction losses (5). With an upconverter the transmission losses can be reduced by adding an intermediate energy band (E_{IL}) in the band gap. After subsequent absorption of two low energy photons, a higher energy photon is emitted (b). The upconverter is electrically isolated. Figure (a) adapted from ref [14].

be absorbed, it is relatively straightforward to demonstrate a positive contribution from the upconversion layer, even if the upconversion efficiency is low. In contrast, proof-of-principle experiments are complicated for downconverters and downshifters. These spectral converters have to be placed at the front of the solar cell and any absorption losses will reduce the overall efficiency of the system. Downconversion with close to 200% quantum efficiency has been demonstrated, but the actual quantum efficiency is lower due to concentration quenching and parasitic absorption processes [18]. Even for a perfect 200% quantum yield system, a higher solar cell response requires a reflective coating to reflect the isotropically emitted photons from the downconversion layer back towards the solar cell. The technology to realize these reflective coatings is available, but so far no proof-of-principle experiments have demonstrated an efficiency gain using downconversion materials. Also an upconverter emits isotropically but since it is placed at the back of the solar cells, the upconverted photons can easily be directed into the solar cell by placing a reflector behind the upconverter layer.

Trupke, Green and Würfel were the first to discuss the potential of increasing the solar cell efficiency through upconversion [19]. They considered an upconverter with an intermediate level band at E_{IL} with energy E_1 above the valence band of the solar cell and E_2 below the conduction band of the solar cell, see figure 1.1b. In this energy level scheme three energy ranges can be absorbed: energy higher than the band gap and two bands giving rise to upconversion: the first band with energy $E_1 < h\nu < E_2$ and a second band of energy $E_2 < h\nu < E_g$. These energy

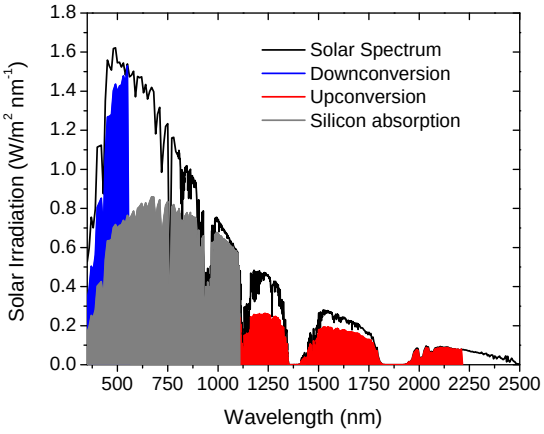

Figure 1.2: The solar spectrum and the part that is absorbed by c-Si directly is shown in gray. The blue area represents the energy range than can be used for downconversion (i.e., photon energy $> 2E_g$) and the red area represents the amount of power that can be upconverted by two photon upconversion (i.e., $E_g >$ photon energy $\geq 0.5E_g$).

levels are electrically isolated from the solar cell. Following the same approach as Shockley and Queisser the upper limit for energy conversion was calculated to be 63.2% for concentrated sunlight and 47.6% for non-concentrated sunlight assuming the sun to be a 6000 K black body for the optimum combination of E_g and E_{IL} [19]. When the same calculations are performed for the AM1.5 spectrum, even higher efficiencies can be obtained (for details, see Refs. [19, 20]).

It is important to note that the calculations were done for a theoretical upconverter with an infinite lifetime for the excited intermediate band state. The intermediate band thus serves as a reservoir for low energy quanta with a 100% upconversion efficiency through subsequent absorption of photons in the energy range of the second band ($E_2 < h\nu < E_g$). In real upconverter materials the lifetime is limited and not all photons are upconverted. The picture is analogous to the principle of the intermediate band solar cells, with slightly lower values for E_1, E_2 and E_g [9], because there are no restrictions to the maximum photon energy that can be absorbed. In both devices photons are subsequently absorbed by an intermediate band, but in an upconverter this results in emission of a higher energy photon and in an intermediate band solar cell this results in an electron-hole pair. An important difference is that the introduction of an intermediate band in the semiconductor materials affects processes in the solar cell and in order to reach high efficiencies it is imperative that the intermediate band levels do not re-trap charge carriers from the valence or conduction band. In case of upconversion materials, the use of sub band gap photons by subsequent absorption steps is

decoupled from the solar cell and it is theoretically possible to apply upconversion to a variety of solar cells.

1.3 Available upconverter materials

Upconverters are materials that are characterized by the fact that the emitted photons are of higher energy than the absorbed photons. This so-called anti-Stokes emission can be achieved in different ways. In second harmonic generation (SHG) birefringent crystals convert highly monochromatic and coherent laser light to higher energies. This process is well known [21] and can be very efficient for high laser powers but for conversion of the solar spectrum it is not efficient. To convert the infrared part of the solar spectrum, upconverters are required with an intermediate excited state. A two-step excitation process raises the system from the ground state via an intermediate state to a high energy state by absorbing two IR photons. This is followed by emission from the high excited energy state. Generally, two available material classes in which this subsequent absorption of low energy photons to give higher energy emission are considered: 1) metal ions in inorganic host materials, mainly lanthanide ions and transition metal ions [22, 23]. And 2) organic chromophores with an extended conjugated π-system [24].

1.3.1 Organic Molecules

The first class of materials for which efficient upconversion has been demonstrated are organic and organo-metallic chromophores. Research on upconversion in these chromophores has gained renewed interest recently. The group of Castellano made important contributions to this field, which are included in a recent review [24]. The upconverters consists of organic molecules with conjugated π-systems, serving as acceptor, and organo-metallic complexes serving as sensitizer. The sensitizer molecules contain a metal ion center and are characterized by metal-to-ligand charge transfer (MLCT) transitions. The activator molecules are organic molecules, which have a high fluorescence quantum yield [25]. The MLCT absorption band of the metal complex sensitizer is usually in the green and red spectral region. The energy of the MLCT absorption bands varies strongly for different organic molecules and metal-ion complexes, which makes it hard to find the most efficient combination of sensitizer and activator for upconversion of a specific spectral region. But the excited singlet state of the sensitizer has a strong absorption, which leads to relative low light intensities that are needed for measurable upconversion efficiencies [26, 27]. Therefore, upconversion of non-concentrated transmitted light by organo-metallic chromophores may be feasible [28]. The photon upconversion in organic molecules is based on triplet-triplet annihilation (TTA) [29], see figure **1.3**. Important requirements are that the triplet and singlet excited state of the sensitizer are nested between the singlet and triplet excited state of the activator. The sensitizer therefore should have a much smaller singlet-triplet

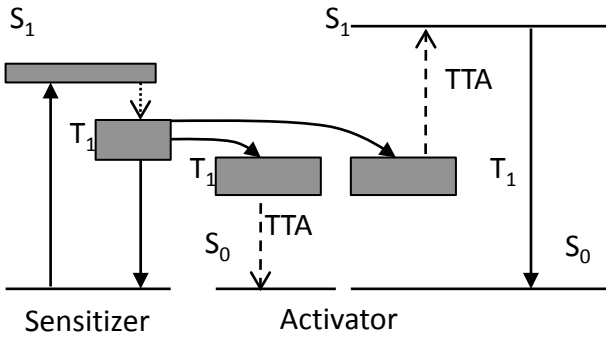

Figure 1.3: Energy scheme for upconversion in organic molecules. The singlet state of the sensitizer is excited and relaxes through fast intersystem crossing to the triplet state of the sensitizer. The energy is then transferred to the triplet state of the activator molecules. When two activator molecules come in close proximity, triplet-triplet annihilation results in one activator in the singlet excited state and one in the ground state. The upconversion emission is observed from the singlet state of the activator molecule.

splitting than the activator, which is usually the case for MLCT transitions on the sensitizer and an aromatic hydrocarbon activator, which generally has a large singlet-triplet splitting. In the upconversion process, first a sensitizer is excited to the lowest singlet state (strong absorption) and relaxes through intersystem crossing (ISC) to the triplet state. This process is faster than spontaneous emission from the singlet state [30] and the triplet state is excited efficiently via the singlet state. The long lived triplet state of the sensitizer transfers the energy to the long lived activator triplet state. Two activator molecules in the triplet state annihilate yielding one activator in the high energy singlet state and one activator in the ground state. Upconverted emission is observed from the singlet state of the activator. In the upconversion process several energy relaxation processes take place, which make the blue shift of the upconverted emission with respect to the excitation wavelength rather small. Typically, blue shifts around 100-200 nm are observed. In Table 1 of Ref. [24] an overview of successful sensitizer-activator combinations for upconversion is given, showing that the wavelengths for these upconversion systems ranges from 780 nm to 560 nm (longest wavelength) up to 442 to 360 nm (shortest wavelength). The presently available wavelength ranges limit the applicability to solar cells. Most solar cells (e.g. c-Si, GaAs, CIGS, CdTe) have an absorption onset at energies lower than 1.6 eV (~780 nm) and the transmission losses can only be reduced by upconverter systems that absorb and upconvert in the spectral region of wavelengths longer than 800 nm. Though the band tails of the upconverters extend into regions above 800 nm [31, 32], the upconversion is rather low in these region because the absorption is so low.

The organic molecules are either dissolved in liquids or dispersed in rubber-like polymeric materials. In general the efficiency of the upconverter in a polymeric environment is much lower than the efficiency in solutions, because the energy transfer rate is limited by the diffusion rate of the molecules [33]. For application in most solar cells polymeric hosts are required, however for dye solar cells also upconverter in solution may be applied [34]. The intensity of the upconversion emission of polymeric upconverters increases with temperature, because the diffusion of the molecules increases. In recent years, substantial progress has been achieved on the power density needed for measurable upconversion luminescence in rubbery media. Initially, polymeric media in which upconversion was observed required excitation densities of MW/cm^2 and kW/cm^2 [35]. Recently, upconversion was reported for excitation intensities below 1 mW/cm^2 and under ambient conditions [36]. The efficiency of upconversion in solid media is still weaker than in inorganic solids [24]. Reports on efficiencies are scarce and usually reported efficiencies are internal quantum efficiencies. Theoretical efficiencies of 40% can be achieved with organic upconverters [37]. They are determined by comparing the emitted upconverted emission with the emission when the band is directly excited. Known quantum yields of the activator molecules are required.

1.3.2 Lanthanides

The second class of upconverter materials are the lanthanides. This class of upconversion is known since the 1960's and an extended review is written by Auzel in 2004 [23]. Lanthanides form the group of elements in the periodic table for which the 4f inner shell is filled with up to 14 electrons. Lanthanide ions are most stable in the trivalent form (Ln^{3+}) and have a [Xe]4f^{n}5s^{2}5p^6 electron configuration with n varying from 0 to 14. For n electrons in 14 available orbitals there are $\binom{14}{n}$ possible configurations which all can have different energies. The partly filled 4f shell is responsible for the characteristic optical and magnetic properties of lanthanide ions. The energy levels within the 4f shell are in the NIR, VIS and UV spectral range. Because the outer 5s and 5p shells shield the inner 4f shell, the electronic transitions are independent of the surrounding host materials, which is a great advantage compared to the unknown position of the absorption band of the organic molecules. The energy levels of the various lanthanide ions are labeled by the term symbols $^{2S+1}L_J$ and are given in the so-called Dieke diagram [38]. The transitions between different 4f^n states are parity forbidden, causing narrow absorption and emission lines and weak absorption. The transitions become allowed through admixture of opposite parity states by odd-parity crystal field components or vibrations. The spectral lines are slightly broadened due the weak coupling with the vibrations.

The large variety of absorption and emission wavelengths, the independence on the host materials and the low vibrational energy losses make lanthanides ideal ions for spectral conversion and in almost all artificial light sources, emission originates from lanthanide ions. Lanthanides are doped in a variety of solids such as crystals,

fibers or glass ceramics, to give these materials the desired optical properties. The ions are embedded in hosts preferably with low phonon energy to decrease multi-phonon relaxation between closely spaced energy levels. Low phonon hosts are e.g. fluorides, chlorides, iodides, bromides [39] and higher phonon energy hosts are usually oxides, such as silicates, borates or phosphates [40]. Though the energy level structure is independent of the host materials, host materials influence the non-radiative transitions due to coupling with phonons. Phonons provide a non-radiative channel between energy levels that competes with the radiative transitions. As a rule of thumb it holds that when energy levels are separated by less than 5 times the maximum phonon energy of the host, non-radiative multi-phonon relaxation will be dominant. For energy differences of more than 5 times the maximum phonon energy, radiative decay will dominate [41].

The most efficient mechanisms behind upconversion with lanthanide ions and transition metals are two-step excitation (ground state absorption followed by excited state absorption, GSA/ESA) and energy transfer upconversion (ETU), that is upconversion by subsequent energy transfer steps of the excited ions. Whereas GSA/ESA is a one-ion process, ETU always involves at least two ions. GSA/ESA is observed for low doping concentration (<1%). The process is schematically depicted in figure 1.4. In case of ETU, the upconversion from a lower excited state to a higher excited state is realized by energy transfer between two excited ions, possibly different types of ions. Different types of energy transfer mechanisms are possible, but mostly non-radiative energy transfer via dipole-dipole interaction is the dominant mechanism. Efficient energy transfer requires the ions to be in close proximity [41] and thus ETU requires high concentration of the dopants; 20% is not uncommon. The ETU transfer process is generally experimentally determined to be the most efficient process. A powerful technique to determine whether energy transfer or excited state absorption is the main upconversion path, is measuring the luminescence decay curve for the upconverted emission after a short excitation pulse. When GSA/ESA is the main pathway for upconversion, the decay curve is a simple exponential decay from the high state without a rise time. For energy transfer upconversion however, there is first a rise in intensity followed by the decay from the high energy state. The rise results from the slow feeding of the emitting state through the energy transfer step [42]. Some materials are doped with more than one specific metal ion. One ion then acts as a sensitizer and the other ion as activator, depicted in the two left diagrams of figure 1.4. A sensitizer ion has preferably a long lifetime, a strong absorption strength and broad absorption spectrum. Sensitized upconverters always involve energy transfer and are therefore in general more efficient than GSA/ESA upconverters. The energy transfer rate is determined by the spectral overlap between the activator absorption and sensitizer emission, the lifetime of the sensitizer emission and the absorption strength of the activator ion.

In contrast to the organic molecules, a large spectral overlap is favored for efficient energy transfer between the sensitizer and activator. The lanthanide couple Er^{3+}, Yb^{3+} is therefore the most efficient couple for NIR-VIS upconversion,

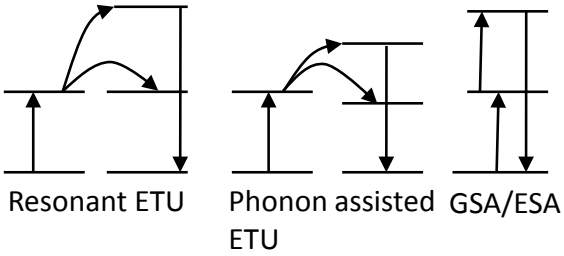

Figure 1.4: The most efficient upconversion mechanisms in lanthanide upconverters. Energy transfer upconversion (ETU), either resonant or phonon assisted and ground state absorption followed by excited state absorption (GSA/ESA). ETU always requires two ions, whereas GSA/ESA one ion.

where Yb^{3+} is the sensitizer and Er^{3+} the activator. Yb^{3+} has only one energy level around 980 nm (10200 cm^{-1}) with a strong oscillator strength, making it an ideal sensitizer for near infrared absorption or emission [43]. Er^{3+} has also an energy level around 980 nm and 490 nm (20400 cm^{-1}), allowing for two close to resonant energy transfer steps from Yb^{3+} to Er^{3+}. The large spectral overlap between Yb^{3+}/Er^{3+} and the efficient ETU for this lanthanide couple, makes Yb^{3+}/Er^{3+} a widely investigated NIR-VIS upconversion couple in a variety of host materials [44, 45, 46, 43, 47, 48] of which $NaYF_4$ host is the one of the most efficient and well investigated material to date [44, 41]. Er^{3+} emits in the green and red after the two-photon and blue after three-photon upconversion process. Another well investigated NIR/VIS upconverter couple is Yb^{3+}/Tm^{3+}, which emits in the blue [46, 49, 50, 51]. Yb^{3+} acts again as sensitizer, but the energy levels between the sensitizer and activator are not resonant and the upconversion requires three-photon absorption. This makes the couple less efficient than Yb^{3+}/Er^{3+}. Next to lanthanides also transition metals have been used for upconversion [23, 52, 53, 54, 55, 56, 57]. They have broad absorption bands, which makes them interesting as sensitizer. The broad absorption bands result from a stronger vibronic coupling of the outer d electrons, involved in the optical transitions. Contrary to the lanthanides, the energy level scheme is strongly dependent on the host. The stronger vibronic coupling is responsible for temperature quenching of the emission at elevated temperatures and often only efficient emission is observed at cryogenic temperatures. As a result, most transition metal upconverters only emit upconverted light at cryogenic temperatures. There is one example of room temperature upconversion with the transition metal Re^{4+}, which absorbs around 1100 nm and emits at 700 nm [56]. An extended review on upconverter materials applicable for solar cells was written by Strümpel et al [58].

1.4 Upconverter efficiency

The feasibility of upconverters to enhance the efficiency of solar cells depends critically on the efficiency of the upconversion process. The efficiency of an upconverter is determined by many variables which influence the radiative, non-radiative and energy transfer rates, e.g. phonon energies, spectral overlap between sensitizer emission and activator absorption, temperature, and defects that quench the emission. Very importantly, as upconversion is a non-linear process, the efficiency strongly depends on excitation power. A reported upconversion efficiency value is only valid for a certain excitation light intensity. This makes it difficult to define and compare the upconversion efficiency. There is no generally excepted definition of upconversion efficiency. Both power conversion and quantum efficiencies are reported. When the quantum efficiency is determined, it is still not always clear how to interpret the reported values. For example, for one emitted photon at least two photons are absorbed. This means that the maximum internal quantum efficiency is 50%, analogous to the fact that downconversion can have an efficiency of 200%. Still, sometimes this maximum efficiency is reported as 100% [59]. Another approach is absolute power conversion efficiency. Here the emitted power intensity is compared with the power of the excitation source, P_{in}. The output power can rather easily be determined by integrating the emission spectra with a calibrated detector. Not all emitted wavelengths are to be included, only those that have an energy higher than the band gap of the solar cell. Typical power efficiencies of NIR-VIS lanthanide upconverters are of the order of 2% or less [43]. As was mentioned above, the most efficient and widely studied upconverter is $NaYF_4$: Er^{3+}, Yb^{3+} with an absolute power conversion efficiency of 5.5% for the conversion of 980 to 540 nm light [60], corresponding to an internal quantum efficiency of 23% [46]. The values are determined at such high powers that the upconverter efficiency is saturated. At $40\,W/cm^2$, the upconverter efficiency is saturated [48]. Clearly, the values reported for upconversion efficiencies are not easily interpreted by just considering the efficiency value reported. The efficiency is dependent on the incident power density, the efficiency saturates at high power, and the maximum efficiencies for different upconverter systems are reached at different power densities. The emitted intensity is proportional to P_{in}^n, and the efficiency is therefore proportional to P_{in}^n/P_{in} i.e. P_{in}^{n-1}. Here n is the number of photons (steps) involved in the upconversion process (e.g. 2 for the NIR to green/red upconversion in Yb^{3+}/Er^{3+} and 3 for the NIR to blue upconversion in Yb^{3+}/Tm^{3+}). This only holds in the absence of saturation. Auzel [23] listed upconversion efficiencies of NIR-VIS upconverters given in cm^{-2}/W^{n-1}. The efficiency was defined as (emitted light intensity)/(absorbed radiation intensity) normalized to a power of $1\ W/cm^2$. Vitroceramics and YF_3 were here listed as the most efficient upconverter with a power efficiency of 28%. However, these high values have never been confirmed experimentally at other laboratories and were based on extrapolation of efficiencies measured at much lower intensities [61]. One problem in the extrapolation of low-power results is that a deviation of the number of 2 or 3 is rather

common, leading to much lower values when extrapolating to high intensities. It is important to note that internal efficiencies are reported; i.e. the power efficiency of absorbed photons. When dealing with power densities of lasers or sunlight, direct comparison is only possible when the absorption strength of the ion is known for that wavelength or when the output power of the laser is given.

1.5 Application of upconverters to solar cells

Both organic and inorganic upconversion systems have advantages and disadvantages and at present it is hard to predict which type of upconversion will be the system of choice for application in solar cells. The upconversion efficiency is low and most demonstrations merely serve as proof of principle showing that an increase in efficiency can in principle be realized by applying an upconversion layer. In general, the upconverter is applied at the back of a cell as an electrically isolated layer. A back reflector reflects all emitted photons back into the solar cell. For a long period of time there were only 2 proof of principle experiments both with lanthanides upconverters applied on GaAs [62] (1996) and c-Si [63] (2005) solar cells. Only recently an organic upconverter was applied [64] (2012) and the solar cells are extended to dye sensitized solar cells [65, 66] (2010). In this thesis upconversion of a-Si:H solar cells is described. Different types of solar cells require different designs for the application of upconverters, as schematically shown in figure 1.5. Except for the design given in ref [66], where the upconverter is not electrically isolated, the solar cell has to be bifacial, i.e. the light enters also from the back, whereas in general, a metal contact is applied at the back to extract the charge carriers generated from the solar cell. With an upconverter the back contact has to be transparent (1.5c), cover only a small part of the back area (1.5a).

The first experiment was done on GaAs solar cells combined with a vitroceramic material doped with Yb^{3+} and Er^{3+} for which the solar cell characteristics was obtained under extremely high excitation densities. An efficiency of the solar cell of 2.5% was obtained even though the excitation wavelength (891 nm) is not resonant with the absorption peak of Yb^{3+} (~980 nm) [40], leading to inefficient upconversion. Secondly the design was such that not all emitted photons were directed to the solar cell, as can be seen from the scheme (Fig. 1.5a). The upconversion photons are emitted isotropically, also in the lateral direction and onto the metal contacts. In 2005 Shalav et al [67] showed upconversion under lower excitation density of 2.4 W/cm^2 reaching 3.4% quantum efficiency at 1523 nm in a crystalline silicon solar cell with $NaYF_4$ doped with Er^{3+} as upconverter. This was for a system optimized for the wavelength of 1523 nm. Intensity dependent measurements showed that the upconversion efficiency was approaching its maximum due to saturation effects [67, 68]. Under broad band excitation upconversion was shown for the same system by Goldschmidt et al [69] (2011) reaching an upconversion efficiency of 1%. Since c-Si has a rather small band gap (1.12 eV), transmission losses due to the low energy photons are not as high as for wider

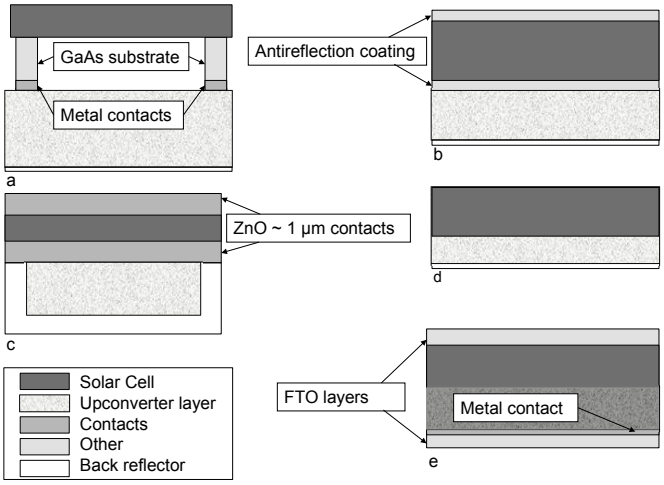

Figure 1.5: Schemes for different solar cells used in combination with upconversion layers. The dark areas are the solar cells, a) GaAs, b) c-Si, c) a-Si, d) DSSC with glass ceramics and e) DSSC with upconverter incorporated inside the solar cell. The shaded areas are the upconverters, darker for e), indicating that it is part of the solar cell. a, b, d and e have a metallic back reflector and c a white back reflector. The light gray areas are the contacts, as shown for GaAs (a)a-Si (c) and DSSC (e). b has also anti reflection layers on both sides of the solar cell.

band gap solar cells. Hence, the efficiency gain for larger band gap solar cells can be higher. Upconversion of 980-nm light was also demonstrated in dye sensitized solar cells [65, 66] and of 750 nm light in ultra thin (50 nm) a-Si:H solar cells in 2012 [64]. In this proof of principle experiment, for the first time an organic upconverter was applied.

1.6 Light intensity and efficient upconversion

Clearly, upconversion for solar cells is an emerging field, whereas the contribution of upconverter research and upconverter solar cells research increases rapidly (figure 1.6). Up to now, only proof of principle experiments have been performed on solar cells, mainly due to the high intensities that had been necessary. Though, especially in the organic field there is a rapid decrease in intensity needed for efficient upconversion, the conversion wavelengths are still not appropriate. Within the lanthanides, large steps in decreasing the necessary intensity are not expected and external sensitization may be a route to increase the efficiency. External sensitization can be achieved by e.g. quantum dots or plasmons. Quantum dots (QDs) can be incorporated in a concentrator plate where the QDs absorb over a broad

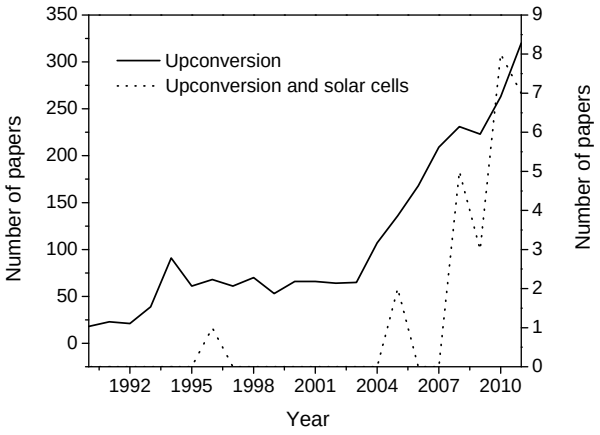

Figure 1.6: Number of publications per year on upconversion (left axis) and upconversion in solar cells (right axis)

spectral range in the IR and emit in a narrow line, e.g. around 1520 nm resonant with the Er^{3+} upconversion wavelength. Energy transfer from the QDs to Er^{3+} in this scheme is through radiative energy transfer. The viability of this concept was proven by Pan et al. [70] in c-Si solar cells, where a layer with quantum dots was placed below the upconverter layer. With the quantum dots more light was absorbed and upconverted, which was proven by measuring the excitation spectra for the upconverted emission. The increased upconverted emission resulted in higher currents in the solar cell. More challenging are options to enhance upconversion efficiencies by manipulating emission and excitation processes through plasmonic coupling [71]. The use of plasmonic effects with upconverter materials is a new and emerging field, with many possibilities and challenges. In general plasmonic resonance can be used in two ways to increase the upconversion efficiency; either by enhancing the absorption strength or the emission strength. When the absorption strength is enhanced, the emission increases with the square of the enhancement in the non-linear regime. In case of resonance between the plasmon and the optical transition strong enhancement can be achieved. A related method is to enhance the absorption strength by nanofocussing of light in tapered metallic structures [72]. At the edges enhancement has been reported due to focusing of the light in these areas.

The other option is enhancing the emission. In this case, the emission of the upconverter is enhanced by nearby plasmon resonances [73]. Since the field enhancement decays away exponentially with the distance to metallic nanoparticle, the upconverter species have to be close to the surface of the nanoparticle to benefit from the field enhancement effects. For organic molecules this presents no problem

because the molecules are small enough to be placed in the field. For lanthanide upconverters, this is more difficult because the ions are typically contained in materials with grain sizes in the micrometer range. Several groups have managed to make nanosize $NaYF_4$ particles [74, 75]. This offers the possibility of plasmonic enhancement for lanthanide upconverters and decrease light intensity required for efficient upconversion.

1.7 Summary and outline

The goal of this research is to investigate the possibility of enhancing the efficiency of solar cells by upconversion of sub band gap light. For this it is necessary to investigate the upconverter material, mainly the conversion efficiency and its dependence on the power density. Second step is designing solar cells that are suitable for application of the upconverter and perform proof of principle experiments. At last, proof of principle experiments should be extended to more realistic situations to investigate to feasibility of an upconverter solar cell device.

In this thesis results on upconversion in a-Si:H solar cells with lanthanide upconverters are presented. Since a-Si:H is a high band gap material, the gain for upconversion is much higher than c-Si solar cells. Results in this thesis may be extended to other high band gap solar cell, for instance GaAs. In this thesis two disciplines in the UC-solar cell field are represented, namely upconverter research itself and application to the solar cells, which requires adaptations of the a-Si:H solar cells.

In chapter 2 experimental methods are described. These are the deposition techniques to make and adapt a-Si:H solar cells and characterization techniques for solar cells and upconverters. The next two chapters, 3 and 4 describe the upconverter materials that are investigated or used for the solar cells. Two upconverter were applied on the solar cells: $NaYF_4 : Er^{3+}$, Yb^{3+} synthesized at the CMI department, and $Gd_2O_2S : Er^{3+}$, Yb^{3+} purchased from Phosphor tech. In the next chapters, the lanthanide doped materials are shortened as $NaYF_4$ and Gd_2O_2S upconverters. In chapter 3, more in depth research is performed on the question why this $NaYF_4$ host is such an efficient upconverter. We found that the high absorption strength may increase the energy transfer between different Yb^{3+} ions. In chapter 4 the $Gd_2O_2S : Er^{3+}$, Yb^{3+} is characterized, by intensity dependent measurements and 2-color excitation. This upconverter is very efficient at low intensities, but saturates readily. Next to characterization of Gd_2O_2S host also ${NaYF_4}^{3+}$: Er^{3+}, Yb^{3+} nanoparticles are described in this chapter. Nanoparticles may be placed in the near field of a metal nanoparticle. Gold nanoparticles have a resonance around 1 µm, where the upconverter absorbs. An increased emission rate is observed at this wavelength, when the particles are placed in the near field of the gold nanorods.

Chapter 5 describes how the a-Si:H cells are made suitable for upconversion. The solar cells normally have a silver back contact, but this has to be replaced by

a transparent back contact without introducing new losses. The solar cells have to become bifacial for further research. This is achieved by applying a TCO layer at the back as contact. With a TCO layer there is a trade off between absorption and resistance, and optimum layer thicknesses has been determined. The solar cells with the TCO back contact had a higher series resistance than silver, but were suitable for further experiment. In the last chapter, chapter 6, the upconverters as described in chapter 3 and 4, and the solar cells as described in chapter 5 are combined. Solar cells with upconverter and reference solar cells were made and illuminated with sub band gap light. The reference solar cells were used to estimate the sub band gap response due to mid gap states in order to correct the measurements of cells with upconverter. Increased response in the solar cells due to upconversion is proven, both under laser light excitation and broad band excitation.

Chapter 2

Experimental methods

Abstract

This thesis describes research aimed at raising the efficiency of solar cells by using upconversion materials. For this solar cells and upconverters are made and characterized. In this chapter a basic description is given of processes occurring in solar cells, followed by the various methods used for characterization of upconversion materials and solar cells. The deposition techniques used for the fabrication of solar cells are similar to those extensively described in previous theses and are therefore only briefly discussed.

2.1 Deposition techniques

2.1.1 PECVD

The amorphous silicon solar cells used in this thesis were made in superstrate p-i-n configuration. As superstrate, either commercially available Asahi U-type $SnO_2 : F$ coated glass [76] or Corning Eagle glass with ZnO:Al coating were used. The p-i-n layers were deposited using plasma enhanced chemical vapor deposition (PECVD). The gasses that are used are, silane (SiH_4) and H_2 for the intrinsic layer, for the p-layer trimethylboron gas ($B(CH_3)_3$) was added and for the n-layer phosphine (PH_3) was added to the silane gas. The molecules are dissociated into radicals in a glow discharge and ions by an applied radio frequency (RF) power between a powered electrode and a grounded electrode, which is the sample holder. A detailed description of the PECVD process can be found in [77, 78].

The a-Si:H layers were deposited in the PASTA (Process equipment for Amorphous Semiconductor Thin Film Applications) ultra high vacuum (UHV) multichamber system. In PASTA system standard RF PECVD operating at 13.56 MHz and hot wire chemical vapor deposition (HWCVD) techniques can be used for deposition of silicon layer, however, for this thesis only the former was employed, and has six separate deposition chambers. The different layers are made in separate chambers. An optimized recipe for p-i-n solar cells on Asahi glass was chosen. For the ZnO:Al superstrate a micro-crystalline p-layer was added between the ZnO:Al layer and the amorphous p-layer to decrease the potential barrier at this interface [79].

2.1.2 Magnetron Sputtering

The TCO layers were deposited with RF magnetron sputtering in the Sputtering Apparatus for Light Scattering Applications (SALSA) using ceramic targets. For our purposes only ZnO:Al with different Al concentration were used. A detailed description on the SALSA apparatus can be found in ref. [79]. With sputtering, atoms and molecules are released from a surface after bombardment with highly energetic ions. The ions (Ar^+) are generated by a RF glow discharge in an argon gas between the grounded sample substrate (anode) and the ceramic target (cathode). Negative ions will be accelerated to the sample and positive ions to the target. In the case of ZnO:Al, the growth is determined by the different ions and Ar neutrals depending on the energy of the bombardment.

2.1.3 Evaporation

The metal contacts were deposited by evaporation in a vacuum chamber. High purity silver and/or aluminum rods (99.99999%) were placed in a tungsten boat. When a high enough current flows through the boat (350 A for Ag, 250 A for Al), the metal evaporates. The sample is placed at a large enough distance from the tungsten boats to avoid heating, but close enough to capture a substantial amount

of the evaporated metal. A mask was placed in front of the sample to determine the shape and size of the metal contacts.

2.2 Characterization techniques

The goal of this research was to make upconverter solar cells and measure an improvement due to the upconverter. To achieve this goal, the solar cells had to be made bifacial. This means, light can enter the solar cells also from the back (through the n-layer). For this a suitable transparent back contact had to be found and characterized. The new solar cells had to be characterized, where the focus was mainly on near infrared response which is the part where we want to improve the response. Most characterization techniques used for the solar cells are described in previous theses as well. Though, sometimes small adaptations were made to measure response in upconverter solar cells. Also a global description on spectroscopy is given, which is used to characterize the upconverter materials separately from the solar cells.

2.3 Material characterization

2.3.1 Reflection transmission

The thickness of TCO and i-layers are determined with eta-optik 2C5/HL R-T mini set-up. This setup is made by W. Theiss Hard- en Software [80]. With this equipment reflection and transmission spectra between 400 and 1050 nm are obtained simultaneously. The apparatus is provided with the computer program SCOUT, which fits the experimentally obtained data to the dielectric function of the materials and gives the thickness of the layer. The calculation follows the procedure described in ref [81]. For silicon also the band gap and band tails are calculated. There was no exact fitting program for ZnO doped with aluminum. Though, the dielectric parameters for ZnO also gave accurate values for the ZnO:Al layer thickness.

2.3.2 Hall Measurements

From Hall measurement mobility (μ) and free carrier concentration (n) can be determined. This is done with van der Pauw method [82]. Hall measurements are performed on the TCO samples. TCO samples require high mobility and low carrier concentration to avoid absorption of light by free carriers. These mobility and carrier concentration are related to the sheet resistance according to $\mathrm{d}\rho = \mathrm{d}/\mu\mathrm{nq}$, with d the thickness of the sample. This measurement is destructive for the sample and for a quick layer quality check, the 4 point probe can better be used.

2.3.3 4-point probe

The sheet resistance of the ZnO:Al layers is determined by 4-point probe. The 4 probes are aligned, between the outer two probes runs a current and the inner two probes a voltage is measured. From this the sheet resistance can be determined: $R_{\square} = V\pi/Iln2$, where V is the applied voltage and I is the current.

Depending on the application of the TCO layer the sheet resistance vary between 1-100 Ω depending on the thickness. For our purpose, the TCO layer is used as front and back contact. For device quality the sheet resistance should be smaller than 10 Ω for front contact in single junction solar cells [83]. In combination with the hall measurements or R-T mini the resistivity $\rho = R_{\square}/d$ with d the layer thickness obtained from the R-T mini, can be determined.

2.3.4 Integrating sphere

With an integrating sphere difference between diffuse and specular reflection and/or transmission can be measured. In the Perkin Elmer Lambda 2S double beam spectrophotometer system in this group, this measurement is done between 200 and 1100 nm. The integrating sphere has a high reflective coating (BaO) inside and a detector within the sphere. The sphere has an entrance for the light and on the other side, light can escape the sphere. Here a specular reflector has to be placed to be able to distinguish between diffuse and specular reflection. Best material to be placed here is silver, because of its high reflectivity. Figure 2.1 shows a schematic view of how the specular and diffuse light can be separated. When the specular reflector is placed perpendicular to the light beam at the other side of the sphere, specular light is reflected in the same direction it entered the sphere and will escape the sphere at the same place where the light is entered. In this configuration only diffuse light is measured. When the specular reflector is placed under a small angle, the light that is reflected specular will have a small angle compared to incoming light. This light will thus not escape the sphere and specular + diffuse light is measured. The difference between diffuse and total light says something about scattering properties of the TCO layers. A measurement for scattering is the Haze, which is defined as:

$$H_{R,T} = \frac{T, R_{diffuse}}{T, R_{total}} \tag{2.1}$$

Haze can be determined from reflection and transmission measurements. When transmission is measured, the scattering happens when the light enters the sphere, which is shown in figure 2.1 by the broken line. Figure 2.2 shows the haze of Asahi glass, which is the textured superstrate used for the a-Si:H solar cells in this thesis. It is important to notice the low haze in the red and near infrared part, where the performance of the solar cells should be increased with the upconverter.

The integrating sphere can also be used to measure the absorption of the upconverter powders. The powders are micro sized small crystals and thus high

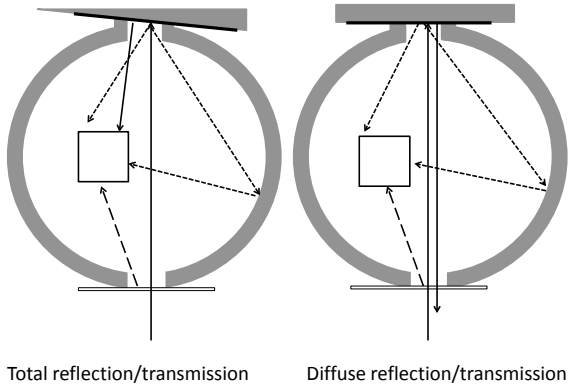

Figure 2.1: Integrating sphere for diffuse or total reflection or transmission. In the left configuration total light is detected, while in the right configuration, specular light is filtered out. Scattering properties can be determined from textured substrates and absorption from strong scattering substances.

scatterers of light. The absorption can be determined from the reflectance. In this case, instead of a silver reflector as reference, a diffuse reflector (BaO) is placed at the exit. The reflectance is determined by:

$$R_{sample} = \frac{R_{measured} - R_0}{100 - R_0} R_{ref} \tag{2.2}$$

Here R_{ref} is the reflectivity of the reference, which are known values of BaO, R_0 is the reflectance measured without any reflector at the exit, which should be 0. $R_{measured}$ is the measured reflectance with the sample placed at the reflectance port. The reflectivity of the sample can then be calculated with formula 2.2 and the absorption is given by $-\log(R_{sample})$. This holds only when the transmission of the sample is 0.

2.3.5 X-ray diffraction

X-ray diffraction is used to determine the crystal structure of the microcrystalline upconverter materials and to determine if they are single phase. X-rays with a wavelength of 0.15428 nm (Cu - Kα radiation) are diffracted by the sample according to Braggs law. The angle between the X-ray beam and the detector is varied to determine the diffraction angles. The positions of the diffraction peaks are characteristic for the crystal structure of the material. The known X-ray diffraction patterns of crystalline materials, as found in the ICDD database, are compared with the measured diffraction pattern to verify the formation of specific crystalline phases.

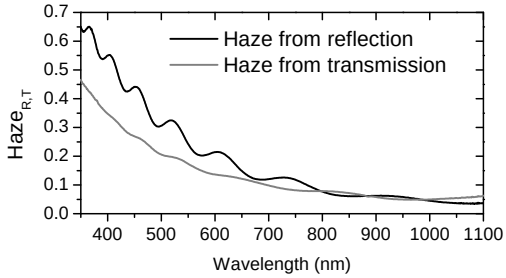

Figure 2.2: The Haze of Asahi U type superstrates, the textured substrates used for the (upconverter) solar cells. The scattering happens mainly in the visible part and is low from 700 nm on.

2.3.6 Spectroscopy

The upconverter materials used in this theses are extensively characterized by luminescence spectroscopy, viz. emission and excitation spectra and luminescence decay curves are measured. For an emission spectrum the sample is excited at a fixed wavelength and the emitted light passes through a scanning emission monochromator and the intensity of the emitted light is measured as a function of wavelength. For an excitation spectrum the emission wavelength is fixed and the excitation light passes through a scanning excitation monochromator. The intensity of the emission is monitored as a function of excitation wavelength and only excitation that results in emission at the fixed emission wavelength gives rise to a signal in the excitation spectrum. In luminescence decay curves the emission intensity is measured as a function of time after a short excitation pulse. Since the photon flux after a single pulse is small, the time evolution of the emission intensity is averaged for many excitation pulses, typically 500-1000.

Figure 2.3 shows the schematic of a spectrofluorometer for emission and excitation measurements. An Edinburgh FLS920 spectrofluorometer was used for the luminescence experiments reported in this thesis. The monochromators use gratings to disperse the light. Gratings with different blazing angles were available to optimize the light throughput in the ultraviolet (UV), visible (VIS) or near infrared (NIR) spectral range. Filters can be placed in filter holders. Neutral density filters are used to change the power incident on the sample. Long pass color filters are used to filter out undesired frequencies, for example a long pass filter is commonly used in the emission path to filter out reflected excitation light that would otherwise give rise to a second order peak at the double wavelength. The emitted light is detected with photomultiplier tubes for the UV-VIS 250-800 nm range (Hamamatsu R928) or the NIR 700-1700 nm range (Hamamatsu R5509-72). The NIR photomultiplier was cooled to 200 K to decrease the dark current. The typical spectra resolution used in the experiments in this thesis is 1 nm but could

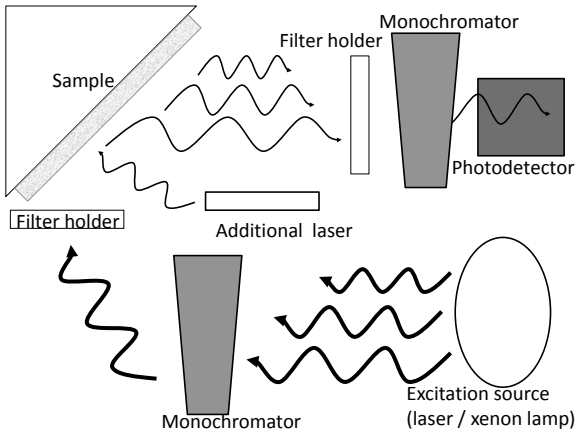

Figure 2.3: A schematic set-up for luminescence measurements to record emission and excitation spectra. For an emission spectrum, the excitation wavelength is fixed and the emission wavelength is scanned. For an excitation spectrum the emission wavelength is fixed and the excitation wavelength is varied. In addition, laser can be used for excitation through a separate access port.

be varied between 0.1 and 10 nm. The spectrofluorometer is equipped with an Oxford Instruments liquid helium flow cryostat for measurements down to 4 K.

Different excitation sources can be used in combination with the spectrofluorometer. The spectrofluorometer is equipped with a 450 W Xe arc lamp. For continuous wave (CW) NIR excitation a 981 nm photodiode was used. Two pulsed excitation sources were used in the NIR. An LPD 3000 dye laser pumped by an LPX 100 excimer laser (308 nm, XeCl) from Lambda Physik was used for life time measurements and NIR excitation. The laser pulses have a 10 ns pulse width and the repetition rate is typically 10 Hz. The laser dye used for NIR excitation is Styryl 14 and covers the 940-990 nm spectral region. Next to the pulsed dye laser, an Optical Parametric Oscillator (OPO) pumped by the third harmonic (355 nm) of a Nd-YAG laser was used. The Opolette 355-I can be scanned between 410 and 2200 nm and gives 10 ns pulses of ~1-5 mJ per pulse [84]. The scanning capability allows for recording excitation spectra in the NIR region of the upconverted shorter wavelength emission. An example is shown in Figure 2.4. Due to the non-linear character of the upconversion process, the intensity of the upconverted emission scales non-linearly with the absorption strength. As a result, the lines in the excitation spectrum are sharper than the corresponding lines in the absorption spectrum. This is demonstrated in Fig. 2.4.

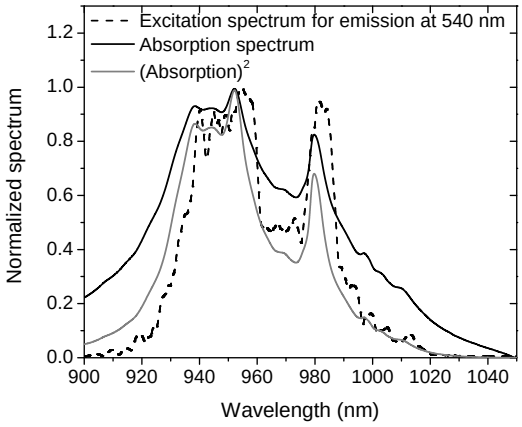

Figure 2.4: Excitation spectrum in the NIR for upconverted 554 nm emission (dotted) and absorption spectrum in the same spectral region. The peaks in the excitation spectrum are sharper, reflecting the non-linear two-photon character of the upconversion process. The excitation spectrum closely resembles the squared absorption spectrum (gray).

2.4 Solar Cell Characterization

2.4.1 Solar Simulator

The performance of the deposited solar cells is measured under AM1.5 light using a dual-beam WACOM super solar simulator. The light is simulated by combining light from a halogen lamp with the light from a xenon arc lamp. The spectrum of the solar simulator is calibrated to the 100 mW/cm^2 AM1.5 solar spectrum and matches the solar spectrum between 300 and 900 nm with 3% deviation and between 900 and 1100 nm with 14% deviation. The spectrum and intensity is verified before every measurement using calibrated reference solar cells for different parts of the spectra. Current-voltage measurements are performed in dark and in light at 25°C, see figure 2.5. Important parameters exstracted from the IV measurements are open circuit voltage (V_{oc}), fill factor (FF), ideality factor (n), series resistance (R_s), parallel resistance (R_p) and short circuit current (I_{sc}). The I-V curve can be described by an adapted ideal diode equation:

$$I(V) = -I_{ph} + I_0(\exp\left(\frac{e(V - IR_s)}{nkT}\right) - 1) + \frac{V - IR_s}{R_p} \tag{2.3}$$

with I_0 the dark saturation current, k the Boltzmann constant and T the absolute temperature. I_0 and n are obtained from dark I-V measurements, where photocurrent $I_{ph} = 0$. From AM1.5 I-V measurements the intersection of the

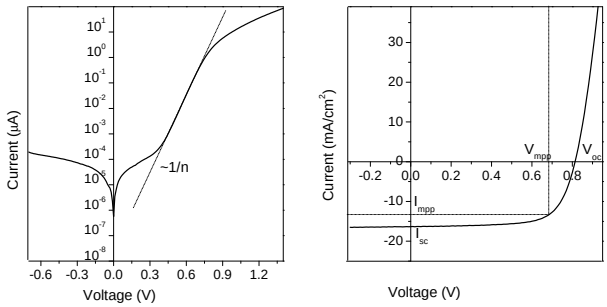

Figure 2.5: IV measurements in dark (left) and light (right). Several parameters can be exstracted from the curves. From dark measurements the ideality factor is calculated from the slope, as shown in the left figure. IV measurements under light give many other parameters, like maximum power point, FF or V_{oc}.

curve with the current axis is identified as I_{sc}. The slope at this point is associated with R_p. The intersection with the voltage axis is identified as V_{oc} . The slope at V_{oc} is associated with R_s. The FF is defined as the squareness of the diode characteristics according to $(I_{mpp}V_{mpp}) / (V_{oc}I_{sc})$ and the efficiency as $(I_{mpp}V_{mpp}) / \left(100\,\mathrm{mW/cm^2}\right)$, where mpp stand for maximum power point.

Next to the dual beam of halogen and xenon lamp, also a small diode laser with a wavelength of 981 nm and maximum power of $3\,\mathrm{W/cm^2}$ was used as light source. The diode laser was mounted inside the box that is used to cover the cells for dark measurement and I-V measurements were performed. From these I-V curves I_{sc} was extracted. Color filters and neutral density filters were used to filter the solar spectrum or decrease the laser intensity. A set-up was made that could concentrate solar light coming from the solar simulator. For this a convex glass lens was attached to a lab jack and the distance was varied. A maximum concentration of 25 times was possible. Long pass filters were used and only sub band gap light (>900 nm) was focused. Since only a small part of the solar spectrum was focused on the solar cell, no cooling system was necessary since the heating was less than 0.5 °C.

2.4.2 Spectral Response

The Quantum Efficiency (QE) of solar cells is defined as the number of collected electrons per incident photon, which varies with the wavelength of the incident light. The photon flux in the wavelength range from 350 to 800 nm is determined using a reference measurement of the spectrum of a Xenon arc lamp using a monochromator and a calibrated photodiode connected to a lock-in amplifier. After the reference measurement the calibrated diode is replaced by the solar cell to be measured, to determine the photocurrent for each wavelength. From the pho-

ton flux, which is known for all wavelengths and the corresponding photocurrent the quantum efficiency can be calculated.

2.4.3 Fourier Transform Photo spectroscopy

In this thesis, the Fourier Transform Photocurrent Spectroscopy (FTPS) is used to measure the spectral response for sub band gap light. FTPS is a sensitive technique for measurement of the photocurrent of solar cells in the range of several orders of magnitude. The light source (NIR) is a halogen lamp. The spectral range is between 500 and 2000 nm. The general principle is to use a Fourier-Transform Infrared (FTIR) spectrometer with an external beam exit and optional external detector. A Fast Fourier Transform algorithm converts the recorded signal from the photodetector from the time domain into the spectral domain. For FTPS measurements calibrated silicon and germanium diodes are used as reference to cover the whole spectral domain. The response of the solar cell is compared with the reference measurements and a response up to 2000 nm for the solar cells can be measured. A more detailed description can be found in ref. [85].

The response for sub gap light is several orders of magnitudes smaller than the response of visible light. The response is plotted on a logarithmic scale and several parameters can be extracted. In the spectral range between 800 and 900 nm the band tails can be determined from the slope [86]. From 1000 nm to longer wavelength the QE is proportional to the absorption which is correlated to the deep defect concentration [87].

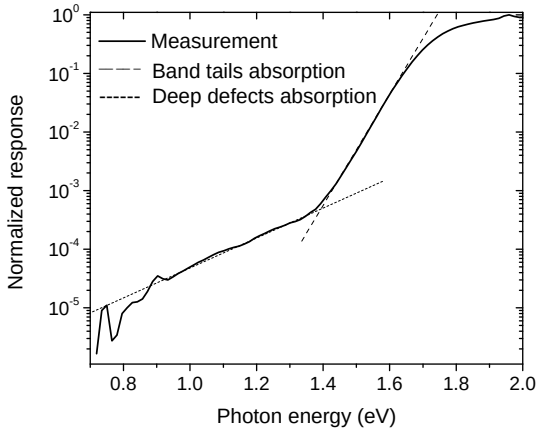

Figure 2.6: FTPS measurement of a-Si:H solar cell. The spectrum is normalized. There are two regimes to be distinguished. At higher energies (>1.4 eV) the slope is determined by the band tails and at lower energies by deep defect states.

Chapter 3

Upconverter material: $NaYF_4$

Abstract

Upconversion is a promising way to increase the efficiency of solar cells. With an upconverter low energy photons are converted to higher energy photons. In this chapter, we focus on upconverters with the Yb^{3+}/Er^{3+} *couple in different crystalline hosts. Previous measurements have shown that* $NaYF_4$ *is a very efficient host for upconversion of near infrared light to visible wavelengths.* $NaYF_4$ *has two crystal structures, an* α *and* β *phase of which* β-$NaYF_4$ *is the more efficient one. The influence of the crystal structure on the emission intensity and upconversion dynamics is investigated. The increased upconversion efficiency in the* β *phase is attributed to the larger absorption strength and more efficient transfer between* Yb^{3+} *and* Er^{3+} *in the hexagonal* β*-phase. Lifetime measurements reveal a slower rise of the upconverted emission. This is consistent with previous measurements, showing that for lanthanides a longer rise time results in higher upconverted emission intensity.*

3.1 Introduction

High efficiency solar cells require absorption of photons of the full solar spectrum followed by effective generation and collection of charge carriers. The high band gap of amorphous silicon of 1.8 eV implies that the material is transparent for sub band gap near infrared (NIR) light, constituting a high photon loss. Upconversion (UC) may enhance the response of solar cells in the infrared. UC is a luminescence process whereby 2 or more low energy photons are converted to 1 higher energy photon. The most efficient UC materials rely on lanthanide ions. Lanthanides form the group of elements in the periodic table for which the 4f inner shell is filled up to 14 electrons. Lanthanide ions are typically trivalent Ln^{3+} and have a $4f^n5s^25p^6$ electron configuration with n=0-14. The partly filled 4f shell is responsible for the unique optical and magnetic properties of lanthanide ions. For n electrons in 14 available orbitals there are 14 over n possible configurations and all configurations can have different energies. This gives rise to a rich energy level structure with energy levels in the NIR, VIS and UV spectral range. Because the outer 5s and 5p shells shield the 4f inner shell, the electronic transitions are independent of the surrounding host materials. The energy levels of the various lanthanide ions are given in the so-called Dieke diagram [38]. The trivalent ions may be doped in different host materials, varying from fluorides to oxides, depending on the application. The transitions between different $4f^n$ states are parity forbidden (no change in dipole moment) and the absorption lines are narrow. The transitions become slightly allowed through admixture of opposite parity states by odd-parity crystal field components or vibrations. The sharpness of the spectral lines results from the weak coupling with the vibrations. There is no Stokes' shift for the optical transitions and this results in the strongly reduced vibrational energy losses. The energy level structure is independent of the host materials, however the phonon energy influences the non-radiative transitions that are possible. Coupling with phonons, albeit weak, provides a non-radiative channel between energy levels that competes with the radiative transitions. An extended review of the lanthanides used for upconversion was written by Auzel [88]. As a rule of thumb it holds that when energy levels are separated by less than 5 times the maximum phonon energy of the host, non-radiative multi-phonon relaxation will be dominant, while for energy differences of more than 5 times, radiative decay will dominate [41].

One of the most efficient upconverter materials for NIR to VIS upconversion was found to be $NaYF_4 : Er^{3+}, Yb^{3+}$ with Yb^{3+} as sensitizer and Er^{3+} as activator [44]. Fluorides are generally low phonon energy host materials and suitable hosts for lanthanides [89]. Yb^{3+} has only one energy level around 980 nm (10 200 cm^{-1}) with a lifetime of ~2 ms [46], making it an ideal sensitizer for near infrared to visible upconversion [43]. Er^{3+} has an energy level around 980 nm and 490 nm (20 400 cm^{-1}), allowing for two close to resonant energy transfer steps from Yb^{3+} to Er^{3+}. The two-step energy transfer process from Yb^{3+} to Er^{3+} is depicted in 3.1. Also other paths are depicted in the graph. Er^{3+} emits in the green and red after the upconversion process. Green emission is observed after two subsequent

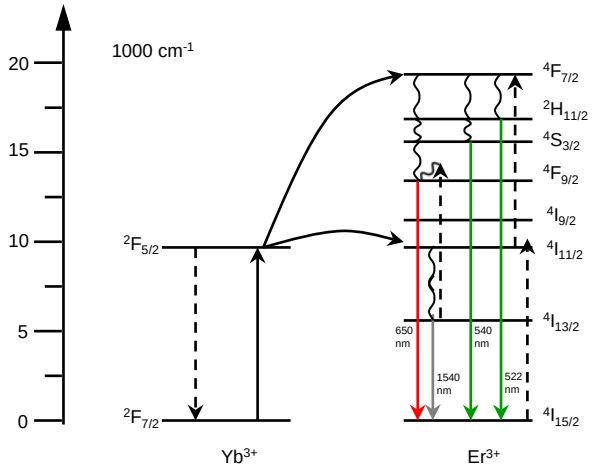

Figure 3.1: Energy levels of the Yb^{3+} and Er^{3+} ions and the interaction between the ions. The full lines represent radiative transitions, curly lines multi-phonon relaxation and the dashed lines non-radiative transitions accompanied by energy transfer, the curved lines. When energy is transferred from Yb^{3+} to Er^{3+} the Yb^{3+} is in its groundstate and Er^{3+} excited to a higher state.

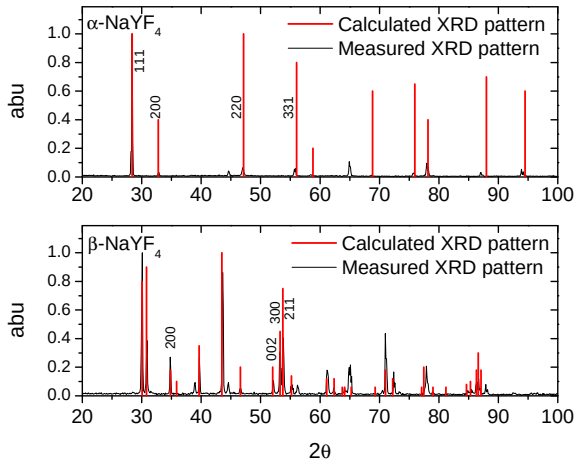

Figure 3.2: XRD diffraction pattern of the $NaYF_4$ crystals. Comparison of theoretical diffraction patterns of the α and β-$NaYF_4$ phases with the experimental data. Overlap reveals that mainly α and β structures were synthesized.

energy transfer steps to the $^4F_{7/2}$ state via the $^4I_{11/2}$ state and multi-phonon relaxation to the $^2H_{11/2}$ and $^4S_{3/2}$ states. The $^4F_{9/2}$ state (red emission) can either be excited in the same way that the $^2H_{11/2}$ and $^4S_{3/2}$ states are excited or after excitation from the $^4I_{13/2}$ state to the $^4F_{9/2}$ state. The $^4I_{13/2}$ state is excited after multi-phonon relaxation from the $^4I_{11/2}$ state of Er^{3+}. Emission from the excited states to ground and intermediate states are observed. The efficient energy transfer and the large spectral overlap between Yb^{3+}/Er^{3+} makes Yb^{3+}/Er^{3+} a widely investigated NIR-VIS upconversion couple in a variety of host materials [43, 45, 46, 47, 48, 90].

The $NaYF_4 : Er^{3+}, Yb^{3+}$ upconverter has two different crystalline structures, a cubic (α) and a hexagonal (β) of which the hexagonal structure is the most efficient. It is not clear why the β-phase is so efficient. Recent research shows that the multiple sites of the Ln^{3+} in the hexagonal phase may increase the energy transfer between the Yb^{3+} and Er^{3+} ions, due to resonance conditions [91]. In this chapter, the different α and β phases are synthesized and the origin of the difference in upconversion efficiency is investigated.

3.2 Experimental

The upconverter that is the most efficient for amorphous silicon solar cells is $NaYF_4 : Yb^{3+}, Er^{3+}$. Micro crystalline $NaYF_4$ samples with different doping concentrations were synthesized with the dry mixture method and two crystal structures were made. The materials are made by mixing appropriate weight mixtures of NaF, YbF_3, ErF_3, and YF_3 and heat the samples with an excess of NH_4F in a nitrogen atmosphere for 7 hours. To make the β-phase the samples were heated up to 700 °C, for the α-phase up to 1050 °C. Samples were prepared with different Er^{3+}/Yb^{3+} concentrations, 20% and 18% 10%, 9% Yb^{3+} and 1% or 2% Er^{3+} and with 1% or 5% Er^{3+} only. XRD patterns of the hexagonal β and cubic α structures are shown in figure 3.2. The lattice constants are 5.49 Å for the cubic and a = 5.95 Å and c= 3.5 Å for the hexagonal structure. In both XRD diffraction patterns peaks from the aluminum substrate are detected at 44.6° and 65.1°. Additional peaks in the β-phase at 38.6°, 56.0° and 70.2° correspond to the NaF crystal structure. Diffuse reflectance spectra were recorded with a Perkin-Elmer Lambda 950 UV/VIS/IR spectrophotometer with integrating sphere. For fluorescence spectra the samples were excited with a tunable dye laser and an Edinburgh instrument spectrofluorometer as described in chapter 2. Excitation of the phosphors at 980 nm was done with a Lambda Physic LPD3000 tunable dye laser filled with a Styrile 14 dye solution. It is pumped by a Lambda Physic LPX100 excimer (XeCl) laser. Lifetime measurements were performed with the dye laser, with a pulse length of 20 ns and a repetition rate of 10 Hz. Upconverted emission spectra recorded under different power intensities of the excitation source, give insight in the power dependence of the upconverted emission. The excitation power of the lasers were varied with neutral density filters. Power dependent measurements

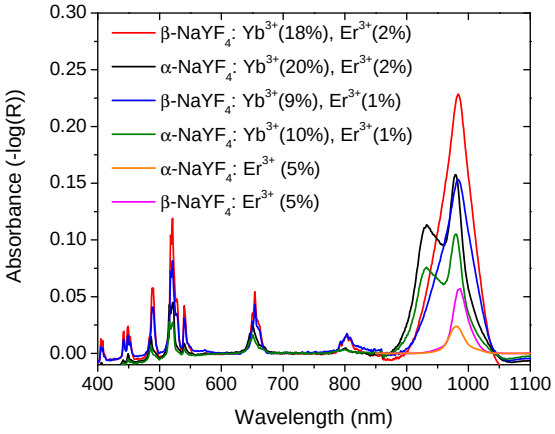

Figure 3.3: Absorption spectra taken from diffuse reflectance spectra of different $NaYF_4$ samples with different concentration.

were performed with the pulsed dye laser and with a continuous diode laser. While the intensity of the pulsed laser was varied, the upconverted emission spectra of different samples were recorded under identical conditions. The emission intensities obtained with the pulsed laser may be compared. Excitation spectra were measured with opotek HE 355 II laser. For the low temperature measurements the Edinburgh spectrofluorometer is equipped with an Oxford helium flow cryostat. The spectra were not corrected for instrumental response.

3.3 Results and discussion

3.3.1 Absorption spectra

In figure 3.3 the absorption spectra are shown for α-$NaYF_4$ and β-$NaYF_4$ doped with different concentrations of Yb^{3+} and Er^{3+}. The absorption around 980 nm is assigned to the $^2F_{7/2} \rightarrow ^2 F_{5/2}$ transition in Yb^{3+} and the $^4I_{15/2} \rightarrow ^4 I_{11/2}$ transition in Er^{3+}. In the samples doped with only $Er^{3+}$the absorption for the $^4I_{15/2} \rightarrow ^4 I_{11/2}$ transition is more than 2 times stronger in β-$NaYF_4$. The higher absorption strength is explained by the lower site symmetry for Er^{3+} in β-$NaYF_4$. α-$NaYF_4$ has a cubic crystal structure and the higher site symmetry for Er^{3+} reduces the absorption strength. The absorption strength for the electric dipole forbidden transitions within the $4f^n$ configuration of lanthanides is induced by mixing opposite parity crystal field components, which is stronger at sites with lower symmetry [92, 93].

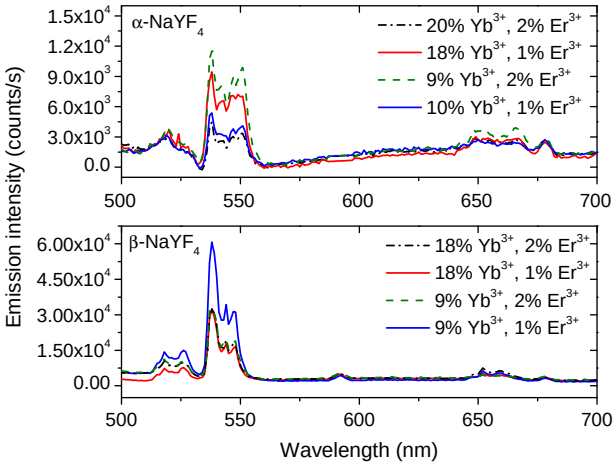

Figure 3.4: Visible upconversion spectra after excitation at 980 nm for the different $NaYF_4$ samples. The most emission is around 550 nm, corresponding to the $^2H_{11/2} \rightarrow ^4 I_{15/2}$ and $^4S_{3/2} \rightarrow ^4 I_{15/2}$ transitions. Maximum UC emission was measured for β-$NaYF_4$: 9% Yb^{3+}, 1% Er^{3+} and for all concentrations the total emission intensity was higher for β-$NaYF_4$.

In samples codoped with Yb^{3+} an extra broader peak around 980 nm is observed due to the $^2F_{7/2} \rightarrow ^2 F_{5/2}$ transition in Yb^{3+}. Also here the absorption strength is ~1.3 times stronger in the β-phase for the 9% and 10% codoped Yb^{3+} samples.

3.3.2 Luminescence spectra

Emission spectra

Emission is observed in the visible part of the spectrum due to upconversion. Figures 3.4 show the upconverted emission. The samples were excited at 980 nm, with a dye laser with styrile dye. The spectra are recorded under identical conditions and intensities may be compared. The emission peaks correspond $^2H_{11/2} \rightarrow ^4 I_{15/2}$, $^4S_{3/2} \rightarrow ^4 I_{15/2}$ and $^4F_{9/2} \rightarrow ^4 I_{15/2}$ transition for 522, 540 (green) and 650 (red) nm emission as shown in figure 3.1. Emission from these states require absorption of 2 photons. Emission spectra in the IR are shown in figure 3.5 for excitation at 950 nm. The peak around 1 µm corresponds to the $^4I_{11/2} \rightarrow ^4 I_{15/2}$ transition from $Er^{3+}$and the $^2F_{5/2} \rightarrow ^2 F_{7/2}$ transition from Yb^{3+} and the peak around 1.5 µm corresponds to $^4I_{13/2} \rightarrow ^4 I_{15/2}$ transition in Er^{3+}, as shown in figure 3.1.

The upconverted emission intensity from the $^4F_{9/2} \rightarrow ^4 I_{15/2}$ transition is the same for all the samples. The green emission intensity varied from being 2 times

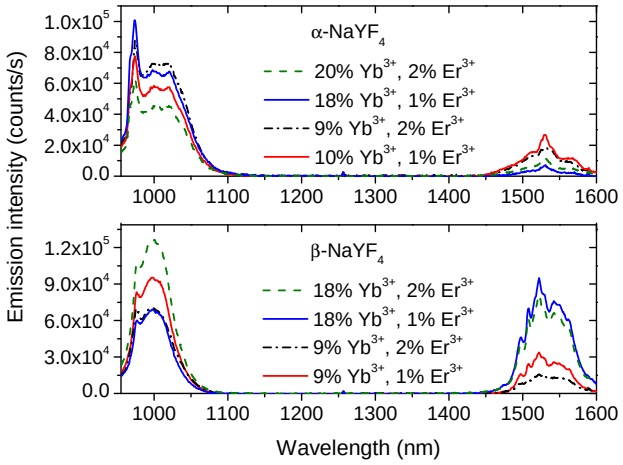

Figure 3.5: Emission after excitation at 950 nm. The emission around 1540 nm corresponds to the $^4I_{13/2} \rightarrow ^4 I_{15/2}$ transition. The emission intensities are always higher for the β-$NaYF_4$ samples.

more efficient for β-$NaYF_4$: 9% Yb^{3+}, 2% Er^{3+} to 9 times more green emission for the β-$NaYF_4$: 9% Yb^{3+}, 1% Er^{3+} compared to the α-samples with same Yb^{3+}/Er^{3+} concentration. Most remarkable is the emission from the $^4I_{13/2}$ state. This is more than ~20 times stronger for the β-$NaYF_4$: 18% Yb^{3+}, 1% Er^{3+} sample compared to the α sample with same dopant concentrations. The increased emission from the $^4I_{13/2}$ state in Er^{3+} and generally higher upconverted emission intensity for the β samples is consistent with reports in the literature [46, 43].

3.3.3 Power Dependence Upconversion

Upconversion involves subsequent absorption of 2 or more photons. The intensity of the upconverted emission is therefore expected to show a quadratic dependence on the incoming light intensity for 2 photon upconversion. Different regimes can be distinguished. The first regime is when no saturation of intermediate energy levels occurs. In figure 3.1 the first excited state N_1 is Yb^{3+} :^{2} $F_{5/2}$ and the upper excited state N_2 is Er^{3+} : $^4F_{7/2}$. The population of the first excited state is proportional to laser intensity P_{in}. Population of the second excited state is dependent on the population density of the first excited state and the laser power density, i.e $N_2 \propto P_{in} \cdot N_1 = P_{in}^2$. In general, when no energy levels are saturated the population of an upper excited $N_n \propto P_{in}^n$. Deviation of the number occur when energy levels are saturated. Photons are either upconverted to an even higher energy state or downshifted. For a two-photon upconversion process, the upconverted intensity is not increasing quadratically anymore and $n < 2$ is observed [45, 94].

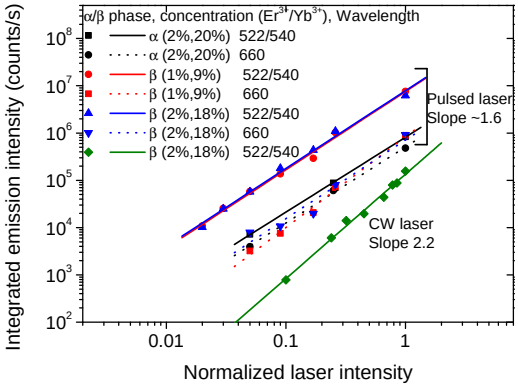

Figure 3.6: Power dependence of different emission wavelengths and samples. The samples were excited with a pulsed laser and continuous laser and slopes of 1.6 and 2.2 were determined respectively. The integrated emission intensity may be compared for the pulsed laser. As what was observed before, the red emission intensity is the same for the α and β phases, while the green emission intensity is stronger in the β-phase.

Power dependence measurement were performed with pulsed laser and continuous laser for different samples. The upconverted emission intensity after excitation with the pulsed laser was recorded under identical conditions and the integrated values may be compared. No large differences between the dependence of the UC intensity on laser power for the samples was found. A significant difference is observed between the pulsed laser and continuous laser light, see figure 3.6. The value for n is approximately 1.6 for all the samples excited with the pulsed laser, while around 2.2 for continuous laser light with a maximum power of $3\,W/cm^2$. The laser power was normalized to 1. Pulsed lasers have very high power density of light and thus energy levels are saturated and slopes < 2 are observed. For the continuous laser a slope of 2 is measured which is expected for the low light intensity of the excitation source.

3.3.4 Energy Transfer

The most efficient mechanisms for upconversion with lanthanide ions are two-step excitation (excitation from the ground state followed by excited state absorption, GSA/ESA) and upconversion by energy transfer (ETU) between the excited ions. Whereas GSA/ESA is a one-ion process, ETU always involves at least two ions. GSA/ESA is observed for low doping concentration (<1%). In case of ETU, the upconversion from a lower excited state to a higher excited state is realized by energy transfer between two excited ions, possibly different types of ions, see figure 3.1. Different types of energy transfer mechanisms are possible, but non-radiative

energy transfer via dipole-dipole interaction is the dominant mechanism [95]. Efficient energy transfer requires the ions to be in close proximity and thus ETU requires high concentration of the dopants. The ETU transfer process is generally experimentally determined to be the most efficient process. Since energy transfer itself can not increase the efficiency, the gain comes from the spatial averaging due to energy diffusion between the ions [88]. The energy transfer efficiency is given by: $\eta_{SA} = (R_0/R_{SA})^6$, with R_0^6 the distance at which the energy transfer rate to the activator is equal to the decay rate of the sensitizer ion and is given by:

$$R_0^6 = \eta f_A (3e^2 c^3 \hbar^5 \pi / 2m) \int g_S(E) g_A(E) / E^4 dE \tag{3.1}$$

with η the quantum efficiency of the sensitizer ion (Yb^{3+}) and f_A the absorption strength of the activator (Er^{3+}). The integral gives the spectral overlap and can be determined by normalized absorption spectrum of Er^{3+} and the normalized emission spectrum of Yb^{3+}, which are the same for the α and β structures. From the absorption in figure 3.3 it was shown that absorption strength of Er^{3+} is two times stronger in β-$NaYF_4$. From diffuse reflection spectra with 5% Er^{3+}(figure 3.3) the absorption for the $^4I_{15/2} \rightarrow ^4 I_{11/2}$ transition was determined to be 2 times stronger for the β-phase. Thus solely from the absorption strength it can be concluded that the energy transfer efficiency will be approximately two times higher in β-$NaYF_4$.

Lifetime Measurements

A powerful technique to examine the dynamics of energy transfer, is measuring the luminescence decay curve for the unconverted emission after a short excitation pulse. When GSA/ESA is the main pathway for upconversion, the decay curve is a simple exponential decay from the high state without a rise time. For energy transfer upconversion however, there is first a rise in intensity followed by the decay. The rise results from the slow feeding of the emitting state through the energy transfer step [42]. Lifetime measurements were performed on the α and β samples with different Yb^{3+} and Er^{3+} concentration. The lifetime curves of upconverted and downshifted emission was fitted by the following formula for the GSA/ETU mechanisms [96]:

$$N_2^{ETU}(t) \propto (1 - \exp[t/\tau_{All}]\exp[-t/\tau_{UC}] \tag{3.2}$$

with $\tau_{All}^{-1} = (k_T - k_R + k_{UC})$ here k_R is the emission rate from the intermediate state to the ground state, k_T is the transfer rate from the intermediate state to the upper excited state and $\tau_{UC}^{-1} = k_{UC}$ the emission rate from the upper excited state to the ground state. Emission from the intermediate state is given by:

$$N_1(t) \propto \exp[t/\tau_{TR}] \tag{3.3}$$

with $\tau_{TR}^{-1} = -k_T - k_R$.

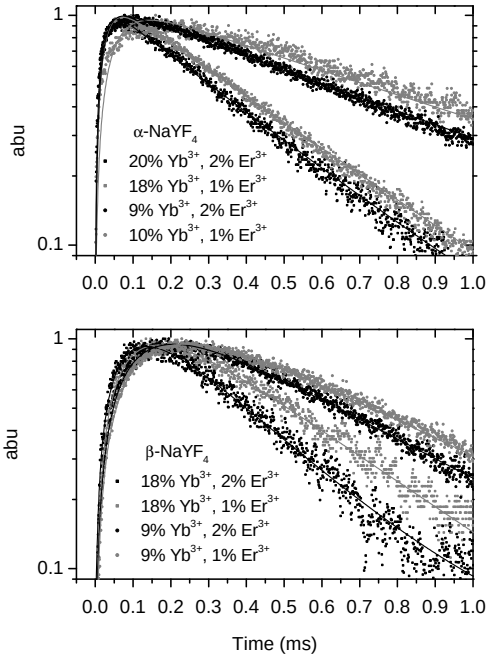

Figure 3.7: Decay curves of α-$NaYF_4$ and β-$NaYF_4$ samples with different concentration of Yb^{3+} and Er^{3+} for upconverted emission of 525 nm. Excitation was at 980 nm. When ETU is the main mechanism, the decay curves will show a rise time followed by a decay, what can be seen in the graphs. The decay rate is increasing with increasing Yb^{3+} concentration, as can be seen clearly in the decay curves of the α-samples.

Time resolved measurement were performed for all samples. Figure 3.7 shows the decay curves for the $^2H_{11/2} \rightarrow ^4 I_{15/2}$ transition after excitation at 980 nm. All emission from the Er^{3+} states showed this rise time followed by the decay of the emitting state and are fitted with equation 3.2. The decay times were consistent with previously measured decay times [46]. Emission from Yb^{3+} was fitted with equation 3.3 and was around 0.5 ms for all samples, which is low compared to previously measured lifetime of 2 ms of the $^2F_{5/2} \rightarrow ^2 F_{7/2}$ transition in Yb^{3+} in β-$NaYF_4$:2% Er^{3+}, 18% Yb^{3+} [46]. The intrinsic lifetime of Yb^{3+} in the $NaYF_4$host was around 2 ms, in both the α and β phases, see figure 3.8. The lifetime may have been shortened due to crystal defects.

For the decay times (τ_{UC}) of upconverted emission no significant differences are found between the different crystal structures, only between the Yb^{3+} and Er^{3+} concentration. As can be seen in the upper graph of figure 3.7, a higher concentration of the sensitizer increases the emission rate. For the rise time however

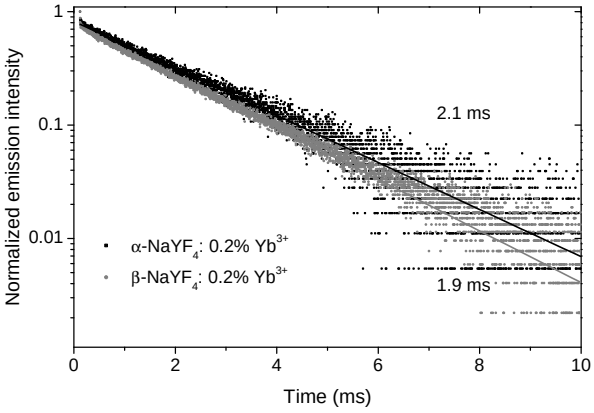

Figure 3.8: Decay curves of Yb^{3+} in α- and β-$NaYF_4$ after excitation at 950 nm. The low concentration avoids interaction between the ions and the intrinsic lifetime is measured.

(τ_{All}), a large difference was found between α and β-$NaYF_4$. Figure 3.9 shows the decay curves for the $^2H_{11/2} \rightarrow ^4 I_{15/2}$ transition in α and β-$NaYF_4$. A distinct difference is rise time is measured. More detailed examination shows that the rise time is 4 times longer in β-$NaYF_4$ for upconverted emission while the decay rates for the 525, 540 and 650 emissions are the same for the different α and β-phases. Also the decay curves for the downshifted $^4I_{13/2} \rightarrow ^4 I_{15/2}$ emission was fitted with equation 3.2 and a longer rise time for the β-phase was found. The rise time for the downshifted emission is 1.3 times longer. The transfer rate is thus lower in β-$NaYF_4$, as determined from the large rise time. Though as explained in section 3.3.4, the transfer is more efficient between Yb^{3+} and Er^{3+} in the β-phase and shown before the (upconverted) emission is larger in the β-phase (see figures 3.4 and 3.5). This seemingly contradiction had been shown before [97], but was not explained. It is possible that the energy is transferred between different Yb^{3+} ions, prior to the Er^{3+} ion. This is likely because the interaction is more efficient and thus smaller chance that the energy is trapped by a defect, leading to non radiative decays. This would increase the rise time but also the emission intensity because more Yb^{3+} ions are transferring their energy to Er^{3+}. As a consequence, in crystal structures with less efficient energy transfer, like the α structure only nearest neighboring Yb^{3+} ions participate in the upconversion process. This will lead to a faster rise time, but lower emission intensity.

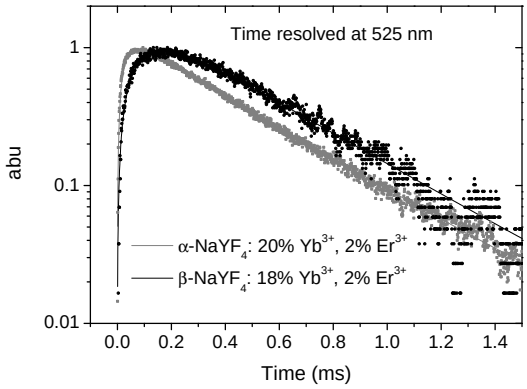

Figure 3.9: Decay curves for emission at 525 nm after excitation at 980 nm for α and β-$NaYF_4$ with same concentration Yb^{3+} and Er^{3+}. Between the α and β samples a distinct difference in rise time was measured. The decay times are the same of the different samples.

3.3.5 Temperature dependence

Temperature dependent measurement will give more insight in phonon assisted transitions. Figures 3.10 and 3.11 show the temperature dependence of the emission of the $^4I_{11/2} \rightarrow ^4 I_{15/2}$ transition, for samples doped with 1% Er^{3+}. Excitation was at 650 nm with the dye laser. To have a high enough signal for the down-shifted emission of the α sample, the slit was slightly larger and the measurement repeated 3 times. Direct comparison of emission intensity between the samples is thus not possible, but the emission of the β samples was much stronger. In the α structure, the transitions between the states are phonon assisted and even at low temperature broad emission lines are measured, though very weak. At higher temperature the high energy peaks become stronger and the total emission increases. The emission is thereby blue shifted. The emission spectra of the $^4I_{11/2} \rightarrow ^4 I_{15/2}$ transition in β-$NaYF_4$ reveals a different mechanism. A 0-phonon peak is visible, which is possible due to the low site symmetry of Er^{3+}. For both samples the peaks are slightly broadened with higher temperature [98]. The emission intensity first decreases with increasing temperature and with higher temperatures the emission intensity is increasing again. At higher temperature phonon assisted energy transfer is possible resulting in especially for the α structure increased emission.

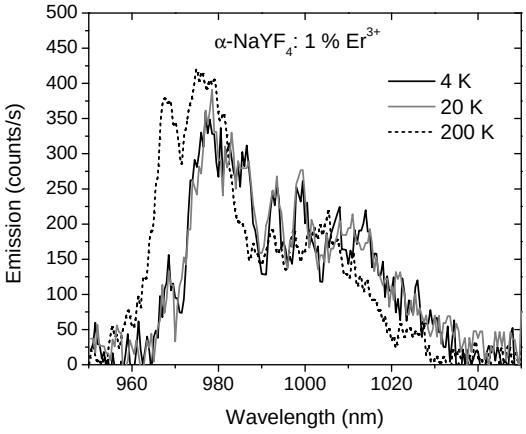

Figure 3.10: Temperature evolution of emission at 980 nm for α-$NaYF_4$:1% Er^{3+}. Excitation was at 650 nm. The resolution was 0.5 nm and repeated 3 times to increase the signal.

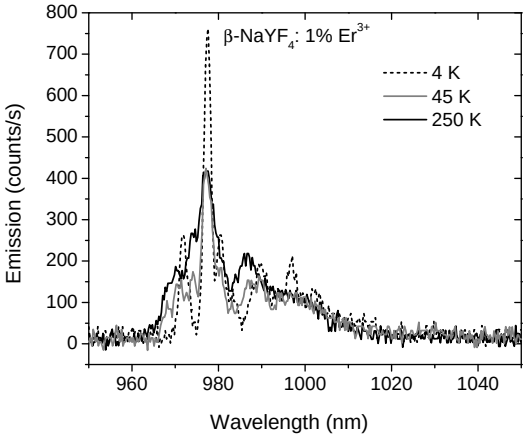

Figure 3.11: Temperature evolution of emission at 980 nm for β-$NaYF_4$:1% Er^{3+}. Excitation was at 650 nm, resolution 0.3 nm.

3.4 Conclusions

The infrared-to-visible upconversion has been investigated in the well-known upconversion material $NaYF_4$:Er^{3+}, Yb^{3+} for the two crystalline modifications, cubic α-$NaYF_4$ and hexagonal β-$NaYF_4$. It is well known that upconversion is more efficient in the hexagonal phase. A quantitative comparison of the UC efficiency confirmed that the efficiency in β-$NaYF_4$:Er^{3+}, Yb^{3+} is about four times stronger. The higher efficiency can be explained by a two times higher oscillator strength of the $^4I_{15/2} \rightarrow ^4 I_{11/2}$ transition on Er^{3+} which is involved in the first $Yb^{3+} \rightarrow Er^{3+}$ energy transfer step. Also for the second transfer step, where the Er^{3+} ion is excited from the $^4I_{11/2}$ to the $^4F_{7/2}$ state, a higher oscillator strength on the Er^{3+}-acceptor may enhance the UC efficiency. For the $^2F_{5/2} \rightarrow ^2 F_{7/2}$ absorption transition on Yb^{3+} and the spectral overlap between the Yb^{3+} emission and Er^{3+} absorption around 1000 nm no significant differences are observed, indicating that these factors cannot explain the higher UC efficiency in β-$NaYF_4$:Er^{3+}, Yb^{3+}. Time resolved measurements confirm that energy transfer by ETU is the dominant mechanism. The slower rise time of the UC emission in β-$NaYF_4$:Er^{3+}, Yb^{3+} is surprising in view of the higher $Yb^{3+} \rightarrow Er^{3+}$ transfer rate and suggests that the rise time is also determined by energy migration over the Yb^{3+}-sub lattice or indicates that alternative transitions- like non-radiative recombination of Yb^{3+} are suppressed.

Chapter 4

Investigation of upconversion efficiencies for low power excitation

Abstract

In this chapter the influence of the absorption strength on the upconversion efficiency under low light intensities is investigated. This is particularly relevant for solar cells since the efficiency of upconverters under solar irradiation is far below the maximum efficiency that is reached under high power infrared radiation. In addition to concentrating solar light, enhanced infrared absorption is a promising avenue to increase the upconversion efficiency. Two systems are studied in this chapter. The first is Gd_2O_2S *:*Yb^{3+}, Er^{3+}. *The upconversion mechanism is similar to that in the model upconversion system* $NaYF_4$*:*Yb^{3+}, Er^{3+}. *The absorption strengths for the intraconfigurational 4f-4f transitions are significantly higher due to the higher covalency of the host lattice. The second method relies on coupling plasmon resonance of gold nanorods. The influence of plasmonic coupling is investigated for* $NaYF_4$*:*Yb^{3+}, Er^{3+} *nanoparticles in close proximity to gold nanorods covered with a silica shell. A faster decay was observed for near infrared emission but no enhanced upconversion was observed.*

4.1 Introduction

Upconversion of near infrared (NIR) to visible (VIS) light may increase the efficiency of solar cells. Upconversion efficiency as high as 10% are possible but are only achieved under high power excitation due to the non-linear character of the two-photon process. To enhance the efficiency of solar cells through upconversion, the upconverter should reach high efficiency under low power NIR excitation. The efficiency of upconversion materials based on lanthanide ions is limited by the weak absorption and narrow bandwidth of the intraconfigurational 4f-4f transitions of lanthanide ions. The upconversion efficiency may be improved in several ways which are depicted in Fig. 4.1. The absorption width can be increased by using a sensitizer, e.g. a transition metal ion incorporated in the host lattice, which absorbs over a broad spectral region and transfer the energy to a nearby lanthanide ion through dipole-dipole interaction [52, 54]. Alternatively, quantum dots to can be used to absorb a broad spectrum of high energy photons and convert these to the absorption wavelength of the lanthanide ion. These processes are depicted on the left hand side of Fig. 4.1. Previous work on the use of transition metal ions has not been successful, mainly due to thermal quenching of the transition metal emission in the infrared spectral region. A problem with quantum dots is that they not only absorb in the IR but also the upconverted visible emission is reabsorbed which complicates the design of the upconversion system. Another approach is to enhance the absorption strength of the 4f-4f transition of the lanthanide ions by changing the host material or by placing the upconverter in a locally enhanced field induced by a metal nanoparticle. The host material influences multi-phonon relaxation rates, energy transfer rates between ions and the absorption strength/radiative decay rate between 4f levels [99]. Plasmonic coupling requires tuning of the plasmon resonance to the desired wavelength of the absorption transition for the upconversion material. The latter two processes are depicted on the right hand side in Fig. 4.1.

The use of metal nanoparticles in combination with upconverter materials has attracted considerable attention recently. Coupling with a plasmon resonance in a nearby metal nanostructure enhances the local field [100]. It has been known since the 1970s that plasmon oscillations enhance nonlinear processes like Raman scattering to the fourth power of the near field enhancement [101]. In the 1980s it has been demonstrated that also a fluorescence signal can be increased in the presence of a local field induced by plasmonic excitations [102]. The enhanced local field influences transition rates and by placing the upconverter in the enhanced local field for the NIR absorption wavelength, the absorption strength and thus the upconversion efficiency can be increased [103].

This chapter explores both options depicted on the right hand side in Fig. 4.1 for the Yb^{3+}, Er^{3+} upconversion couple. By changing the host material from the standard material $NaYF_4$ to the more covalent Gd_2O_2S the absorption strength of the 4f-4f transitions increases. The upconversion in Gd_2O_2S :Yb^{3+}, Er^{3+} appeared to be more efficient at low light intensities and also saturation effects for

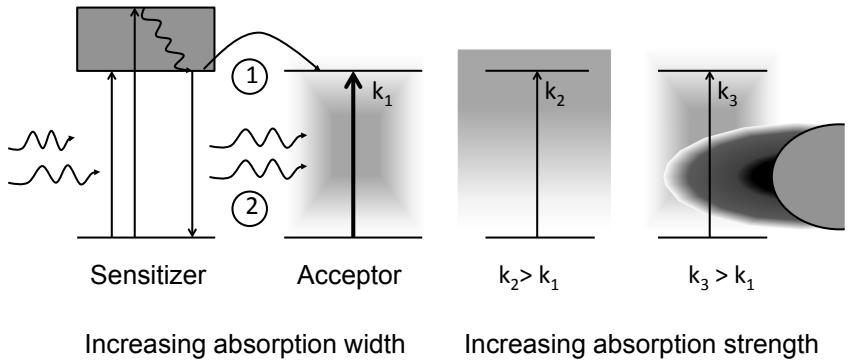

Figure 4.1: Different methods for increasing the upconversion efficiency. The transition rates are given by $k_{1,2,3}$, the curved lines represent photons, the drawn lines represent absorption and emission transitions and the curved gray line represents multi-phonon relaxation. On the left hand side the enhanced absorption through non-radiative (1) or radiative (2) energy transfer from a broad band absorbing sensitizer is shown, on the right hand side the enhanced absorption is induced by changing the host lattice or by local field enhancement by a nearby metal nanoparticle.

the two-photon processes occurred at relatively low light intensities and higher order processes were observed. Gold nanorods were synthesized with an aspect ratio giving rise to a plasmon resonance around 1000 nm, at the wavelength of the absorption for the Yb^{3+} ion. Combining $NaYF_4$:Yb^{3+}, Er^{3+} nanocrystals with gold nanorods covered with a thin layer of silica resulted in a faster decay for the NIR emission of Yb^{3+} around 1000 nm and, to a lesser extent, for the 1500 nm emission from Er^{3+} . The present experiments are initial studies to realize enhanced upconversion efficiencies and further research is required to obtain a complete understanding of the effects observed and to design a upconversion system that provides a significant increase of the solar cell efficiency.

4.2 Experimental

Both NIR to VIS upconversion systems described in this chapter are based on the Yb^{3+}/Er^{3+}couple. The Gd_2O_2S: Er^{3+} , Yb^{3+} upconverter was purchased from Phosphor Technology Ltd. XRD analysis confirmed the crystal structure and with ICP (Inductive Coupled Plasma) elemental analysis the concentration of Er^{3+} and Yb^{3+} were determined to be 5% and 10%, respectively. Core-shell nanoparticles of β-$NaYF_4$: Er^{3+} , Yb^{3+} (15 nm diameter, dissolved in octadecanol) were obtained from prof. M. Haase of the University of Osnabrück. The synthesis method is

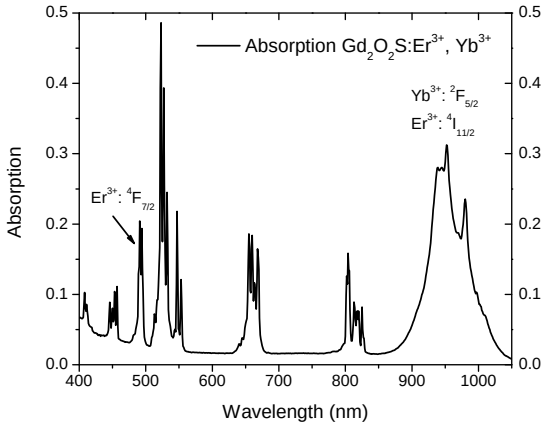

Figure 4.2: Absorption spectra of Gd_2O_2S taken from diffuse reflectance spectra. The absorption around 950 is the highest, though absorption around 980 nm leads to resonant energy transfer to the $^4F_{7/2}$ state.

described in Ref. [104]. Gold nanorods were synthesized using a seed-mediated growth method described in Ref. [105]. Absorption spectra were measured using a Perkin Elmer 950 UV/VIS/NIR spectrophotometer. Luminescence spectra were recorded using an Edinburgh FLS920 spectrofluorometer. For excitation spectra in the NIR and for time resolved measurements, the samples were excited with a pulsed Opotek system (Opolette HE355 I) tunable between 410 and 2200 nm. Emission spectra were also recorded for dual NIR excitation combining the Opotek system with a CW diode laser at 981 nm.

4.3 Upconversion in Gd_2O_2S

The host lattice Gd_2O_2S is well known for phosphor materials and is used for example as a scintillator material in x-ray imaging and CT scanners when doped with Tb^{3+} or Pr^{3+} [106, 107]. As a host for upconversion materials the oxysulfide host is not well known, but the upconversion material Gd_2O_2S: Er^{3+}, Yb^{3+} is commercially available. The phonon frequency of the host is low (450 cm^{-1} cut-off frequency [108]) and is only slightly higher than for the standard upconversion material host NaYF4 (400 cm^{-1}). Systematic studies have been conducted on upconversion in La_2O_2S:Er, Yb (Ln=Y, La, Gd) doped with the Yb^{3+}/Er^{3+} and the Yb^{3+}/Tm^{3+} couples and showed a weaker power dependence that expected for the two and three photon upconversion processes [109]. It was also found that the optimum concentration for the sensitizer ion Yb^{3+} was lower than for

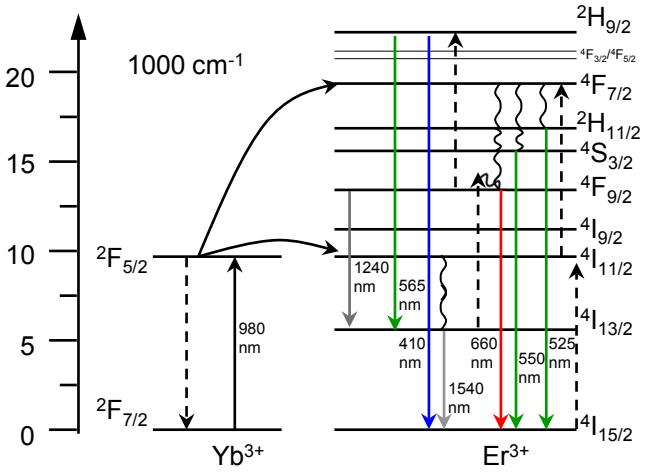

Figure 4.3: Different transitions in Gd_2O_2S host after excitation at 980 nm in Yb^{3+}. The dashed lines represent energy transfer, the curly line non-radiative decay and the full lines radiative decay. When the excitation power density is low, main emission is observed from $^2H_{11/2}$ and $^4S_{3/2}$ states. At higher intensities also emission is observed from the $^2H_{9/2}$ state, which requires absorption of 3 photons to reach.

the same upconversion couple in the fluoride host. More recent studies on Y_2O_2S doped with Yb^{3+}/Ho^{3+} [110] and studies for Gd_2O_2S nanoparticles [111] did show a quadratic dependence of the upconversion emission intensity on NIR excitation power.

4.3.1 Absorption spectra

Absorption spectra for microcrystalline powders are recorded by measuring diffuse reflection spectra. In Figure 4.2 the diffuse reflection spectrum for Gd_2O_2S: Er^{3+} , Yb^{3+} is shown. The strong absorption band with maxima at 950 and 980 nm is assigned to the $^2F_{7/2} \rightarrow ^2 F_{5/2}$ transition on Yb^{3+} and also the $^4I_{15/2} \rightarrow ^4 I_{11/2}$ transition on Er^{3+}. All other absorption lines between 400 and 800 nm can be assigned to transitions on Er^{3+}. In Fig. 4.3 the energy level schemes for Yb^{3+} and Er^{3+} are depicted. The lines around 490 nm in the diffuse reflection spectrum correspond to transitions to the $^4F_{7/2}$ state of Er^{3+}. This state is at twice the energy of the $^4I_{11/2}$ state of Er^{3+} and is crucial in the upconversion process since this state is reached in the two step energy transfer process from Yb^{3+} to Er^{3+}.

4.3.2 Luminescence spectra

In Fig. 4.3 the upconversion process for the Yb^{3+}/Er^{3+} couple is depicted. Excitation in the $^2F_{5/2}$ level of Yb^{3+} is followed by energy transfer to the $^4I_{11/2}$ level of Er^{3+} . A subsequent energy transfer step from a second excited Yb^{3+} ion can raise the Er^{3+} to the $^4F_{7/2}$ level. Fast multi-phonon relaxation to the $^2H_{11/2}$ and $^4S_{3/2}$ levels is followed by emission from these levels which has the strongest transition to the ground state of Er^{3+} and is in the green spectral region (around 540 nm). Relaxation to the $^4F_{9/2}$ emission results in red emission around 660 nm. Besides upconversion processes involving two 980 nm photons, also higher order processes have been observed resulting in population of higher energy levels like the $^4H_{9/2}$ level.

Emission spectra

To study upconversion in Gd_2O_2S: Er^{3+} , Yb^{3+} emission spectra were recorded for excitation at 980 nm and at 1510 nm using the Opolette laser. The upconversion emission spectra is shown in Fig. 4.4. The transitions are mostly from higher energy levels to the $^4I_{15/2}$ ground state and are assigned in the figure. Excitation at 980 nm gives rise to emission from the ($^2H_{11/2}$, $^4S_{3/2}$) and $^4F_{9/2}$ states, both resulting from a two-photon process (see Fig. 4.3). Emission from the higher energy $^4H_{9/2}$ level is also observed and requires a three photon process. Excitation at 1510 nm into the $^4I_{13/2}$ level leads to a dominant red emission from the $^4F_{9/2}$ level, resulting from a three photon process. Higher energy emission from the $^2H_{11/2}$, $^4S_{3/2}$ states is also observed and requires a four photon process. The higher order of the process resulting in green emission under 1510 nm excitation is consistent with the lower relative intensity. It is clear from the upconverted emission spectra that 3 or 4 photon upconverted emission is easily achieved in this material.

In Fig. 4.5 the NIR emission spectra are shown after excitation in the $^4S_{3/2}$ level at 546 nm and into the $^4F_{9/2}$ level at 669 nm. In these spectra emission from Yb^{3+} and from the lower energy levels of Er^{3+} is observed. Also emission from the $^4F_{9/2}$ level to an intermediate state ($^4I_{13/2}$) is observed in the NIR region. No emission are observed in the NIR corresponding to transition from the ($^2H_{11/2}$, $^4S_{3/2}$) level to intermediate levels, showing that the emission to the ground state dominates for the levels.

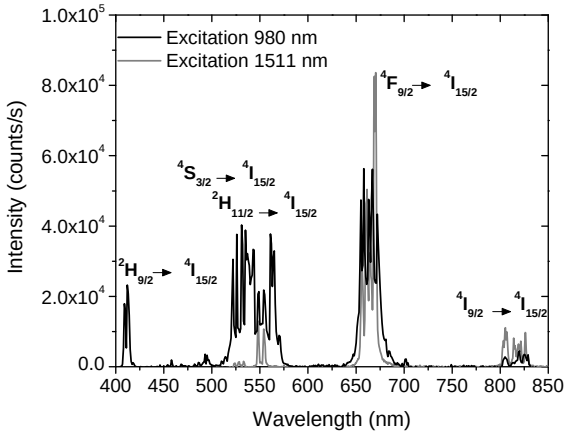

Figure 4.4: Upconverted emission spectra after excitation in the near infrared. The black line shows the upconverted emission spectra after excitation at 980 nm and the red line after excitation at 1511 nm. The basic transitions to the ground state are assigned in the graph.

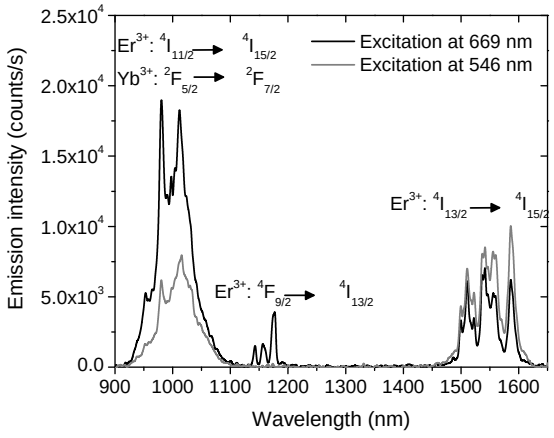

Figure 4.5: Emission spectra after excitation in the visible. Excitation in the $^4S_{3/2}$ state leads to emission from the lower lying states to the ground state. Excitation in the $^4F_{9/2}$ state leads to emission from lower lying states to the ground state but also the an intermediate state.

Excitation spectra

Excitation spectra were recorded in the infrared spectral region for the upconversion emission in green and red spectral region, both around 960 nm (excitation in the $^2F_{5/2}$ level of Yb^{3+}) and around 1530 nm (excitation in the $^4I_{13/2}$ level of Er^{3+}). The graphs are shown in figure 4.6 and figure 4.7 for the spectral region around 960 and 1530 nm respectively. The excitation spectra show lines corresponding to transitions to the various crystal field split components of the $^2F_{5/2}$ level of Yb^{3+} (around 960 nm) and the $^4I_{13/2}$ level of Er^{3+} (around 1530 nm). The lines in the spectra are narrower than the corresponding lines in the diffuse reflection spectra due to the non-linear character of the upconversion process.

In addition to the one-color excitation spectra, also excitation spectra were recorded for simultaneous excitation with the CW diode laser at 981 nm and tunable excitation with the pulsed OPO around 1530 nm and around 960 nm. The excitation spectrum around 960 nm shows stronger excitation lines at the edges and around 970 nm, where the single color excitation spectrum shows the lowest intensity. This is an unexpected observation. It may be explained by saturation of absorption to the $^2F_{5/2}$ level. Comparison of the excitation spectra around 1530 nm for the 536 nm and the 669 nm emission shows generally the same sharp transition corresponding to transitions to the different crystal field split components of the $^4I_{13/2}$ level of Er^{3+}. Some interesting differences are observed in the relative intensities, for example the line around 1526 nm. Possibly, some of the lines correspond to pairs/clusters of Er^{3+} in which the ratio of the red to green emission is different. The two-color excitation spectrum of the 669 nm emission is clearly broadened in comparison to the single color excitation spectra. The simultaneous excitation with the 981 nm diode makes that only a single photon absorption is required to raise the Er^{3+} ion from the $^4I_{11/2}$ level (populated under 981 nm excitation) to the $^4F_{9/2}$ level. The similarity of the peak positions between the one-color and the two-color spectra suggest that the dominant mechanism is absorption in the $^4I_{13/2}$ level followed by energy transfer from the $^4I_{13/2}$ level to a neighboring Er^{3+} ion in the $^4I_{13/2}$ state raising this ion to the $^4F_{9/2}$ state. The alternative mechanism, excited state absorption from the $^4I_{11/2}$ level to the $^4F_{9/2}$ level is not likely, since this would result in different positions of the excitation lines, resonant with energy differences between the $^4I_{11/2}$ and $^4F_{9/2}$ crystal field split components.

4.3.3 Power dependence upconversion

The power dependence of the upconversion emission in Gd_2O_2S: Er^{3+} , Yb^{3+} was measured using the pulsed OPO (with ~mJ maximum pulse energy) as well for CW excitation with the 981 diode laser with a maximum power density of 3 W/cm^2. In Figure 4.8 two typical upconversion emission spectra are shown for excitation with the OPO at 980 nm, one for low power excitation (7% of maximum laser power) and one for full laser power. The relative intensity of the red emission

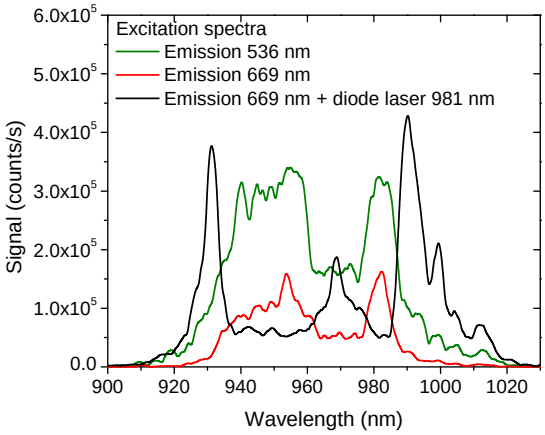

Figure 4.6: Excitation spectrum for emission at 536 nm and 674 nm with and without diode laser. The excitation spectra without additional diode laser are the same for emission at 536 and 674 nm. When the diode laser (981 nm) is added, side bands are visible and the main excitation peaks at 950 and 980 nm are gone.

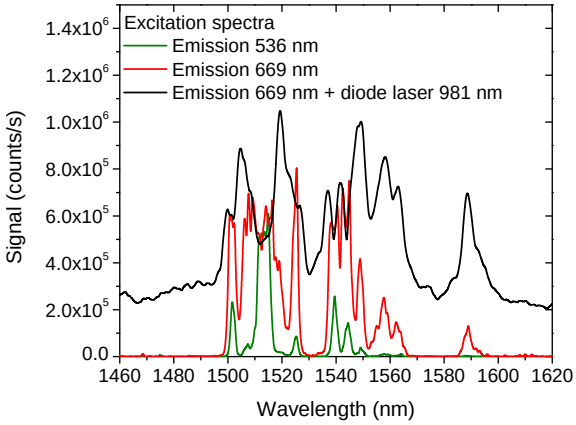

Figure 4.7: Excitation spectra of emission at 536 and 669 nm. The change in spectra is attributed due to broadening when fewer photons are necessary to reach the upconverted state. For emission at 536 nm, this are 4 photons for 669 nm 3 photons, but when excited with the diode laser (981 nm) only 1 photon is required to reach the $^4F_{9/2}$ state.

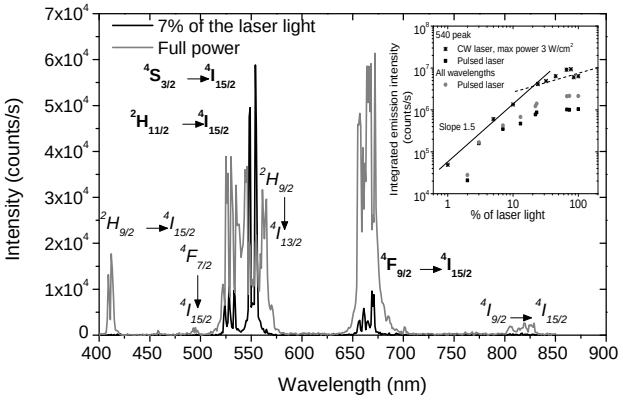

Figure 4.8: Intensity dependence upconverted emission. The emission intensity may be compared. the graph shows the change of the shape of the peaks and the additional peaks at 410, 490 and 810 nm and the intermediate transition at 565 nm (italic). The inset shows the total integrated emission intensity for green (500-570 nm) and all peaks.

increases with increasing laser power which can be explained by cross-relaxation processes between excited Er^{3+} neighbors populating the $^4F_{9/2}$ state, similar to what has been observed for $NaYF_4 : Er^{3+}$, Yb^{3+}. At higher excitation densities also additional peaks are observed around 410, 460, 490, 565, 705 and 810 nm. All these lines are assigned in italics in Fig. 4.8. The additional peaks partly result from higher order processes leading to population of higher energy levels and partly due to population of intermediate levels by cross-relaxation between neighboring excited Er^{3+} ion (e.g. the $^4F_{9/2}$ emission line around 810 nm).

The power dependence of the integrated green emission is depicted in the inset of Fig. 4.8 for CW excitation with the 981 diode laser with and the pulsed OPO. The power dependence has a slope less than two in the low power regime (slope ~ 1.5). The upconversion emission intensity saturates at a 1 W/cm^2 power density. This low power is consistent with results reported in Ref. [109]. The deviation is from the expected slope of 2 for a two-photon upconversion process in a log-log plot of the upconversion emission intensity and excitation power is commonly observed and is ascribed to saturation effects and competing depopulation processes for excited states that are involved in the upconversion process [94]. The saturation power of 1 W/cm^2 is lower than observed for the Er, Yb couple in fluoride host lattices . This is consistent with the higher absorption strengths for the transitions on Er^{3+} and Yb^{3+} in the more covalent oxysulfide hosts and the better performance of this upconversion material at low power densities, in comparison to $NaYF_4 : Er^{3+}$, Yb^{3+}.

Intermediate transitions and broadening

In addition to the intensity changes between different spectral regions for different excitation powers, also other changes are observed in the emission spectra, viz. the spectra broaden for higher excitation power, line shifts and extra emission lines appear. As an example more detailed emission spectra are shown in the spectral region around 540 nm, 670 nm and 820 nm for three or four different excitation powers of the OPO, operating at 5, 20, 60 or 100% of the maximum power, see figure 4.9. Around 540 nm an increase of the relative intensity of the higher energy 525 nm emission is observed. This emission originates from the $^2H_{11/2}$ level which is in thermal equilibrium with the $^4S_{3/2}$ level. The increase of the relative intensity from this level can be explained by laser induced heating of the sample. The broadening and small spectral shifts of the emission lines may also be attributed to laser induced heating. Extra lines appearing in the emission spectra result from emission from higher excited states which are populated through three photon processes at higher excitation powers. Emission from higher excited states to intermediate levels can occur in the spectra regions investigated and explain the appearance of the extra emission.

4.3.4 Comparison with β-$NaYF_4$

It is interesting to compare the upconversion properties in $Gd_2O_2S : Er^{3+}, Yb^{3+}$ with those for β-$NaYF_4 : Er^{3+}, Yb^{3+}$. Both upconverter materials have a hexagonal crystal structure and the f-f transitions are dominated by forced electric dipole transitions. Due to the higher covalency and lower energy opposite parity states, the forced electric dipole transitions are stronger in the oxysulfide. The higher absorption strengths give rise to lower saturation powers. The presently reported experiments (see Fig. 4.8) show saturation of the upconversion emission above 1 W/cm^2. This is indeed much lower than the saturation power reported for $NaYF_4 : Er^{3+}, Yb^{3+}$of 20 W/cm^2[45]. It is also interesting to compare the emission spectra under pulsed laser excitation around 980 nm. In Fig. 4.10 the upconverted emission spectra are shown for β-$NaYF_4 : Er^{3+}$ 1%, Yb^{3+} 18%, (discussed in Chapter 3) and Gd_2O_2S: Er^{3+} 5%, Yb^{3+} 10%. Under the high power pulsed excitation the emission intensity has saturated. The emission spectra are different. For the $NaYF_4$ host the emission is dominated by the green ($^2H_{11/2}$, $^4S_{3/2}$) emission around 545 nm while for the Gd_2O_2S host there is strong contribution from the $^4F_{9/2}$ red emission around 660 nm. For upconversion emission in application where the human eye is used to detect the upconverted light, the green emission is favorable due to the high eye sensitivity in this spectral region. For solar cells however, the response in the green and red spectral region is similar and the red $^4F_{9/2}$ emission can be used for efficient generation of electrical power. The present comparison between $Gd_2O_2S : Er^{3+}, Yb^{3+}$ and β-$NaYF_4 : Er^{3+}, Yb^{3+}$ is limited to a few concentrations and no optimization has been done in concentration and synthesis procedure.

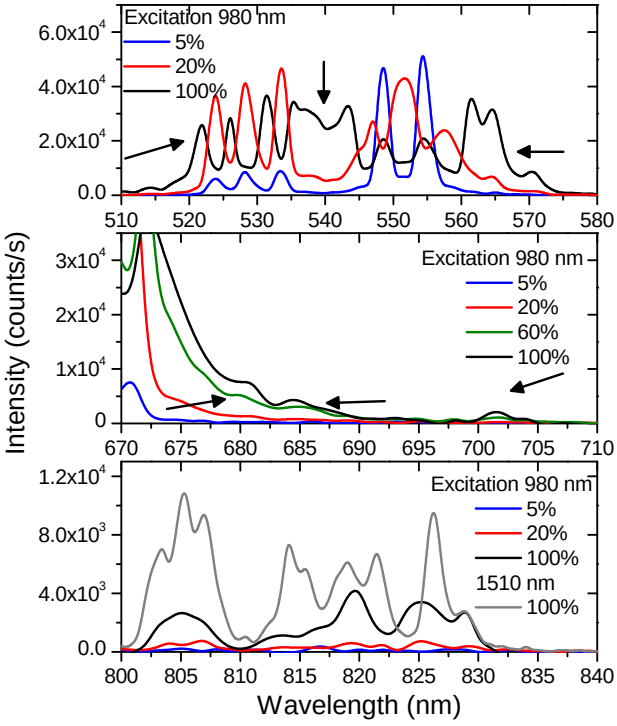

Figure 4.9: Broadening of the green and red emission peaks and appearance of peaks around 815 nm with increasing laser power. The percentage in the graphs represent the fraction of the maximum laser power.

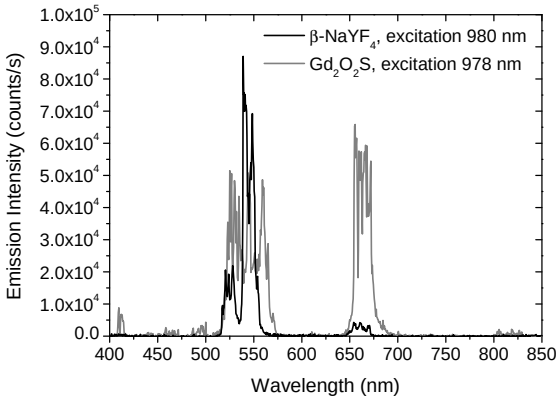

Figure 4.10: Upconversion emission spectra of β-$NaYF_4$:Er^{3+} 1%, Yb^{3+} 18% and Gd_2O_2S:Er^{3+} 5%, Yb^{3+} 10% recorded under identical alignment and excitation density at 980 nm ($NaYF_4$) and 978 nm (Gd_2O_2S).

4.4 Upconversion in β-$NaYF_4$: Er^{3+}, Yb^{3+} nanocrystals near gold nanorods

In the second part of this chapter we describe experiments aimed at increasing the absorption strength through coupling with plasmons in gold nanorods. Coupling of transitions resonant with plasmon resonances on nearby metal nanostructures is known to increase transition rates [100]. When an upconverter nanocrystal is placed close to a metal nanoparticle, the upconversion efficiency may increase due to an increased absorption strength. In order to investigate the feasibility $NaYF_4$: Er^{3+}, Yb^{3+} upconversion nanocrystals were combined with gold nanostructures. The upconversion nanocrystals (NCs) of β-$NaYF_4$: Er^{3+}, Yb^{3+} were kindly provided by prof. Haase from the University of Osnabrück. Gold nanostructures with a plasmon resonance close to the absorption transition of Yb^{3+} (around 1000 nm) were synthesized. Gold nanocrystals have plasmon resonances in the visible part of the spectrum. However, for gold nanorods or gold nanospheres, the resonance frequency can be tuned towards the near infrared [112, 113, 114, 115]. The synthesis of gold nanorods with different aspect ratios, including the ratio that gives rise to a 1000 nm plasmon resonance, is known in the literature [115]. To optimize the distance between the gold nanorod and the upconverter nanoparticle, the gold nanorods were coated with a thin layer of silica. If the distance is too small, the emission of the upconversion nanocrystal will be quenched due to fast energy transfer to the gold nanorod. If the distance is too large, the coupling will be weak. Typical distances for which an enhancement can be expected are between 10 and 30 nm [116].

4.4.1 Gold nanorods synthesis

Gold nanorods were synthesized via the seed-mediated growth method. The method relies on reduction of a gold precursor in solution. After reduction of gold ions to atoms, nucleation of seeds starts, forming the seed solution. The seed solution is added to a growth solution in which the gold is not fully reduced and the gold ions form a gold reservoir for further growth of the seeds. Surfactants in the solution are used to control the growth and shape of the nanoparticles and to prevent agglomeration of the seed clusters. The shape control arises from the absorption of surfactants at specific crystal facets. The particle is forced to grow in certain directions and different shapes are obtained depending on the type of and concentration of surfactants and reducing agent. The synthesis method used to grow gold nanorods is described in Ref. [105]. It used the following compounds: hexadecylmethysammonium bromide (CTAB), benzyldimethylammoniumchloride (BDAC), $HAuCl_4$, $AgNO_3$, Ascorbic Acid (AA), $NaBH_4$ and distilled water (18.2MΩ). CTAB and BDAC are used as surfactants. Ascorbic acid and $NaBH_4$ serve as reducing agents. The shape at the end of gold nanorod is influenced by the curvature of the absorbed surfactant molecules and BDAC gives a smaller curvature than CTAB. As a result, a higher aspect ratio (length/diameter) is achieved by using BDAC [105]. The length of the rods depends critically on the BDAC/CTAB concentrations and the silver concentration. Silver attaches on the long side of the rods and prevents growth in this direction. By varying the silver concentration and the BDAC/CTAB concentrations the aspect ratio and length can be tuned [105]. The aspect ratio determines the frequency of the plasmon peak, which should be around 1 µm for enhancing Yb^{3+} absorption. An aspect ratio of 7-8 is required [105].

To prepare the seed solution 5 ml of 0.2 M CTAB was mixed with 5 ml of 5 mM $HAuCl_4$. While stirring the solution, 0.6 ml of 10 mM $NaBH_4$, dissolved in ice cold water, was added to the solution. The solution was stirred for two more minutes and kept at 25 ^oC. To lower the pH, 2.5 ml 0.1 M HCl solution was added to the seed solution. The growth solution contained 125 ml of 0.2 M CTAB mixed with 100 ml of 0.125 M BDAC. To this solution 3 ml of a 10 mM $AgNO_3$ and 12.5 ml of 10 mM $HAuCl_4$ was added. The most crucial steps involve the addition of the AA and the seed solution. 1.5 ml of the 0.1 M AA solution was added, followed immediately by 0.25 ml of the seed solution. The mixture was stirred for 24 hours at 25 ^oC, after which 62 µl of 10 mM AA was added to 114.6 ml of the solution.

To coat the gold nanorods with silica the standard method using tetraethylorthosilicate (TEOS) and NaOH was applied [117]. Silica layers of 10, 20 and 30 nm were grown. Fig. 4.11 shows a TEM image of gold nanorods with a 10 nm silica coating. Absorption spectra were recorded to verify that the position of the plasmon resonance is around 1 µm. The absorption spectra of the gold nanorods coated with 10 nm, 20 nm and 30 nm silica coatings are shown in Fig. 4.12. The plasmon resonance around 1000 nm is clearly observed. Note that a second plasmon resonance is also present, around 540 nm. Coupling with this plasmon

peak may enhance the transition rate for the green emission making these gold nanorods suitable for enhancing the upconversion emission through both increased absorption in the NIR and enhanced upconversion emission in the visible.

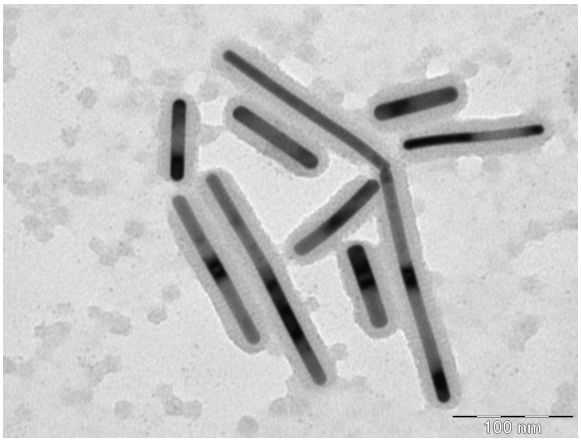

Figure 4.11: TEM picture of the gold nanorods with silica coating.

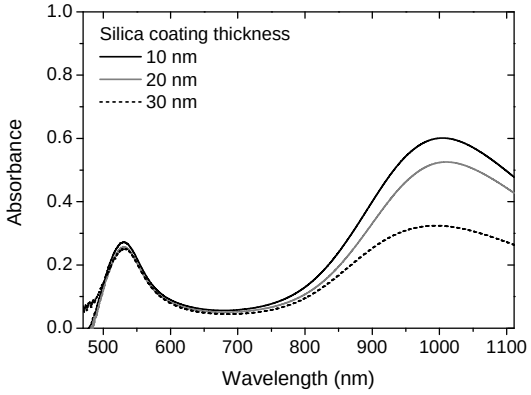

Figure 4.12: Absorption spectra of gold nanorods with silica coating. The plasmon peak around 530 nm is independent of the shape of the nanoparticle and is the surface plasmon peak of gold. The plasmon peak around 1 µm is the longitudinal plasmon peak that depends on the aspect ratio. With a higher aspect ratio, this peak shifts to the red. The reduction in the longitudinal plasmon peak is due to the silica coating.

4.4.2 $NaYF_4$:Er^{3+}, Yb^{3+} NCs and gold nanorod aggregates

To investigate the influence of the plasmon coupling on the luminescence properties of the $NaYF_4$:Er^{3+}, Yb^{3+} UC NCs, aggregates were made of the UC NCs and the silica coated gold nanorods. A complicating factor is the large difference in concentration. The nanorods synthesis yields very low concentrations, typically 10^7 lower than the $NaYF_4$ NC concentration. To bring a substantial fraction of the $NaYF_4$ NCs in contact with the silica coated gold nanorods, a 4 µl volume of $NaYF_4$ NCs was combined with 5 ml of gold nanorod solution. For this volume ratio, the ratio of gold nanorods to UC NCs was ~ 1:250. Since a large number upconversion NCs can absorb on single silica coated nanorods, most upconversion NCs can be in close proximity to the gold nanorod. To combine the UC NCs with the silica coated gold nanorods, the UC NCs were first transferred to ethanol. This was required since the UC NCs were dissolved in octadecanol and the silica coated gold nanorods in water and water and octadecanol do not mix. Transfer to ethanol was realized by first drying the UC NC solution and redissolving the UC NCs in ethanol. The combined solution of silica coated gold nanorods and UC NCs was thoroughly mixed in an ultrasonic bath and next the solution was dried. Experiments were done only for the gold nanorods coated with 30 nm silica. To make a valid comparison possible, control experiments were conducted on dried samples without gold nanorods.

4.4.3 Luminescence

In Chapter 3 the luminescence and upconversion in β-$NaYF_4$:Er^{3+}, Yb^{3+} has been described in detail. To study the influence of coupling with plasmon resonances in nearby gold nanorods, emission spectra were recorded for the dried $NaYF_4$:Er^{3+}, Yb^{3+} nanocrystal as reference and for the aggregates with the gold nanorods described above. In Fig. 4.13 the emission spectrum is shown for the upconverted emission of the $NaYF_4$:Er^{3+}, Yb^{3+} nanocrystals. The emission spectrum is similar to that for microcrystalline β-$NaYF_4$:Er^{3+}, Yb^{3+} but the efficiency is two orders of magnitude lower. This observation is consistent with earlier work by Van Veggel et al. who demonstrated that upconversion efficiencies are a strong function of particle size and that nanocrystalline materials show very low upconversion efficiencies [118]. For the aggregate sample of $NaYF_4$ NCs and gold nanorods with a 30 nm layer of silica, no upconversion emission could be detected. The low efficiency can be due to competing absorption by the gold nanorods in the dense aggregate. The aggregate of $NaYF_4$:Er^{3+}, Yb^{3+} and silica coated gold nanorods does show infrared luminescence upon excitation in the $^2F_{7/2}$ level of Yb^{3+} at 975 nm. The infrared emission spectrum is shown in Fig. 4.14, together with the emission spectrum for the $NaYF_4$:Er^{3+}, Yb^{3+} NC reference sample. The emission spectra show transitions from the $^4I_{11/2}$ and the $^4I_{13/2}$ level to the $^4I_{15/2}$ ground state of Er^{3+}. The spectra are similar for the two systems.

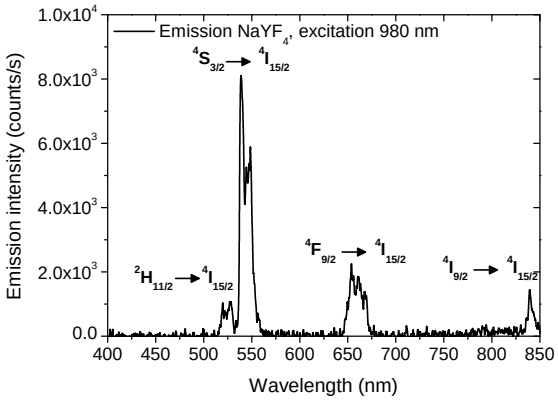

Figure 4.13: Upconverted emission spectra of the $NaYF_4$ nanoparticles after excitation at 980 nm.

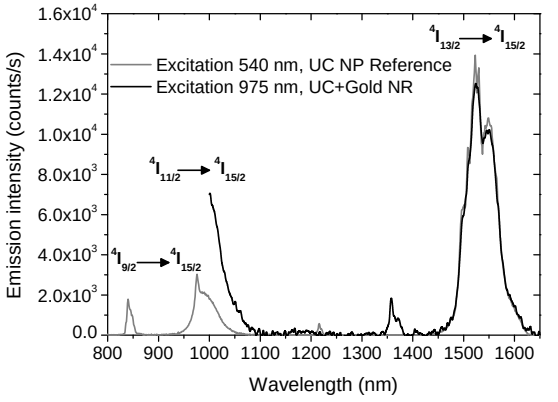

Figure 4.14: Near infrared emission spectra of the nano upconverters with and without gold nanorods.

4.4.4 Lifetime

To investigate the influence of plasmonic coupling, luminescence decay curves were recorded for the infrared emission under pulsed excitation with the OPO system at 975 nm. The decay curves for the 1010 nm and the 1540 nm emission are shown in Figs. 4.15 and 4.16. Fitting the curves to a single exponential decay function leads to a decay time of 0.36 ms for the 1010 nm emission in the system without gold nanorods and a 0.16 ms decay time for the mixed aggregate with gold nanorods. The pronounced shortening of the life can be explained by plasmon coupling. For the 1540 nm emission also a shortening of the life time is observed (from 3.8 ms to 3.1 ms) but due to the weak signal around 1540 nm, the luminescence decay curves do not yield very accurate luminescence life times. The small decrease in life time is not unexpected since the plasmon resonance extends to longer wavelengths (see fig. 4.12) and will still have an influence around 1540 nm.

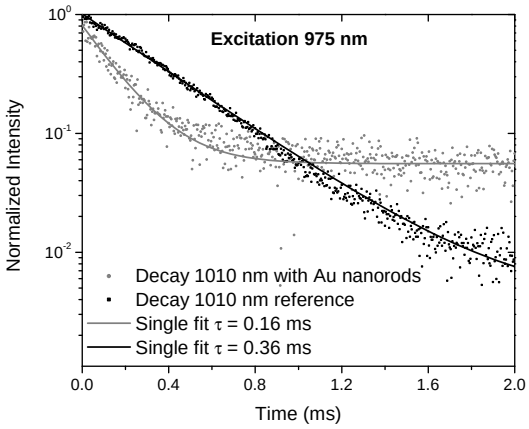

Figure 4.15: Luminescence decay curves for the 1010 nm emission in $NaYF_4$:Er^{3+}, Yb^{3+} nanocrystals (black line) and $NaYF_4$:Er^{3+}, Yb^{3+} nanocrystals in a mixed system with $NaYF_4$:Er^{3+}, Yb^{3+} NCs with gold nanorods in 30 nm silica (gray line).

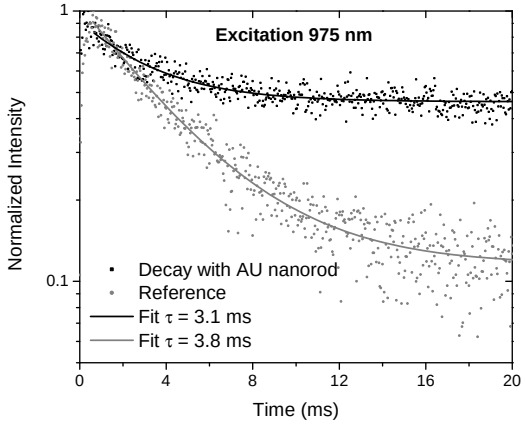

Figure 4.16: Luminescence decay curves for the 1540 nm emission in $NaYF_4$:Er^{3+}, Yb^{3+} nanocrystals (black line) and $NaYF_4$:Er^{3+}, Yb^{3+} nanocrystals in a mixed system with $NaYF_4$:Er^{3+}, Yb^{3+} NCs with gold nanorods in silica (gray line).

4.5 Discussion and conclusion

In this chapter two upconversion systems have been investigated, aimed at enhancement of the upconversion efficiency at low excitation powers through increasing the absorption strength around 1000 nm. The first system investigated was Gd_2O_2S doped with Yb^{3+} and Er^{3+}. The higher degree of covalency and lower energy position of opposite parity states in comparison to $NaYF_4$:Er^{3+}, Yb^{3+} results in stronger absorption strengths for 4f-4f transitions. Strong upconversion emission was observed for Gd_2O_2S :Er^{3+}, Yb^{3+} with efficiencies similar to those for $NaYF_4$:Er^{3+}, Yb^{3+}. Saturation is observed at much lower powers (~1W/cm^2) for Gd_2O_2S :Er^{3+}, Yb^{3+} in comparison with $NaYF_4$:Er^{3+}, Yb^{3+} (20 W/cm^2). This observation is consistent with a higher absorption strength for the f-f transitions and makes this material promising for solar cell applications. The second system investigated relies on coupling between 4f-4f transitions and plasmon excitations in gold nanorods. By combining upconversion nanocrystals with silica coated nanorods, an enhanced absorption can be expected around the plasmon resonance frequency. Gold nanorods with a plasmon resonance around 1000 nm were successfully prepared and coated with 10-30 nm silica. In the mixed upconversion nanoparticle – gold nanorod system, no upconversion emission could be observed. The luminescence life time of the 1000 nm emission was however strongly reduced which can be explained by plasmon coupling.

Chapter 5

Thin film a-Si:H Solar Cells

Abstract

To apply an upconverter onto a-Si:H solar cells, the solar cells have to be bifacial. Bifacial solar cells can be made by applying a TCO layer as back contact instead of a metal. Aluminum doped ZnO TCOs with high transparency in the red and near infrared part, besides high conductivity can be made with proper process optimization. Requirements for a good TCO are: electrical resistance less than 10 $\Omega_{\square}$ *and optical transparency higher than 85%. Different layers are characterized and a 1.5* μ*m ZnO:Al layer from a* $ZnO : Al_2O_3$ *0.5% target fullfilled these requirements. Solar cells made with this ZnO:Al as back contact had a slightly higher series resistance, 5 vs 7* $\Omega_{\square}$*, but other electrical parameters were in the same range as the solar cells with silver back contact. To increase the transparency further, flat solar cells were made. The* V_{oc} *increased 30 to 40 mV for i-layer thickness of 230 and 500 nm respectively, because of decreased surface recombination. The current however was 3 to 2* mA/cm^2 *lower. The transparency increased from 40% to 84% for 980 nm light. This is attributed to lower absorption for near infrared light due to smaller number of defect states in the band gap. For 980 nm light, the EQE of flat solar cells was also less than that for solar cells on textured superstrate, with an EQE measured of 0.002 ± 0.0001% for flat solar cells and of 0.009 ± 0.001% for textured solar cells with an i-layer thickness of 500 nm.*

5.1 Introduction

Hydrogenated amorphous silicon (a-Si:H) has an optical band gap around 1.8 eV. It has the characteristic of a direct band gap semiconductor and thus has a stronger absorption than crystalline silicon. Amorphous silicon (a-Si) can be made by chemical vapor deposition (CVD) and due to its higher absorption strength, less material is needed. This makes a-Si:H a cheap material, which is an important factor for solar cells. Because the structure is amorphous, a-Si has as well as structural as electronic defects: dangling bonds, voids, micro structures and internal surfaces. By incorporating hydrogen in the a-Si structure (a-Si:H), dangling bonds can be passivated and the mid gap states are reduced [119]. Solar cells made of a-Si:H have a typical layer thickness between 200 and 500 nm and a stabilized efficiency of approximately 10% [120]. Thicker layers will lead to stronger light induced degradation (Staebler Wronski effect [121]) and thus there is a trade off between absorption and degradation. Great improvements have been achieved by increasing the light absorption; with scattering, light capture techniques and the use of a back reflector. Nevertheless, even if great improvement are achieved the Shockley Queisser limit of conversion efficiency is still 28% considering the band gap of a-Si:H of 1.8 eV. Other significant improvements can be achieved if the solar spectrum can be used more efficiently and certainly for the infrared part, of which almost 50% is lost in a-Si:H. This can be done by so called upconversion, whereby a luminescent active layer at the back of the solar cell absorbs the transmitted part of the solar spectrum and re-emits higher energy light back. To have a solar cell with active luminescent layers at the back some adaptations have to be made for amorphous silicon solar cells. These adaptations are at the front side of the solar cell by increasing the transparency for infrared light and at the back by applying highly transparent back contacts. This means that the 100 nm ZnO/Ag back contact/reflector [122, 123] has to be replaced by a transparent back contact. At the front; the textured TCO is replaced by a flat TCO layer to increase the transmittance of sub band gap light. Further, the thickness of the intrinsic a-Si:H layer is varied for optimizing the transmittance. A diffuse back reflector will scatter the (upconverted) light back into the solar cell, causing the necessary increase of pathlength for a good absorption, see figure 5.1.

5.2 Experimental

The ZnO:Al layers were deposited on corning glass by RF magnetron sputtering. Electrical and optical properties were determined with a 4-point probe, Hall measurements and R-T mini reflection/transmission spectroscopy (chapter 2). Thickness of the TCO layers was calculated from the reflection and transmission data. Standard p-i-n a-Si:H solar cells were made by RF Plasma Enhanced Chemical Vapor Deposition (PECVD) at 13.56 MHz with an area of 0.16 cm^2. Superstrates were either Asahi U type SnO_2 : F coated glass or ZnO:Al layer deposited on Corn-

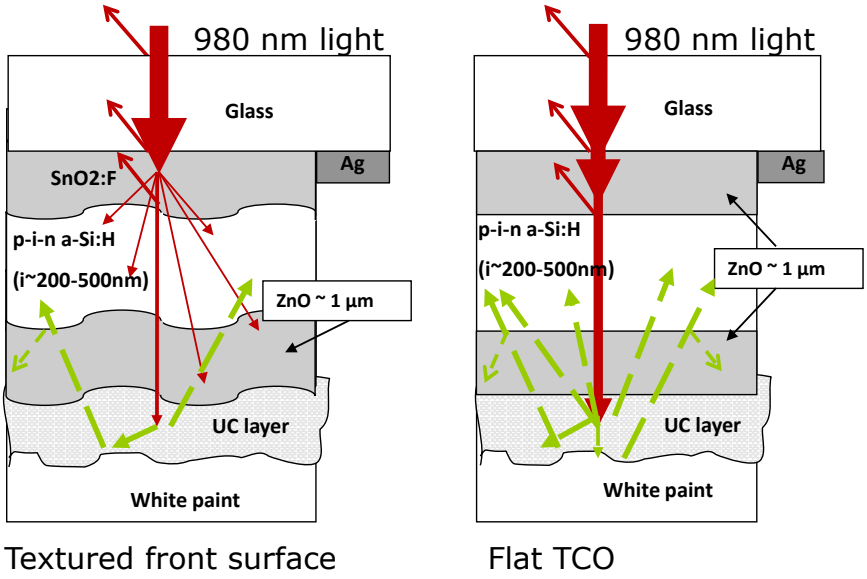

Figure 5.1: Design of solar cells used for upconversion. The back contact consists of a TCO layer after which the upconversion layer and a diffuse back reflector is places.

ing glass. The solar cells were characterized by spectral response, FTPS and I-V characteristics, and optical properties are obtained from transmission and reflection measurement with R-T mini set-up and diffuse reflectance with the integrating sphere. As back reflector either white foil or white paint was applied. White foil was melted on the ZnO:Al back contact at 80 degrees. As reference also silver was applied at the back of the cell by thermal evaporation.

5.3 Results and discussion

5.3.1 TCO

To have a new type solar cell with upconverter layer at the back the 100 nm ZnO/Ag back [122, 123] contact had to be replaced by a thicker layer TCO that serves as new back contact. This TCO layer has to be highly transparent for NIR photons and highly conductive to minimize resistance losses. A TCO that is widely used in thin film silicon solar cells and also commercially available that fulfills most of the requirements for a standard thin film silicon solar cell is fluorine-doped tin oxide ($SnO_2 : F$), developed by Asahi Glass company [76]. TCOs are commonly used as front electrode but most the requirements apply for the back

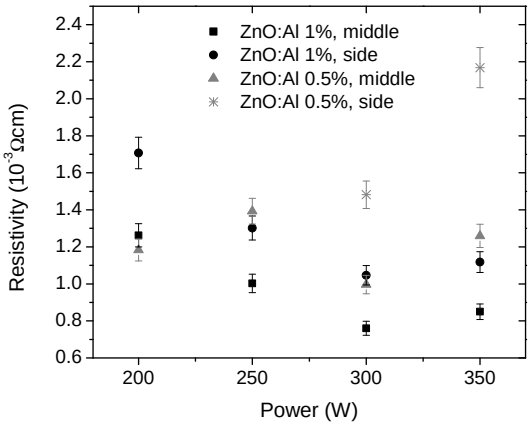

Figure 5.2: Applied RF power dependency of the electrical resistivity of the ZnO:Al layers for 1% and 0.5% ZnO : Al_2O_3 targets.

contact too. One of the differences is that the band gap for the back contact TCO doesn't have to be so high, because all blue light is absorbed at the front of the solar cell. For our upconverter solar cells, in addition, the TCO has to be highly transparent for near infrared light, which is not a requirement for front TCO, because the a-Si:H solar cell itself absorbs only to ~ 800 nm. A good TCO that fulfills these requirements is ZnO:Al. ZnO has a band gap around 3.3 eV increasing with the alumina concentration [124] and is transparent in the near infrared with a proper doping concentration [123, 125]. Different ZnO:Al_2O_3 targets with alumina concentrations of 0.5%, 1% and 2% were used for sputter depositing the TCOs. The films were characterized by optical transmission and reflection measurements, four point probe sheet resistance and Hall effect measurements.

Resistivity and power

With an aim to develop a suitable infrared transparent material, sputter depositions with the new ZnO 0.5 % Al_2O_3 target, had to be optimized and characterized before they were applied as back contact on solar cells and compared with the high dopant concentration (1% and 2%) ZnO:Al TCOs. Requirements are a sheet resistance of less than 10 $\Omega_\square$ and a transparency higher than 85% [83]. First an applied power series for sputter deposition was made, to obtain the lowest resistivity. Films were prepared by magnetron sputtering, the pressure was kept at 1 micro bar, time 6800 s, electrode-substrate distance 125 mm and the RF power was varied between 200 and 350 W. The lowest resistance was measured at 300 W for both targets, see figure 5.2. The deposition rate was almost the same for the

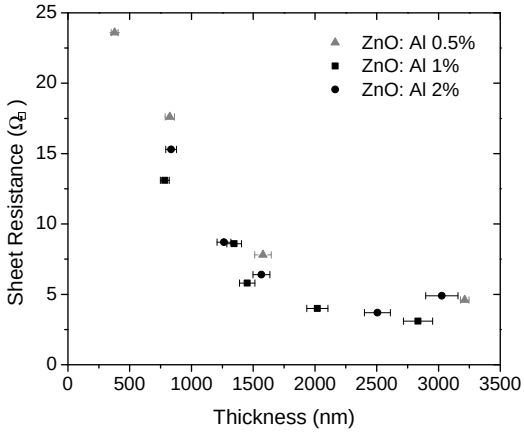

Figure 5.3: The sheet resistance as measured with the 4-point probe for the different $ZnO : Al_2O_3$ targets.

Table 5.1: Electrical and optical parameters for the layer made from ZnO targets with different alumina concentrations.

ZnO:Al	Mobility (μ_e, $cm^2(Vs)^{-1}$)	Absorption coefficient at 980 nm (cm^{-1})
0.5%	28 ± 2	13 ±1
1%	21 ± 1	126 ± 14
2%	16 ± 2	625 ± 40

different targets, 0.37 nm/s for the 0.5% Al_2O_3 target at 300 W and 0.38 nm/s for 1% Al_2O_3 target at 350 W, the standard RF power for ZnO:Al 1% sputter depositions on glass. The deposition time was varied for different layers, with a constant power, 350 W for 1% and 2% targets and 300 W for 0.5% target to determine the optimal sheet resistance. Figure 5.3 shows the sheet resistance of the layers. For the ZnO:Al 0.5% target, the layers thicker than ~1.5 µm have a sheet resistance smaller than 10 $\Omega_\square$.

Transmittance

Equally important for the TCO back contact are the transmittance and absorbance of the layers. Figure 5.4 shows the transmission curves for the layers with a thickness of approximately 3 µm on glass and a sheet resistance of less than 5 $\Omega_\square$. For the transparency, especially in the infrared, the lower aluminum concentration is very suitable for our solar cells. Significant increase of transparency with decreasing aluminum concentration is found. From the slopes of the curves of figure

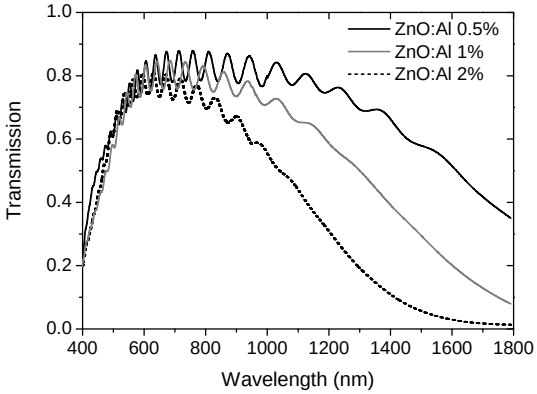

Figure 5.4: Transmittance of different ZnO:Al layers on Corning glass. The band edge of the ZnO:Al is at 400 nm, in the red part there is free carrier absorption. Lower aluminum concentration leads to less absorption, due to lower free carrier concentration.

5.5 the absorption coefficient at 980 nm for the ZnO:Al layers sputter deposited from different targets was calculated and table 5.1 showed the absorption coefficients. For the 2% target the absorption coefficient was previously determined to be $308 \pm 12\,\mathrm{cm}^{-1}$ at 800 nm [126]. Hall measurements give information on the transmittance (free carrier absorption) and conductivity properties. Ideally a good TCO has a high carrier mobility and low free carrier concentration. Table 5.1 gives the mobility for samples of approximately 3 µm made from different targets, these materials have a resistance of smaller than 5 $\Omega_{\square}$. To reach the same resistance, the carrier concentration has to be higher for lower mobility, which results in more absorption, which is in agreement with the absorbance measurement.

5.3.2 Solar Cells

Solar cells were made on Asahi TCO or ZnO:Al superstrates according to the schemes in figure 5.1. The silicon layers were deposited by PECVD, with a deposition rate of 10 nm/min. The standard back contact/reflector for p-i-n solar cells is 100 nm ZnO:Al 2%/Ag. This back contact was replaced by a 1.5 µm thick ZnO:Al 0.5% layer contact. On the back this TCO back contact a non-conducting diffuse back reflector can be applied. A diffuse reflector should increase the current more than a metallic reflector, because the light is scattered back into the solar cells [127]. For the new configuration different back reflectors will be applied.

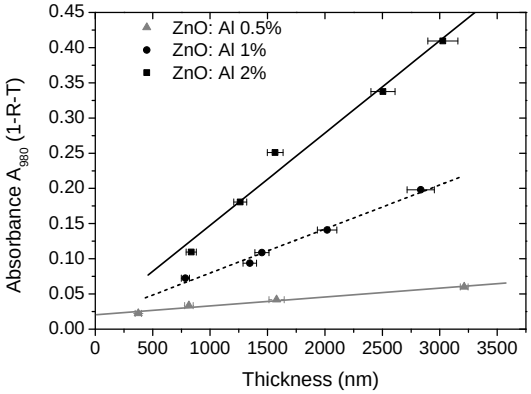

Figure 5.5: Absorbance at 980 nm of flat ZnO:Al layers. From the slope the absorption coefficient is determined.

TCO back contact

At first the solar cells were made on Asahi U-type TCO glass. A standard recipe for ZnO:Al 1% (3400 s at 350 W) and a new optimized recipe for ZnO:Al 0.5% were used for the respective TCO layers. Solar cells with i-layers of 500 and 350 nm were made on Asahi glass with 1% and 0.5% ZnO:Al back contact. As back reflector commercial white paint was used. The back contact with white paint back reflector replaces the optimized 100 nm ZnO:Al 2%/Ag back contact/reflector (reference solar cells). The current was determined from spectral response curves, all other parameters from light and dark I-V measurements with solar simulator. Only from solar cells with and ideality factor smaller than 1.5 the electrical values were averaged, see table 5.2. The parameters were averaged over 20 cells, except for the short circuit current, which were obtained from spectral response measurements, averaged over 2 or 3 cells. The series resistance is slightly higher and therefore the deposition time for the 0.5%, which was 3600 seconds, was increased to 4000 seconds to decrease further the series resistance. The current is the same, though the i-layer is much thicker for the cells with TCO/paint back contact. From figure 5.4 it can be seen that the ZnO:Al layer does absorb at least around 10 % of the light for one way and thus current losses are expected [128]. We may add that as front electrode, the higher transmittance of textured ZnO:Al in the near infrared is beneficial compared to the Asahi superstrate, which will result in a higher current [129, 130].

To investigate the absorption in the ZnO:Al layer, new series were made with different i-layer thickness and the two different back contacts. Variation of the i-layer thickness shows significant different trends in current densities between the silver and the TCO back contact, see figure 5.6. In the silver configuration, the

current density decreases with increasing i-layer thickness. This is explained by bad collection in the blue part. However, the current is increasing with increasing i-layer thickness when a TCO back contact is applied, which is shown mostly in the red part. To absorb red light, thicker i-layers are necessary. When layers are too thick the carrier collection will decrease again, because the electron hole pairs recombine before they are collected at the contacts. It has to be mentioned, that the silver solar cells had a relatively high ideality factor of around 1.5.

Back reflector

By applying a back reflector the current in a solar cell increases. Two different back reflectors were applied in this study, a specular silver and a diffuse white reflector. It is expected that a diffuse back reflector will increase the current more than a specular back reflector [127]. Diffusely scattered light will be better absorbed in the solar cell due to increased path length. Moreover, there is no plasmonic absorption loss, the type of which has been reported for Ag reflector. As a diffuse back reflector all kinds of white paint can be used [131]. Here we have used commercial white paint and white foil [132]. The reflection is more than 98% up to 1100 nm and the current increase is 11% compared to no back reflector. The silver back reflector delivers an increase of current of 7% compared to no back reflector, see the spectral response in figure 5.7. Here the silver layer was added on the thick TCO layer by evaporation. The diffused scattering back reflector increases current more than the silver back reflector, mainly because metallic back reflector has a lower reflectivity for higher wavelengths and reflects specular, in addition to the plasmonic loss. White foil reflected slightly better than the white paint, though no difference on their effect on current was measured in solar cell configuration. The only difference noticed is the series resistance, it increased with white paint, which dissolved the ZnO:Al back contact by time. With white foil only an increase in current was measured. The foil was melted on the ZnO:Al back reflector at 80 degrees.

Flat superstrate and i-layer thickness variation

As shown in figure 5.1 two different types of solar cells were made, either on structured (Asahi glass) or on flat ZnO:Al 0.5% on Corning glass superstrates. The solar cells on Asahi glass appeared to be transmitting only 40% of the sub band gap light. With flat solar cells, light will not be scattered, defect density will be smaller hence transmission of sub band gap light will be increased. Besides that, by adapting the i-layer thickness constructive interference at 980 nm will increase the transmission even more. From simulation of reflection/transmission data it was determined that maximum interference is at 270 and 550 nm thickness. The layer is therefore adapted to 230 nm and 500 nm thickness, so that with the p and n layers the total silicon layer is around 270 and 550 nm. Though, large decrease in J_{sc} was measured compared to textured surface the V_{oc} was increased,

Table 5.2: Electrical parameters of solar cells on Asahi U-type Front TCO and ZnO:Al with TCO back contact.

Back Contact	100 nm ZnO:Al 2%/Ag	1.5 μm ZnO:Al 0.5%/paint	1.5 μm ZnO:Al 1%/paint
V_{oc} (V)	0.815±0.003	0.817±0.003	0.821±0.003
J_{sc} (mA/cm^2)	14.3±0.1	14.42±0.02	14.2±0.4
R_s (Ω_)	5.1±0.3	7.6±0.9	7.2±0.5
R_p (kΩ)	1.7±0.4	1.6±0.2	1.2±0.1
FF	0.70±0.01	0.67±0.01	0.66±0.01
n	1.39±0.02	1.46±0.02	1.47±0.01

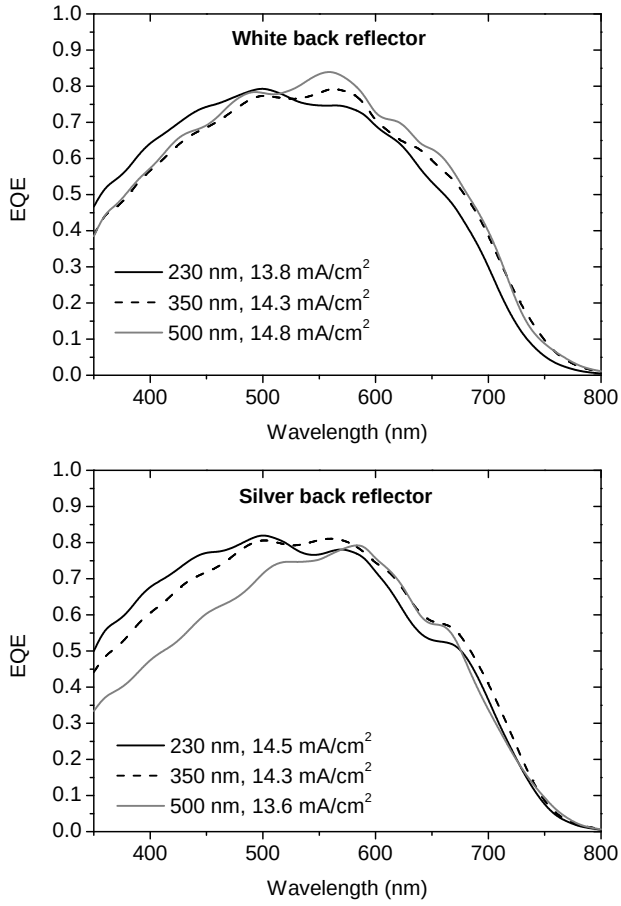

Figure 5.6: Solar cells with TCO/white back reflector contact and silver back contact (ref) on Asahi U type superstrate. The curves are averaged over 3 or 4 solar cells. For the TCO solar cells, an increase in current is measured due to more absorption of the longer wavelength for thicker i-layers (upper graph). In contrast, the current is decreasing when a silver back reflector is applied, mainly due to decreasing carrier collection of short wavelengths (lower graph).

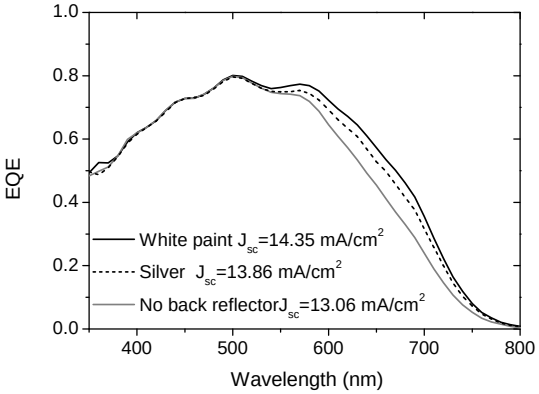

Figure 5.7: Spectral response of one solar cells with different back reflector in dark.

Table 5.3: Electrical parameters of flat and textured solar cells.

Solar Cell	V_{oc}(V)	J_{sc}(mA/cm^2)	FF
Textured 500 nm	0.83	13.8	0.69
Textured 230 nm	0.84	11.7	0.65
Flat 500 nm	0.86	10.8	0.67
Flat 230 nm	0.88	9.3	0.67

see table 5.3 and a transmission of more than 85% at 980 nm was measured for the flat solar cells.

Sub band gap response

To investigate the sub band gap response of the solar cells, spectral response measurements were performed by Fourier Transform Photocurrent Spectroscopy (FTPS) [86] and intensity dependent diode laser excitation. The FTPS set up has a NIR/VIS source with a low intensity light beam. The sample is excited with a broadband light and the detected signal is converted from time domain to frequency domain by a Fast Fourier Transform technique. Figure 5.8 shows the response of 2 solar cells on different superstrates. One on flat TCO and another on Asahi U type TCO. Two regimes can be distinguished. For wavelengths shorter than 900 nm the valence band tails determine the absorption and for wavelengths higher than 900 nm the absorption is due to dangling bonds [133]. From the slope between 1.5 and 1.8 eV the valence band tail edge can be determined. Under exposure of the cell to light the dangling bonds will increase, the so called Staebler Wronski effect [121], thus increasing the response above 900 nm. The solar cells were also excited with a diode laser, with an excitation wavelength of 981 nm.

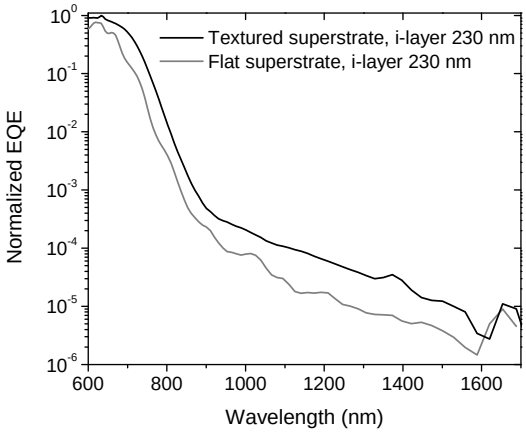

Figure 5.8: Sub bandgap response of different solar cells on different superstrates

The EQE for the laser excitation was calculated as:

$$\mathrm{EQE} = \frac{\mathrm{I_{SC}}}{\mathrm{P_{in}}/(1248/\lambda)} \tag{5.1}$$

with $\mathrm{I_{sc}}$ the current measured in mA, $\mathrm{P_{in}}$ the laser power in mW and $1248/\lambda$ the photon energy of the laser light in eV. The response at 981 nm varied between 0.002% and 0.01% depending on the texture type of superstrate and the thickness of the i-layer, see figure 5.9. The variation was larger for solar cells on Asahi glass. Intensity dependent measurements do not show a significant change in EQE (figure 5.9), implying that the response requires only 1 photon and comes from the midgap defect states. While dangling bonds normally act as recombination centers, the reverse process (i.e., generation) is dominant with sub band gap light, what is known from constant photocurrent method (CPM) studies of sub band gap absorption, that an electron from partially filled midgap states gets excited to the conduction band after absorption of a photon. However excitation from an intermediate state to the conduction band requires also excitation from the valence band to the intermediate state, which may require 2 photons. This was not measured, the states might independently be excited by thermal excitation, resulting in an intensity independent sub band gap response.

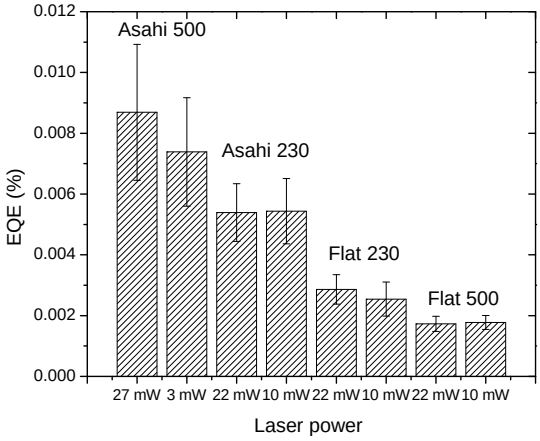

Figure 5.9: EQE at 981 nm at different intensities of laser excitation.

5.4 Conclusion

New type a-Si:H solar cells were made to use them with an upconverter. First the optimal TCO properties have to be determined before applying it on a standard p-i-n solar cell. ZnO:Al sputter deposited from a $ZnO : Al_2O_3$ 0.5% target has shown good electrical and optical properties, which means a high transparency in the NIR, because it is applied at the back of a solar cell and a sheet resistance smaller than 10 $\Omega_\square$. Solar cells were made with these optimum properties and the parameters of these solar cells are compared with that of reference standard solar cells with silver back contact. There is a small difference between the solar cells made on textured superstrates with silver back contact, mainly because of the higher series resistance of the ZnO layer. The solar cells were transparent of only 45% in NIR, mainly because of the high defect density of a-Si:H. Next to textured solar cells also flat solar cells were made, mainly to increase the transparency in the near infrared. These solar cells lack the trapping properties of textured superstrates and thus low current densities were measured. The V_{oc} was slightly higher due to lower density of defects. Moreover, the sub band gap response was much lower and the transparency was increased up to 84%. While the current generation for flat solar cells is much lower than standard reference cells on textured superstrates, when an upconverter is applied the current generation should be higher and more noticeable. The solar cells described in this chapter will be used for further experiments with upconverter material attached at the back.

Chapter 6

Solar Cells with Upconverter

Abstract

To increase the response in the near infrared two different upconverters are applied onto a-Si:H solar cells. The upconverters are $NaYF_4$ *and* Gd_2O_2S*. The a-Si:H solar cells were made on either flat superstrate or textured superstrate configuration. Under laser light excitation a clear increase of current was measured. The current was almost quadratically increasing when the* $NaYF_4$ *upconverter was applied, while for the* Gd_2O_2S *upconverter, current was increasing linearly. A maximum quantum efficiency was measured at a power density of* $0.6\,W/cm^2$ *for this upconverter, resulting in an EQE of 0.1%. With* $NaYF_4$ *the maximum EQE measured was 0.03% under an excitation density of* $3\,W/cm^2$*, which is far from saturation. This implies that a higher response can be achieved for higher power densities. Next to upconversion response due to laser excitation also upconverter response under broad band light excitation was measured. As upconverter* Gd_2O_2S *was used, because of the relatively high efficiency under low excitation densities. For a concentration of 25 Suns a current of* $0.2\,mA/cm^2$ *was measured, due to upconversion of near infrared light.*

6.1 Introduction

Highly efficient solar cells require the absorption of photons over the broadest possible range of the solar spectrum followed by an effective generation and collection of charge carriers. Thin film a-Si:H cells have a high absorption in the visible range, but the wide band gap of amorphous silicon (E_g ~1.8 eV) implies that the material is almost transparent for near-infrared (NIR) radiation, constituting a significant efficiency loss known as transmission losses. Upconversion (UC) may enhance the response of solar cells in the infrared region [19, 20, 134]. UC is a luminescence process whereby two or more low energy photons are converted to one higher energy photon. When a layer containing an UC phosphor is attached at the rear of a solar cell, sub-band gap photons that are transmitted by the solar cell can be absorbed by the UC layer and converted into higher energy photons. These photons are emitted isotropically and with the help of a reflector behind the upconverter layer, all emitted photons are directed to the cell, where they can be absorbed in the active layer.

Recently the use of UC was demonstrated to enhance the efficiency for crystalline Si (c-Si) solar cells [63, 135]. The band gap of c-Si is relatively narrow (1.1 eV) and the part of the solar spectrum that cannot be absorbed is limited (wavelengths larger than 1100 nm). Nevertheless, upconversion of photons in this spectral range and subsequent carrier generation in the solar cell will enhance the solar cell efficiency. Upconversion of ~1500 nm photons to 980 nm in the UC material $NaYF_4 : Er^{3+}$ on the back of c-Si solar cells was reported with an external quantum efficiency (EQE) of 2.5% for excitation with a focused 5.1 mW laser at 1523 nm [135].

In this chapter upconversion is applied for wider band gap solar cells, specifically a-Si:H solar cells. The transmission losses are much higher in these solar cells compared to c-Si cells and the potential gain from UC is therefore higher. Two different upconverter materials were used. $NaYF_4 : 2\% Er^{3+}, 18\% Yb^{3+}$ and $Gd_2O_2S : Er^{3+}, Yb^{3+}$ a phosphor purchased from Phosphor Technology Ltd., which turns out to be very efficient at low intensities. The upconversion phosphors with Er^{3+} and Yb^{3+} are very suitable for upconversion for wide band gap solar cells (E_g up to ~2 eV) as it is to date among the most efficient upconversion couple for converting NIR radiation around 980 nm to green (525, 550 nm) and red (650 nm) emission. The collection efficiency of a-Si:H cells is high for these wavelengths, making these phosphors suitable candidates for upconversion in this type of solar cells.

Response due to upconversion is measured under laser light and concentrated light from the solar simulator. Because a-Si:H has a large defect density causing absorption and response due to sub band gap light, corrections for this response were made. Comparison of the power density of monochromatic laser light with the solar spectrum are made and losses that influence the performance of the upconverter solar cell device are analyzed.

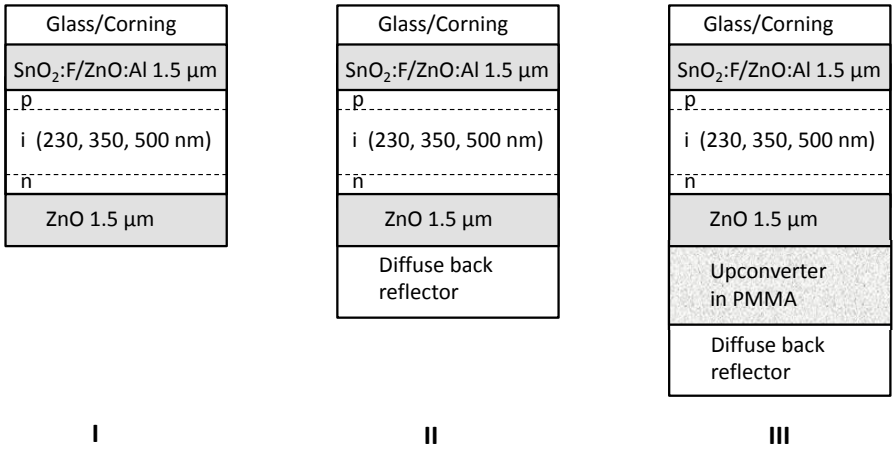

Figure 6.1: The different solar cell structures used for the experiments: I) solar cell without back reflector, II) solar cell with back reflector, mostly used as reference solar cell and III) the upconverter solar cell with back reflector.

6.2 Experimental

Standard p-i-n amorphous silicon solar cells were made by 13.56 MHz Plasma Enhanced Chemical Vapor Deposition (PECVD) with an area of 0.16 cm^2 on Asahi or ZnO/corning glass superstrates. As back contact 1.5 µm sputtered aluminum doped zinc oxide from a $ZnO : Al_2O_3$ 0.5% target was used. Upconverter powders were dropcasted on the back contact and a small area was kept free to make electrical contact. The upconverter powders were dissolved in chloroform with PMMA, (Poly(methyl methacrylate)) a transparent plastic with refractive index of ~1.53, with a volume ratio chloroform:PMMA of 10:1. An upconverter layer thicknesses of 200-300 µm was obtained. As back reflector white paint or white foil was applied. The structures of the used solar cells are depicted in figure 6.1. The infrared response was measured with FTPS set up and intensity dependent measurement were performed with diode laser excitation (981 nm) and concentrated light from the solar simulator. Current-voltage characteristics were measured with the solar simulator set up, of which the light source was either the diode laser or simulated solar light. For broad band light excitation, the light from the solar simulator was filtered with a 900 nm long pass filter. Additional to this, spectral response and reflection and transmission measurements were performed.

6.3 Results and discussion

6.3.1 Solar cells with $NaYF_4$ upconverter

Three sets of solar cells were made, without back reflector, with back reflector and with upconverter and back reflector and an i-layer thickness of 500 nm on Asahi superstrate, see figure 6.1. Front side illumination yields a power conversion efficiency of 8% and back side illumination (through the n-layer) an efficiency of 5% of the cell without back reflector (solar cell I). The white paint back reflector was applied on the PMMA-UC layer and increased the current by 10%. The upconverter material used was β-$NaYF_4$: 2% Er^{3+}, 18% Yb^{3+}, which has the highest efficiency recorded for NIR to VIS upconversion [136].

FTPS

With the FTPS set up, the response was measured in the near infrared. Figure 6.2 shows the spectral response of the solar cells with and without upconverter layer. As reference a solar cell without back reflector is used (solar cell I, figure 1.1). A value larger than 1 is an increase in response compared to the solar cell without back reflector. For both solar cells, (II and III in figure 1.1), an increase in response in measured for all wavelengths in the red and near infrared. This is expected because of the back reflector, that reflects photons back into the solar cell that are not absorbed after a single pass of light. Higher energy photons are already efficiently absorbed in the intrinsic layer after a single pass of the light. Though, both solar cells show an increase in response, the increase is smaller when an UC-layer is attached to the cell, see figure 6.2. This is mainly due to absorption in the PMMA/UC layer, as is shown by the normalized absorption spectra of β-$NaYF_4$. The vertical dotted lines point out at which wavelengths even a larger decrease in response of the upconverter solar cell was measured. These wavelengths correspond with the absorption of Er^{3+} and Yb^{3+} ions in the upconverter layer. Especially the decrease in response around the wavelengths where Yb^{3+} absorbs light ($\sim$980 nm) and converts it to shorter wavelengths is remarkable. At the wavelengths where Yb^{3+} absorbs an increase in response is expected, however the opposite was measured. The explanation may be, that the light intensity in this experiment is too low for efficient upconversion. The absorbed 980 nm light is not upconverted efficiently and not reflected back into the solar cell. This explains the observed reduction in the sub band gap response around 980 nm due to absorption of Yb^{3+}. To measure a positive effect of the upconverter layer, higher light intensities are needed to increase the upconverter efficiency.

Diode laser excitation

Higher light intensities were achieved with diode laser excitation. To demonstrate the enhancement of solar cell performance due to UC, current-voltage (I-V) measurements were performed. The solar cells were illuminated with a NIR diode

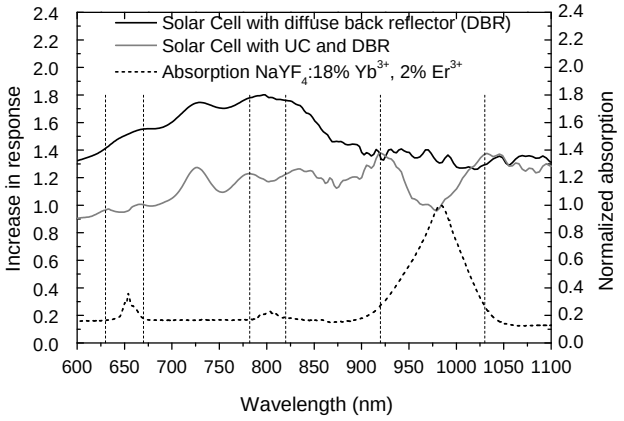

Figure 6.2: FTPS measurement on a-Si:H solar cells with and without upconverter layer. A solar cell with white back reflector increases the response from 30% to almost twice at the band edges (800 nm), compared to a solar cell without any back reflector (black line). The solar cell with UC, however, increases the response in the NIR by approximately 20% (gray line). This is slightly lower due to absorption in the PMMA/UC layer. Around 653, 800 and 980 nm there is a decrease in the response, which is consistent with the peaks in absorbance of β-$NaYF_4$:Er^{3+} (2%), Yb^{3+} (18%) depicted in the lower graph (dotted).

laser, with a maximum power of 28 mW. The laser emits light at wavelengths of 981 and 986 nm, which are suitable wavelengths for absorption by Yb^{3+}. The laser beam was not focused and the area was 1 mm^2 which results in a power density of 3 W/cm^2. Maximum efficiency of the upconverter was obtained at 40 W/cm^2 [46], thus the power of the laser used in this experiment is far below the power for which the highest upconversion efficiency of 5% [136] has been obtained.

It is well known for a-Si:H that sub band gap absorption arises due to a continuous density of localized states. As a result, a part of the NIR radiation is absorbed by the cell, before it reaches the backside of the cell where it can be upconverted. To distinguish the response to upconverted light from the primary response due to absorption of sub band gap radiation, the response to NIR radiation of the solar cell without the upconverter but with otherwise the same cell structure as reference was measured as well. The solar cells were mounted in a box in which no light from outside can penetrate, so that the response of the solar cell is only due to the diode laser. Figure 6.3 shows the I-V curves of two cells, one with and one without upconverter (denoted as reference). The reference cell shows a short-circuit current of 2.1 μA. There is a clear three-fold improvement due to UC leading to a short-circuit current of 6.2 μA. The EQE is calculated as:

$$\mathrm{EQE_{UC}}(\lambda) = \frac{\mathrm{I_{SC}}}{\mathrm{P_{in}}/(1240/\lambda)} \tag{6.1}$$

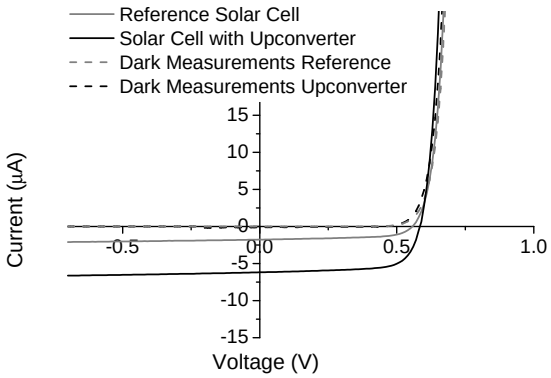

Figure 6.3: Measured I-V curves of solar cells with and without $NaYF_4$ upconverter under 981 nm laser light excitation and dark. A three times higher I_{SC} is measured for the upconverter solar cell compared to the reference solar cell.

with I_{SC} the photogenerated short circuit current in A, $1240/\lambda$ the energy of the photon in eV and P_{in} the laser power in W. A value of 0.03% was calculated for 980 nm photon energy. This EQE is dependent on the UC efficiency, the photo-carrier generation efficiency, and the collection efficiency of the device. Unfortunately, we cannot compare the obtained EQE with that reported for $NaYF_4 : Er^{3+}$ and c-Si solar cells using a 1523 nm laser [63] directly. First, the upconverter route undertaken in $NaYF_4 : Er^{3+}$ is different, namely excited state absorption while with the Yb^{3+}/Er^{3+} couple this is energy transfer upconversion. Second, upconversion of 1523 nm light to 980 nm light is more efficient than upconversion of 980 nm to 546/650 nm for the light intensities used in the experiments [68]. Third, the response of the c-Si solar cells for 980 nm and transmission and response of the 1523 nm light are not known.

Intensity dependence

The upconverted photon flux Θ_{UC} is strongly dependent on the excitation power density (W/cm^2), ie $\Theta_{UC} \propto P_{in}^n$, see chapter 3 section 1.3.3. The current of solar cells due to non-linear processes like UC is dependent on the illumination intensity $I_{SC} \propto \Theta_{UC}$ and the EQE is expected to follow the relationship:

$$EQE \propto \frac{I_{SC}}{P_{in}} = \frac{P_{in}^n}{P_{in}} = P_{in}^{n-1} \tag{6.2}$$

When increasing the power intensity of 981 nm laser light we find that EQE increases with increasing intensity, with a slope of 0.72, see figure 6.4. A very weak dependence on the illumination intensity of the reference cell was found inferring that the sub band gap response is almost a linear process, which was already

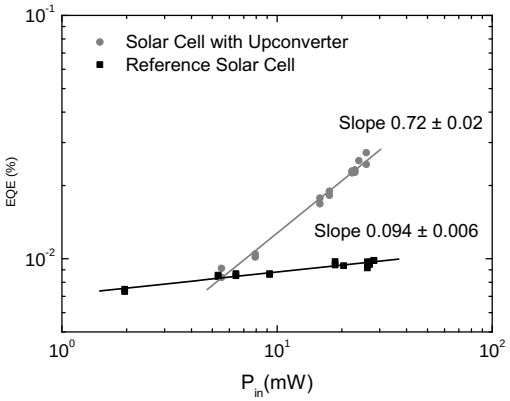

Figure 6.4: Double logarithmic plot of EQE as a function of excitation power. The slope in case of the solar cell with up converter (gray line) matches the expected power dependence of P_{in}^{n-1}, with n close to 2. The EQE of the reference cell is approximately constant which was expected for the sub band gap response.

found in chapter 5 section 1.3.4. The relative contribution of UC will become more significant at higher excitation powers.

6.3.2 Device modifications

To investigate the influence of the light intensity on the solar cell response, two new solar cells designs are proposed: solar cells deposited on textured superstrates and on flat superstrates. Ideally the solar cells with upconverter layer at the back do not scatter the sub band gap light and are highly transparent for sub band gap light to hold a high power density of the transmitted light. Solar cells with texture increase the absorption but decrease the efficiency of the upconverter due to light scattering and they are less transparent also for 980 nm light. Solar cells made on flat superstrates are more transparent and due to interference between the different layers, the transparency can be increased even more for suitable wavelengths by adapting the layer thickness. We adapted the solar cells in such a way that an interference maximum occurs in the solar cells at a wavelength of 980 nm, thereby increasing the light that is transmitted at this wavelength which can be upconverted. As front contact a TCO layer of 1.5 µm ZnO:Al (from a 0.5% Al_2O_3/ZnO target) was sputtered on corning glass and textured Asahi glass superstrate was used. As back contact a 1.5 µm ZnO:Al layer (also 0.5% doped) was sputtered on both solar cells. Changing only the i-layer thickness does not increase the transparency of the textured solar cells. Transmittance values varying between 40% and 55% are measured for 980 nm light, which were almost independent of the i-layer thickness. This is mainly because the variation in sub

band gap absorption is much larger for textured solar cells, as was shown in chapter 5 section 1.3.2 sub band gap response. For flat solar cells however, the transmission was generally higher and a transmittance up to 84% was measured. Therefore, the light intensity that reaches the upconverter layer is approximately two times higher and thus higher upconverter efficiency is expected, resulting in a higher response of the solar cell in the near infrared. As upconverter Gd_2O_2S was used, because of the higher efficiency at the low light intensities used in the experiments.

Saturation of Gd_2O_2S upconverter

Figure 6.5 shows the total current measured under laser light excitation with a wavelength of 981 nm with Gd_2O_2S upconverter. When applying the Gd_2O_2S upconverter at the back of the solar cells different results are obtained compared to $NaYF_4$. The current is increasing almost linear with the light intensity, which is unexpected because the photogenerated current is directly proportional to the upconverted emission and thus a quadratic dependence is expected (see section 6.3.1). From a power of $0.6\,W/cm^2$ slopes smaller than 1 are even measured for the flat solar cells, see figure 6.5. This means that there is a decrease in efficiency of the upconverter solar cell device. Also, at low intensities the sub band gap response of the textured solar cells is dominating. This means that the EQE of the upconverter is in the same order and thus the current for the textured solar cells is higher than for flat solar cells at low light intensities. For higher light intensities the response is better for the flat solar cells, because more light reaches the upconverter layer leading to more efficient upconversion.

EQE and sub band gap correction

Figure 6.6 shows the calculated EQE corrected for the sub band gap response. Several effects can be distinguished. First, the EQE is higher for all power densities for the flat solar cells. This can be expected when higher transparency for sub band gap light leads to higher light intensity in UC layer. A higher light intensity leads to increased upconverter efficiency and thus the flat solar cell configuration has higher response than the textured solar cell under the same light intensities. Second, the correction for sub band gap response does not make a big difference because the efficiency of the upconverter is one order of magnitude higher than the EQE of sub band gap response. Only at low light intensities differences between figures 6.5 and 6.6 are visible. For the textured solar cell the current is higher than for flat solar cells, see figure 6.5, but after subtraction of the sub band gap response, the flat solar cells have a higher EQE. The EQE is dependent on the power density according to formula 6.2. In figure 6.5, it was shown that for light intensities of $0.6\,W/cm^2$ and higher a value smaller than one was measured for the current in flat solar cells. This means that the EQE is decreasing for a power higher than $0.6\,W/cm^2$, which can be seen in figure 6.6. For textured solar cells the EQE is almost constant for a power higher than $0.6\,W/cm^2$, which could also be expected from figure 6.5.

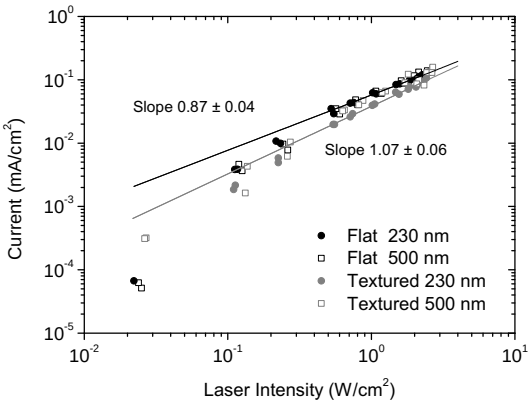

Figure 6.5: Photogenerated I_{SC} under 981 nm laser light excitation with Gd_2O_2S upconverter. The flat solar cells have a slightly higher current, which is due to better upconverter performance, because more light reaches the upconverter layer. The difference between the i-layer thicknesses is less pronounced.

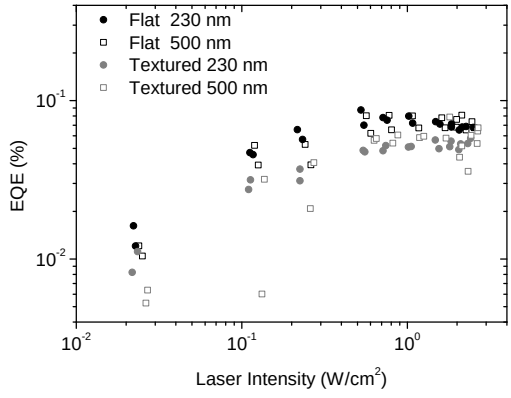

Figure 6.6: The EQE of the different solar cells with Gd_2O_2S upconverter corrected for the sub band gap response. The black figures are the EQEs measured for the flat solar cells and for all power intensities a higher EQE was measured.

6.3.3 Laser light and equivalent number of suns

To make upconversion a real possibility for improving the response of solar cells in the infrared, it is important to know what the necessary concentration would be. Because, the laser light is monochromatic and the sunlight polychromatic in nature, direct comparison of light power densities is not straightforward. The best way to compare these intensities, is by multiplying the solar spectrum with the absorption spectrum of the upconverter and integrate the area to find the power that can be absorbed by the upconverter under 1 Sun. When the intensity of the laser is not corrected for the amount that is absorbed by the upconverter, the spectra of the upconverter has to be normalized for comparison. The upconverter materials used with the solar cells have Yb^{3+} (900-1050 nm) and Er^{3+} (1400-1650 nm) as absorber, see figure 6.7. When these normalized absorption bands are multiplied with the solar spectrum the absorbed power densities are then $3.8\,mW/cm^2$ for Yb^{3+} absorption and $1.4\,mW/cm^2$ for Er^{3+} absorption in the $NaYF_4$ host; these number will differ slightly depending on the host materials. Then, from the photon flux of the laser and the solar spectrum the required light concentration can be determined.

For a-Si:H only Yb^{3+} is a relevant absorber and in the experiments described in this chapter only Yb^{3+} contributed to the upconverted emission. Figure 6.8 shows the power (in W/cm^2) vs the concentration that is necessary to reach this power. Hereby two different situations are compared, first absorption by Yb^{3+} only (black line) and the situation in which all light can be absorbed from the band edge of a-Si:H (800 nm) to the red end of Yb^{3+} (1050 nm). This can theoretically be achieved by downshifting the wavelengths between 800 and 900 nm by quantum dots or broadening the absorption spectra by transition metals. According to these calculation and the power densities used in the experiments described above, the concentration varies from 400 suns for the $0.6\,W/cm^2$ with the Gd_2O_2S host to 2000 suns for $3\,W/cm^2$ for the $NaYF_4$ host. The gray line shows how much power can be absorbed with a concentration of 500 Sun. This number is chosen as a realistic maximum that is actually used in real concentrated solar cell systems [137]. From this it becomes clear that a laser power of more than several W/cm^2 is actually too high, compared to the power that can be absorbed by concentration of solar light. Though, one thing that has to be considered is that upconversion may be more efficient under broad band light. Especially, when the two steps of excitations as shown in chapter 3 figure 2 are not exactly in resonance, which was also taken as assumption by the calculation of Trupke et. al. [19].

6.3.4 Broad band excitation

Though Gd_2O_2S is not the best upconverter to achieve high quantum efficiencies with, it had relatively high efficiencies under low light intensities as was shown in the experiments above. Therefore this upconverter was used for broad band excitation of UC-solar cells. Two sets of solar cells were made, on ZnO superstrate

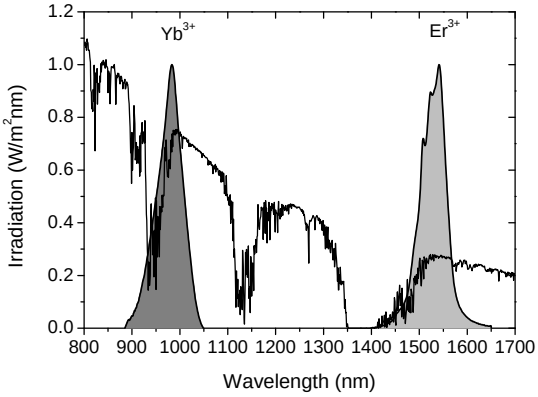

Figure 6.7: Part of the solar spectrum that is not absorbed by a-Si:H solar cells and the normalized absorption spectra of Yb^{3+} and Er^{3+} in $NaYF_4$ host. These two ions absorb the sub band gap light and contribute to upconversion.

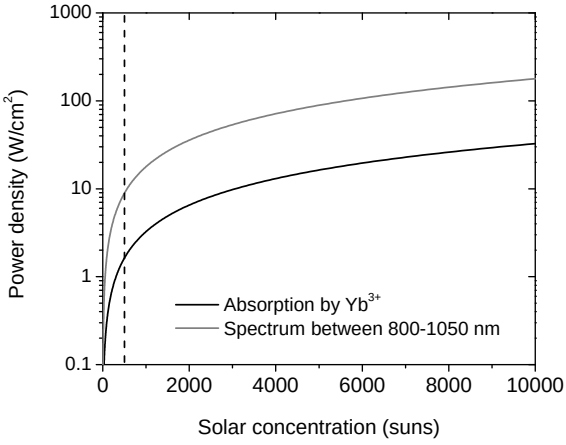

Figure 6.8: The power absorbed when Yb^{3+} is the absorber and when all light between 800 and 1050 can be absorbed with increasing concentration of the AM 1.5 solar spectrum.

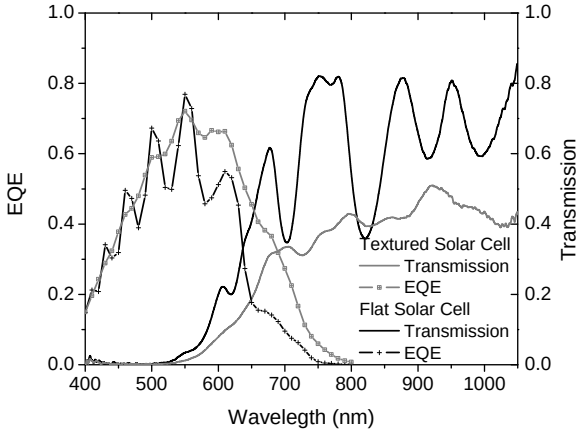

Figure 6.9: Spectral response (through the n-layer) and transmission of the flat and textured solar cells used for broad band excitation.

and Asahi with an i-layer thickness of 350 nm. As back reflector white foil was applied. The transparency for 900-1040 nm was between 80% and 60% for flat solar cells, with a maximum around 950 nm and 45% for textured solar cells, see figure 6.9. The solar cells were illuminated with sub band gap light longer than 900 nm from the solar simulator. By positioning the lens, the light could be concentrated up to 25 times. The upper graph in figure 6.10 shows the total current measured in the upconverter and reference solar cells and the lower graph the current measured in the upconverter solar cells corrected for the sub band gap response. The slope for the sub band gap current (reference), was as expected 1 for the textured and flat solar cells. The current due to the upconverter, corrected for the sub band gap response, followed an almost quadratic law of 1.8 for flat solar cells and 1.5 for textured solar cells, see the lower graph in figure 6.10. These values are smaller than 2, which is common for the oxysulfide phosphors [109]. Though, the difference in slopes between the solar cells can not be explained by saturation of the upconverter. It is therefore more likely that the deviations are due to decreasing carrier collection efficiency with increasing concentration. This effect would play a larger role in textured solar cells, because they have a higher defect density than flat solar cells. This may explain why for flat solar cells the value n is closer to 2, than the value n for the textured solar cells.

For a comparison of the response due to the broad band excitation and laser light excitation the responses of the textured solar cells were also measured under laser light excitation. Monochromatic laser light with wavelength at 981 nm and power density of 0.2 W/cm^2 , gave a current density of 0.14 mA/cm^2 for the upconverter solar cells and 0.04 mA/cm^2 for the reference solar cells. The

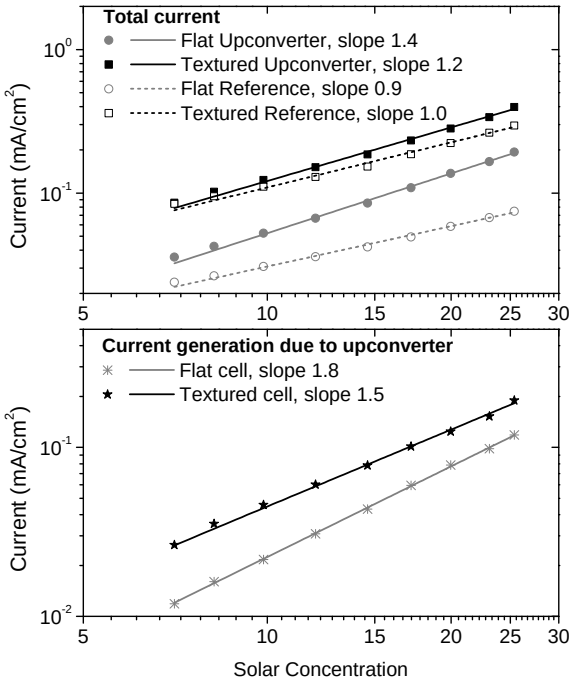

Figure 6.10: Current densities under broad band excitation. Upper graph: the total current measured for the references solar cells and the upconverter solar cells. The current of the upconverter solar cells is only slightly higher, where for the flat solar cells the difference is larger. Lower figure: the current corrected for the sub band gap response, thus solely due to the upconverter.

contribution of sub band gap absorption is much smaller, with monochromatic laser light, because only 981 nm light high laser intensity is contributing while for the broad band excitation all wavelengths longer than 900 nm add to the current. More revealing is the current generated in the upconverter solar cell. The current due to the upconverter is comparable to the current measured under 20 sun: ~0.1mA/cm^2 (see figure 6.10). This is remarkable in two ways. First, the results are in contrast with previously reported experiments with broad band excitation of c-Si solar cells [69], where the current under broad band excitation was much smaller than under laser light excitation. However, in [69] another upconverter was applied ($NaYF_4$) and different processes are undertaken in the upconverter, namely excited state absorption. In the upconverter in this work (Gd_2O_2S) ETU is the main upconverter path and the broad band absorption of Yb^{3+} may increase the transfer between Yb^{3+} and Er^{3+}. Second, the power that is absorbed by Yb^{3+} is 3.44 mW/cm^2 which yields a broad band power density of 70 mW/cm^2 under a concentration of 20 sun. This is 3 times less than the power density of the laser.

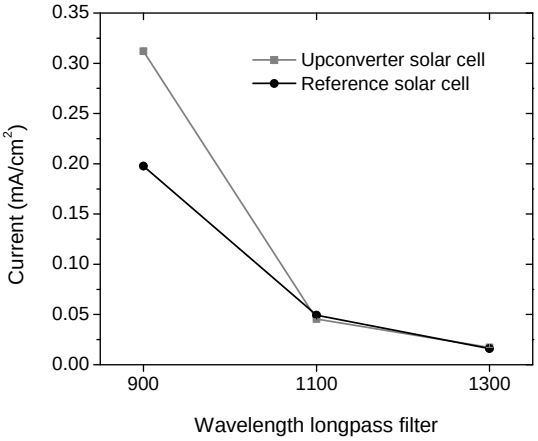

Figure 6.11: Current under a concentration of 20 sun with different filters. If other path would contribute to the current, ie 2 color direct excitation of Er^{3+}: $^2I_{13/2}$ state followed by excite state absorption (ESA) from $^2I_{13/2}$ to $^2F_{9/2}$ the current of the upconverter should be higher with an 1100 nm filter. Only difference is measured when Yb^{3+} can be excited and for longer wavelengths the current is the same.

A large difference here is that light of the solar simulator extends to further than 1600 nm, thus also the Er^{3+}: $^2I_{13/2}$ state is excited directly. Addition of other paths that lead to upconverted light may contribute to the current. These paths may be non resonant excited state absorption between the energy levels of Er^{3+} or 3-photon absorption around 1540 nm at Er^{3+}: $^2I_{13/2}$, see figure 3, chapter 4. Direct excitation of the Er^{3+} :$^2I_{13/2}$ state followed by excited state absorption (ESA) from $^2I_{13/2}$ to $^2I_{9/2}$ results in a visible photon around 650 nm, while 3 photon absorption around 1540 nm, results in emission from the $^2I_{9/2}$ state too. Wavelengths required for these transition are around 1540 nm and 1200 nm, which are present within the broad spectrum the solar cell is illuminated with. Contribution of these upconversion routes, increases the emission and thereby the current in the solar cells. To see if there is a contribution of excited state upconversion, the solar cells are illuminated with 900, 1100 and 1300 nm long pass filters under a concentration of 20 sun. The results are shown in figure 6.11. There is a distinct difference in response between the upconverter and reference solar cell with the 900 nm filter. However, the current measured under the other filters is the same for the upconverter and reference solar cells. It therefore seems that the contribution of the upconverter is due to absorption of Yb^{3+} only and its efficient energy transfer to Er^{3+}.

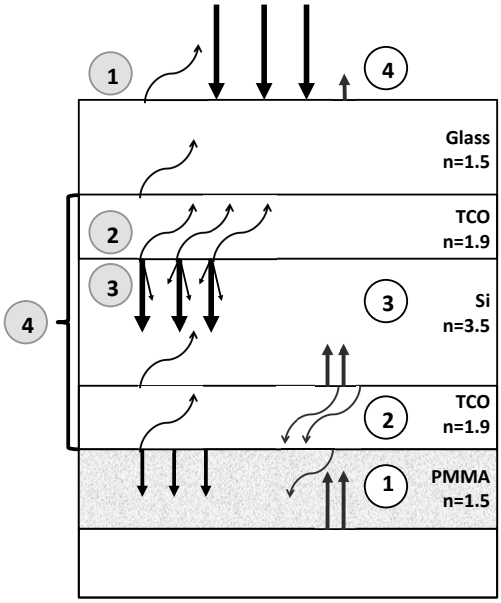

Figure 6.12: Schematic overview of losses in solar cells for upconversion. The gray circles represents losses of incoming light: reflection (1, 2), scattering (3) and absorption (4) and the white circles losses of upconverted light: parasitic absorption (1, 2), collection efficiency of smaller than 1 (3) and transmission (4).

6.3.5 Upconversion luminescence efficiency

From figure 6.6 a maximum quantum efficiency of the upconverter can be determined, taking losses in consideration. These losses can be divided in different ways: either losses of incoming light due to reflection at the interfaces (1 and 2), scattering (3) of light before it reaches the upconverter layer and absorption (4), and losses of upconverted light due to parasitic absorption in non active layers (1 and 2), a collection efficiency (3) less than unity and overall transmission (4), see figure 6.12. For flat solar cells, the scattering is less than 5% for and the specular transmission is~80%. The absorption in the PMMA layer is very low,~1.5%. When measuring the EQE for 550 nm from the back, incoming light though n-layer, 2 and 4 are taken into account as well. Ignoring scattering of light, which is allowed for flat cells and even for textured cell since the haze is very low at 1 µm, (see figure 2.2 in chapter 2) [138], the luminescence quantum efficiency (LQE) of the upconverter can be determined as follows:

$$\mathrm{LQE} = \frac{\mathrm{EQE_{UC}}}{\mathrm{T_{980}}(1 - \mathrm{A_{PMMA}})\mathrm{EQE_B}(\lambda_{\mathrm{UC}})} \tag{6.3}$$

with $\mathrm{EQE_{UC}}$ given by formula 6.1. This leads to a LQE of 0.2% of Gd_2O_2S. However, when an upconverter is saturated other paths are possible. Emission will increase at 660 and 800 nm and even 410 nm. Unfortunately, for the a-Si:H solar cells the quantum efficiencies are rather low at these wavelengths.

6.4 Conclusions

In this chapter we have shown an increase in response in the near infrared due to upconversion. As an excitation source either laser light or concentrated light from a solar simulator was used. The upconverters that were applied were $NaYF_4$ and Gd_2O_2S. Under laser light excitation the current was almost quadratically increasing when the $NaYF_4$ upconverter was applied, while for Gd_2O_2S upconverter, current was increasing linearly because the upconverter was saturated. A maximum quantum efficiency was measured at a power density of $0.6\,\mathrm{W/cm^2}$ for Gd_2O_2S upconverter, resulting in an EQE of 0.1%. With $NaYF_4$ the maximum EQE measured was 0.03% under an excitation density of $3\,\mathrm{W/cm^2}$. Under broad band excitation the upconverter Gd_2O_2S was used, because of the relatively high efficiency under low excitation densities. An increase of current was measured that was almost quadratically increasing with concentration factor for flat solar cells. Under a concentration of 25 sun a current of $0.2\,\mathrm{mA/cm^2}$ was measured, due to upconversion of near infrared light.

Bibliography

[1] D.J.D. Mackay. Sustainable energy without the hot air. *UIT Cambridge*, 2008.

[2] W. Shockley and H. J. Queisser. Detailed balance limit of efficiency of p-n junction solar cells. *Journal of Applied Physics*, 32(3):510–519, 1961.

[3] M. A. Green, K. Emery, Y. Hishikawa, and W. Warta. Solar cell efficiency tables (version 37). *Progress in Photovoltaics: Research and Applications*, 19(1):84–92, 2011.

[4] G. Conibeer. Third-generation photovoltaics. *Materials Today*, 10(11):42–50, 2007.

[5] G. F. Brown and J. Wu. Third generation photovoltaics. *Laser and Photonics Reviews*, 3(4):394–405, 2009.

[6] R. P. Kenny, A. Ioannides, H. Müllejans, W. Zaaiman, and E. D. Dunlop. Performance of thin film PV modules. *Thin Solid Films*, 511-512:663–672, 2006.

[7] P. Würfel. Solar energy conversion with hot electrons from impact ionisation. *Solar Energy Materials and Solar Cells*, 46(1):43–52, 1997.

[8] M. J. Keevers and M. A. Green. Extended infrared response of silicon solar cells and the impurity photovoltaic effect. *Solar Energy Materials and Solar Cells*, 41-42:195–204, 1996.

[9] A. Luque and A. Martí. Increasing the efficiency of ideal solar cells by photon induced transitions at intermediate levels. *Physical Review Letters*, 78(26):5014–5017, 1997.

[10] M. C. Hanna and A. J. Nozik. Solar conversion efficiency of photovoltaic and photoelectrolysis cells with carrier multiplication absorbers. *Journal of Applied Physics*, 100(7), 2006.

[11] R. D. Schaller and V. I. Klimov. High efficiency carrier multiplication in PbSe nanocrystals: Implications for solar energy conversion. *Physical Review Letters*, 92(18):186601–1, 2004.

[12] R. J. Ellingson, M. C. Beard, J. C. Johnson, P. Yu, O. I. Micic, A. J. Nozik, A. Shabaev, and A. L. Efros. Highly efficient multiple exciton generation in colloidal PbSe and PbS quantum dots. *Nano Letters*, 5(5):865–871, 2005.

[13] J. J. H. Pijpers, R. Ulbricht, K. J. Tielrooij, A. Osherov, Y. Golan, C. Delerue, G. Allan, and M. Bonn. Assessment of carrier-multiplication efficiency in bulk PbSe and PbS. *Nature Physics*, 5(11):811–814, 2009.

[14] B. S. Richards. Enhancing the performance of silicon solar cells via the application of passive luminescence conversion layers. *Solar Energy Materials and Solar Cells*, 90(15):2329–2337, 2006.

[15] W. G. J. H. M. Van Sark, A. Meijerink, R. E. I. Schropp, J. A. M. Van Roosmalen, and E. H. Lysen. Enhancing solar cell efficiency by using spectral converters. *Solar Energy Materials and Solar Cells*, 87(1-4):395–409, 2005.

[16] B. M. Van Der Ende, L. Aarts, and A. Meijerink. Lanthanide ions as spectral converters for solar cells. *Physical Chemistry Chemical Physics*, 11(47):11081–11095, 2009.

[17] W. G. J. H. M. Van Sark, A. Meijerink, and R. E. I. Schropp. Nanoparticles for solar spectrum conversion, nanotechnology for photovoltaics. *Taylor Franscis*, chapter 10, 2009.

[18] R. T. Wegh, H. Donker, K. D. Oskam, and A. Meijerink. Visible quantum cutting in $LiGdF_4 : Eu^{3+}$ through downconversion. *Science*, 283(5402):663–666, 1999.

[19] T. Trupke, M. A. Green, and P. Würfel. Improving solar cell efficiencies by down-conversion of high-energy photons. *Journal of Applied Physics*, 92(3):1668, 2002.

[20] T. Trupke, A. Shalav, B. S. Richards, P. Würfel, and M. A. Green. Efficiency enhancement of solar cells by luminescent up-conversion of sunlight. *Solar Energy Materials and Solar Cells*, 90(18-19):3327–3338, 2006.

[21] P. A. Franken, A. E. Hill, C. W. Peters, and G. Weinreich. Generation of optical harmonics. *Physical Review Letters*, 7(4):118–119, 1961.

[22] G. Blasse and B.C. Grabmaier. *Luminescent Materials*. Springer Berlin, 1994.

[23] F. Auzel. Upconversion and anti-Stokes processes with f and d ions in solids. *Chemical reviews*, 104(1):139–173, 2004.

[24] T. N. Singh-Rachford and F. N. Castellano. Photon upconversion based on sensitized triplet-triplet annihilation. *Coordination Chemistry Reviews*, 254(21-22):2560–2573, 2010.

[25] R. R. Islangulov, D. V. Kozlov, and F. N. Castellano. Low power upconversion using MLCT sensitizers. *Chemical Communications*, (30):3776–3778, 2005.

[26] T. N. Singh-Rachford, A. Haefele, R. Ziessel, and F. N. Castellano. Boron dipyrromethene chromophores: Next generation triplet acceptors/annihilators for low power upconversion schemes. *Journal of the American Chemical Society*, 130(48):16164–16165, 2008.

[27] R. R. Islangulov, J. Lott, C. Weder, and F. N. Castellano. Noncoherent low-power upconversion in solid polymer films. *Journal of the American Chemical Society*, 129(42):12652–12653, 2007.

[28] S. Baluschev, T. Miteva, V. Yakutkin, G. Nelles, A. Yasuda, and G. Wegner. Up-conversion fluorescence: Noncoherent excitation by sunlight. *Physical Review Letters*, 97(14), 2006.

[29] H. Sternlicht, G. C. Nieman, and G. W. Robinson. Triplet-triplet annihilation and delayed fluorescence in molecular aggregates. *The Journal of chemical physics*, 38(6):1326–1335, 1963.

[30] M. Kasha. Discussions of the Faraday Society. 9:14–19, 1950.

[31] T. N. Singh-Rachford, A. Nayak, M. L. Muro-Small, S. Goeb, M. J. Therien, and F. N. Castellano. Supermolecular-chromophore-sensitized near-infrared-to-visible photon upconversion. *Journal of the American Chemical Society*, 132(40):14203–14211, 2010.

[32] V. Yakutkin, S. Aleshchenkov, S. Chernov, T. Miteva, G. Nelles, A. Cheprakov, and S. Baluschev. Towards the IR limit of the triplet-triplet annihilation-supported up-conversion: Tetraanthraporphyrin. *Chemistry - A European Journal*, 14(32):9846–9850, 2008.

[33] J. Mezyk, R. Tubino, A. Monguzzi, A. Mech, and F. Meinardi. Effect of an external magnetic field on the up-conversion photoluminescence of organic films: The role of disorder in triplet-triplet annihilation. *Physical Review Letters*, 102(8), 2009.

[34] B. E. Hardin, E. T. Hoke, P. B. Armstrong, J. . Yum, P. Comte, T. Torres, J. M. J. Fréchet, M. K. Nazeeruddin, M. Grätzel, and M. D. McGehee. Increased light harvesting in dye-sensitized solar cells with energy relay dyes. *Nature Photonics*, 3(7):406–411, 2009.

[35] P. E. Keivanidis, S. Baluschev, T. Miteva, G. Nelles, U. Scherf, A. Yasuda, and G. Wegner. Up-conversion photoluminescence in Polyfluorene Doped with Metal(II)-Octaethyl Porphyrins. *Advanced Materials*, 15(24):2095–2098, 2003.

[36] P. B. Merkel and J. P. Dinnocenzo. Low-power green-to-blue and blue-to-UV upconversion in rigid polymer films. *Journal of Luminescence*, 129(3):303–306, 2009.

[37] Y. Y. Cheng, T. Khoury, R. G. C. R. Clady, M. J. Y. Tayebjee, N. J. Ekins-Daukes, M. J. Crossley, and T. W. Schmidt. On the efficiency limit of triplet-triplet annihilation for photochemical upconversion. *Physical Chemistry Chemical Physics*, 12(1):66–71, 2010.

[38] G.H. G. H. Dieke and H.M Crosswhite. The spectra of the doubly and triply ionized rare earths. *Applied optics*, 2(7):675–683, 1963.

[39] Junichi Ohwaki and Yuhu Wang. Efficient 1.5 μm to visible upconversion in Er^{3+}-doped halide phosphors. *Japanese Journal of Applied Physics, Part 2: Letters*, 33(3 A):L334–L337, 1994.

[40] F. Auzel, D. Pecile, and D. Morin. Rare earth doped vitroceramics: New, efficient, blue and green emitting materials for infrared up-conversion. *Journal of the Electrochemical Society*, 122(1):101–107, 1975.

[41] J. F. Suyver, J. Grimm, K. W. Krämer, and H. U. Güdel. Highly efficient near-infrared to visible up-conversion process in $NaYF_4$:Er^{3+},Yb^{3+}. *Journal of Luminescence*, 114(1):53–59, 2005.

[42] H. Yersin. Transition metals and rare earth compounds II. *springer Verlag Telos*, 214(1):12, 2001.

[43] R. H. Page, K. I. Schaffers, P. A. Waide, J. B. Tassano, S. A. Payne, W. F. Krupke, and W. K. Bischel. Upconversion-pumped luminescence efficiency of rare-earth-doped hosts sensitized with trivalent ytterbium. *Journal of the Optical Society of America B: Optical Physics*, 15(3):996–1008, 1998.

[44] N. Menyuk, K. Dwight, and J. W. Pierce. $NaYF_4 : Yb, Er$ - an efficient upconversion phosphor. *Applied Physics Letters*, 21(4):159–161, 1972.

[45] J. F. Suyver, A. Aebischer, S. García-Revilla, P. Gerner, and H. U. Güdel. Anomalous power dependence of sensitized upconversion luminescence. *Physical Review B - Condensed Matter and Materials Physics*, 71(12):1–9, 2005.

[46] J. F. Suyver, J. Grimm, M. K. Van Veen, D. Biner, K. W. Krämer, and H. U. Güdel. Upconversion spectroscopy and properties of $NaYF_4$ doped with Er^{3+}, Tm^{3+} and/or Yb^{3+}. *Journal of Luminescence*, 117(1):1–12, 2006.

[47] A. M. Pires, S. Heer, H. U. Güdel, and O. A. Serra. Er, Yb doped yttrium based nanosized phosphors: Particle size, "host lattice" and doping ion concentration effects on upconversion efficiency. *Journal of Fluorescence*, 16(3):461–468, 2006.

[48] K. W. Krämer, D. Biner, G. Frei, H. U. Güdel, M. P. Hehlen, and S. R. Lüthi. Hexagonal sodium yttrium fluoride based green and blue emitting upconversion phosphors. *Chemistry of Materials*, 16(7):1244–1251, 2004.

[49] D. C. Hanna, R. M. Percival, I. R. Perry, R. G. Smart, J. E. Townsend, and A. C. Tropper. Frequency upconversion in Tm- and Yb:Tm-doped silica fibers. *Optics Communications*, 78(2):187–194, 1990.

[50] X. Wu, J. P. Denis, G. Özen, and F. Pellé. Infrared-to-visible conversion luminescence of Tm^{3+} and Yb^{3+} ions in glass ceramics. *Journal of Luminescence*, 60-61(C):212–215, 1994.

[51] G. Wang, W. Qin, L. Wang, G. Wei, P. Zhu, and R. Kim. Intense ultraviolet upconversion luminescence from hexagonal $NaYF_4$:Tm^{3+}/Yb^{3+} microcrystals. *Optics Express*, 16(16):11907–11914, 2008.

[52] J. F. Suyver, A. Aebischer, D. Biner, P. Gerner, J. Grimm, S. Heer, K. W. Krämer, C. Reinhard, and H. U. Güdel. Novel materials doped with trivalent lanthanides and transition metal ions showing near-infrared to visible photon upconversion. *Optical Materials*, 27(6):1111–1130, 2005.

[53] C. Reinhard, K. Krämer, D. A. Biner, and H. U. Güdel. V^{3+} sensitized upconversion in $Cs_2NaScCl_6$:Pr^{3+};V^{3+} and K_2NaScF_6 :Er^{3+};V^{3+}. *Journal of Alloys and Compounds*, 374(1-2):133–136, 2004.

[54] D. R. Gamelin, M. Wermuth, and H. U. Güdel. Up-conversion processes of 5d transition metal ions in crystals. *Journal of Luminescence*, 83-84:405–410, 1999.

[55] C. Reinhard, P. Gerner, F. Rodríguez, S. García-Revilla, R. Valiente, and H. U. Güdel. Near-infrared to green photon upconversion in Mn^{2+} and Yb^{3+} doped lattices. *Chemical Physics Letters*, 386(1-3):132–136, 2004.

[56] D. R. Gamelin and H. U. Güdel. Spectroscopy and dynamics of Re^{4+} near-IR-to-visible luminescence upconversion. *Inorganic chemistry*, 38(22):5154–5164, 1999.

[57] P. Gerner, K. Krämer, and H. U. Güdel. Broad-band Cr^{5+}-sensitized Er^{3+} luminescence in YVO_3. *Journal of Luminescence*, 102-103(SPEC):112–118, 2003.

[58] C. Strümpel, M. McCann, G. Beaucarne, V. Arkhipov, A. Slaoui, V. Švrček, C. del Cañizo, and I. Tobias. Modifying the solar spectrum to enhance silicon solar cell efficiency-An overview of available materials. *Solar Energy Materials and Solar Cells*, 91(4):238–249, 2007.

[59] C. Ronda. *Luminescence: From Theory to Applications*, chapter 6, page 153. Wiley-VCN, 2008.

[60] M.P. Hehlen, M.L.F. Philips, N.J. Cockroft, and H.U. Güdel. Encyclopedia of Materials: Science of Technology. *Pergamon, New York*, 10:9458, 2001.

[61] F. Auzel and D. Pecile. Comparison and efficiency of materials for summation of photons assisted by energy transfer. *Journal of Luminescence*, 8(1):32–43, 1973.

[62] P. Gibart, F. Auzel, J. . Guillaume, and K. Zahraman. Below band-gap IR response of substrate-free GaAs solar cells using two-photon up-conversion. *Japanese Journal of Applied Physics, Part 1: Regular Papers and Short Notes and Review Papers*, 35(8):4401–4402, 1996.

[63] A. Shalav, B. S. Richards, T. Trupke, K. W. Krämer, and H. U. Güdel. Application of $NaYF_4$:Er^{3+} up-converting phosphors for enhanced near-infrared silicon solar cell response. *Applied Physics Letters*, 86(1):013505–1–013505–3, 2005.

[64] Y-Y. Cheng, B. Fückel, R. W. MacQueen, T. Khoury, R. G. R. C. Clady, T. F. Schulze, N. Ekins-Daukes, M.l J. Crossley, B. Stannowski, L. Klaus, and T. Schmidt. Improving the light-harvesting of amorphous silicon solar cells with photochemical upconversion. *Energy Environ. Sci.*, 2012.

[65] M. Liu, Y. Lu, Z. B. Xie, and G. M. Chow. Enhancing near-infrared solar cell response using upconverting transparentceramics. *Solar Energy Materials and Solar Cells*, 95(2):800–803, 2011.

[66] G. . Shan and G. P. Demopoulos. Near-infrared sunlight harvesting in dye-sensitized solar cells via the insertion of an upconverter-TiO_2 nanocomposite layer. *Advanced Materials*, 22(39):4373–4377, 2010.

[67] B. S. Richards and A. Shalav. Enhancing the near-infrared spectral response of silicon optoelectronic devices via up-conversion. *IEEE Transactions on Electron Devices*, 54(10):2679–2684, 2007.

[68] S. Fischer, J. C. Goldschmidt, P. Löper, G. H. Bauer, R. Brüggemann, K. Krämer, D. Biner, M. Hermle, and S. W. Glunz. Enhancement of silicon solar cell efficiency by upconversion: Optical and electrical characterization. *Journal of Applied Physics*, 108(4), 2010.

[69] J. C. Goldschmidt, S. Fischer, P. Löper, K. W. Krämer, D. Biner, M. Hermle, and S. W. Glunz. Experimental analysis of upconversion with both coherent monochromatic irradiation and broad spectrum illumination. *Solar Energy Materials and Solar Cells*, 95(7):1960–1963, 2011.

[70] A. C. Pan, C. Del Cañizo, E. Cánovas, N. M. Santos, J. P. Leitão, and A. Luque. Enhancement of up-conversion efficiency by combining rare earth-doped phosphors with PbS quantum dots. *Solar Energy Materials and Solar Cells*, 94(11):1923–1926, 2010.

[71] W. L. Barnes, A. Dereux, and T. W. Ebbesen. Surface plasmon subwavelength optics. *Nature*, 424(6950):824–830, 2003.

[72] E. Verhagen, L. Kuipers, and A. Polman. Enhanced nonlinear optical effects with a tapered plasmonic waveguide. *Nano Letters*, 7(2):334–337, 2007.

[73] S. Schietinger, T. Aichele, H. . Wang, T. Nann, and O. Benson. Plasmon-enhanced upconversion in single $NaYF_4$:Er^{3+}/Yb^{3+} codoped nanocrystals. *Nano Letters*, 10(1):134–138, 2010.

[74] J. . Boyer, L. A. Cuccia, and J. A. Capobianco. Synthesis of colloidal up-converting $NaYF_4$:Er^{3+}/Yb^{3+} and Tm^{3+}/Yb^{3+} monodisperse nanocrystals. *Nano Letters*, 7(3):847–852, 2007.

[75] H. Schäfer, P. Ptacek, R. Kömpe, and M. Haase. Lanthanide-doped $NaYF_4$ nanocrystals in aqueous solution displaying strong up-conversion emission. *Chemistry of Materials*, 19(6):1396–1400, 2007.

[76] K. Sato, Y. Gotoh, Y. Wakayama, Y. Hayasahi, K. Adachi, and H. Nishimura. Highly textured SnO_2 : F TCO films for a-si solar cells. *Rep Res. Lab. Asahi Glass Co. Ltd.*, 42:129–137, 1992.

[77] Yanchao Liu. *Very high frequency plasma deposited amorphous/nanocrystalline silicon tandem solar cells on flexible substrates.* PhD thesis, Utrecht University, 2009.

[78] Jan Willen Schuttauf. *Amorphous and crystalline silicon based heterojunction solar cells.* PhD thesis, Utrecht University, 2011.

[79] Ronald Franken. *Transparant conducting oxide contancts and textured metal back reflectors for thin film silicon solar cells.* PhD thesis, Utrecht University, 2006.

[80] Hard W. Theiss and Software. http://www.wtheiss.com, 2012.

[81] S. K. O'Leary, S. R. Johnson, and P. K. Lim. The relationship between the distribution of electronic states and the optical absorption spectrum of an amorphous semiconductor: An empirical analysis. *Journal of Applied Physics*, 82(7):3334–3340, 1997.

[82] L.J. van der Pauw. A methods of measuring the resistivity and Hall coefficient on lamellae of arbitrary shape. *Physics Technical Review*, 20:220–224, 1958.

[83] R.E.I. Schropp and M. Zeman. *Amorphous and microcrystalline silicon solar cells*, page 74. Kluwer Academic Publishers, 1998.

[84] VIBRANT 355 II. http://www.opotek.com/vibrant.html, 2012.

[85] Arjan Verkerk. *Plasma deposition of thin film silcon at low substrate temperature and high deposition rate*. PhD thesis, Utrecht university, 2009.

[86] A. Poruba, M. Vaněček, J. Meier, and A. Shah. Fourier transform infrared photocurrent spectroscopy in microcrystalline silicon. *Journal of Non-Crystalline Solids*, 299-302(PART 1):536–540, 2002.

[87] N. Wyrsch, F. Finger, T. J. McMahon, and M. Vaněček. How to reach more precise interpretation of subgap absorption spectra in terms of deep defect density in a-Si:H. *Journal of Non-Crystalline Solids*, 137-138(PART 1):347–350, 1991.

[88] F. Auzel. Upconversion and anti-stokes processes with f and d ions in solids. *Chemical reviews*, 104(1):139–173, 2004.

[89] R. Srivastava, H. V. Lauer Jr., L. L. Chase, and W. E. Bron. Raman frequencies of fluorite crystals. *Physics Letters A*, 36(4):333–334, 1971.

[90] A. Aebischer, S. Heer, D. Biner, K. Kramer, M. Haase, and H. U. GÃŒdel. Visible light emission upon near-infrared excitation in a transparent solution of nanocrystalline $\beta-NaGdF_4:Er^{3+}/Yb^{3+}$. *Chemical Physics Letters*, 407(1-3):124–128, 2005.

[91] C. Renero-Lecuna, R. Martín-Rodríguez, R. Valiente, J. González, F. Rodríguez, K. W. Krämer, and H. U. Güdel. Origin of the high upconversion green luminescence efficiency in $\beta - NaYF_4$:2%Er^{3+}/20%Yb^{3+}. *Chemistry of Materials*, 23(15):3442–3448, 2011.

[92] B. R. Judd. Optical absorption intensities of rare-earth ions. *Physical Review*, 127(3):750–761, 1962.

[93] G.S. Ofelt. Intensities of crystal spectra of rare-earth ions. *Journal of Chemical Physics*, 37(3):511–520, 1962.

[94] M. Pollnau, D. R. Gamelin, S. R. Lüthi, H. U. Güdel, and M. P. Hehlen. Power dependence of upconversion luminescence in lanthanide and transition-metal-ion systems. *Physical Review B - Condensed Matter and Materials Physics*, 61(5):3337–3346, 2000.

[95] C. Ronda. *Luminescence: From Theory to Applications*, chapter 1, pages 15–18. Wiley-VSH, 2008.

[96] C. Ronda. *Luminescence: From Theory to Applications*, chapter 6, pages 143–144. Wiley-VSH, 2008.

[97] F. Auzel and D. Pecile. Comparison and efficiency of materials for summation of photons assisted by energy transfer. *Journal of Luminescence*, 8(1):32–43, 1973.

[98] A. Ellens, H. Andres, M. L. H. Ter Heerdt, R. T. Wegh, A. Meijerink, and G. Blasse. Spectral-line-broadening study of the trivalent lanthanide-ion series.II. the variation of the electron-phonon coupling strength through the series. *Physical Review B - Condensed Matter and Materials Physics*, 55(1):180–186, 1997.

[99] B. M. Walsh, N. P. Barnes, M. Petros, J. Yu, and U. N. Singh. Spectroscopy and modeling of solid state lanthanide lasers: Application to trivalent Tm^{3+} and Ho^{3+} in $YLiF_4$ and $LuLiF_4$. *Journal of Applied Physics*, 95(7):3255–3271, 2004.

[100] K. L. Kelly, E. Coronado, L. L. Zhao, and G. C. Schatz. The optical properties of metal nanoparticles: The influence of size, shape, and dielectric environment. *Journal of Physical Chemistry B*, 107(3):668–677, 2003.

[101] J. A. Creighton, C. G. Blatchford, and M. G. Albrecht. Plasma resonance enhancement of Raman scattering by pyridine adsorbed on silver or gold sol particles of size comparable to the excitation wavelength. *Journal of the Chemical Society, Faraday Transactions 2: Molecular and Chemical Physics*, 75:790–798, 1979.

[102] M. Moskovits. Surface-enhanced spectroscopy. *Reviews of Modern Physics*, 57(3):783–826, 1985.

[103] R. Esteban, M. Laroche, and J. . Greffet. Influence of metallic nanoparticles on upconversion processes. *Journal of Applied Physics*, 105(3), 2009.

[104] M. Haase and H. Schäfer. Upconverting nanoparticles. *Angewandte Chemie - International Edition*, 50(26):5808–5829, 2011.

[105] B. Nikoobakht and M. A. El-Sayed. Preparation and growth mechanism of gold nanorods (NRs) using seed-mediated growth method. *Chemistry of Materials*, 15(10):1957–1962, 2003.

[106] C. Greskovich and S. Duclos. Ceramic scintillators. *Annual Review of Materials Science*, 27(1):69–88, 1997.

[107] R. Morlotti, M. Nikl, M. Piazza, and C. Boragno. Intrinsic conversion efficiency of X-rays to light in $Gd_2O_2S : Tb^{3+}$ powder phosphors. *Journal of Luminescence*, 72-74:772–774, 1997.

[108] M. Mikami and S. Nakamura. Electronic structure of rare-earth sesquioxides and oxysulfides. *Journal of Alloys and Compounds*, 408-412:687–692, 2006.

[109] P. N. Yocom, J. P. Wittke, and I. Ladany. Rare-earth-doped oxysulfides for GaAs-pumped luminescent devices. *Metallurgical Transactions*, 2(3):763–767, 1971.

[110] X. . Luo and W. . Cao. Upconversion luminescence of holmium and ytterbium co-doped yttrium oxysulfide phosphor. *Materials Letters*, 61(17):3696–3700, 2007.

[111] T. Hirai and T. Orikoshi. Preparation of Gd_2O_3:Yb,Er and Gd_2O_2S:Yb,Er infrared-to-visible conversion phosphor ultrafine particles using an emulsion liquid membrane system. *Journal of colloid and interface science*, 269(1):103–108, 2004.

[112] M. A. Mahmoud and M. A. El-Sayed. Gold nanoframes: Very high surface plasmon fields and excellent near-infrared sensors. *Journal of the American Chemical Society*, 132(36):12704–12710, 2010.

[113] Yu-Ying Yu, Ser-Sing Chang, Chien-Liang Lee, and C. R. C. Wang. Gold nanorods: electrochemical synthesis and optical properties. *Journal of Physical Chemistry B*, 101(34):6661–6664, 1997.

[114] S. J. Oldenburg, J. B. Jackson, S. L. Westcott, and N. J. Halas. Infrared extinction properties of gold nanoshells. *Applied Physics Letters*, 75(19):2897–2899, 1999.

[115] P. K. Jain, K. S. Lee, I. H. El-Sayed, and M. A. El-Sayed. Calculated absorption and scattering properties of gold nanoparticles of different size, shape, and composition: Applications in biological imaging and biomedicine. *Journal of Physical Chemistry B*, 110(14):7238–7248, 2006.

[116] S. Kühn, G. Mori, M. Agio, and V. Sandoghdar. Modification of single molecule fluorescence close to a nanostructure: Radiation pattern, spontaneous emission and quenching. *Molecular Physics*, 106(7):893–908, 2008.

[117] I. Gorelikov and N. Matsuura. Single-step coating of mesoporous silica on cetyltrimethyl ammonium bromide-capped nanoparticles. *Nano Letters*, 8(1):369–373, 2008.

[118] J. . Boyer and F. C. J. M. Van Veggel. Absolute quantum yield measurements of colloidal $NaYF_4 : Er^{3+}, Yb^{3+}$ upconverting nanoparticles. *Nanoscale*, 2(8):1417–1419, 2010.

[119] B. Schröder. Thin film technology based on hydrogenated amorphous silicon. *Materials Science and Engineering A*, 139(C):319–333, 1991.

[120] M. A. Green, K. Emery, Y. Hishikawa, W. Warta, and E. D. Dunlop. Solar cell efficiency tables (version 39). *Progress in Photovoltaics: Research and Applications*, 20(1):12–20, 2012.

[121] D. L. Staebler and C. R. Wronski. Reversible conductivity changes in discharge-produced amorphous Si. *Applied Physics Letters*, 31(4):292–294, 1977.

[122] R.H. Franken, H. Yu, Y. Liu, R.L. Stolk, C.H.M. van der Werf, J.K. Rath, and R.E.I. Schropp. Texture-grown Ag and ZnO:Al as back reflectors for hot-wire CVD microcrystalline NIP solar cells. *Proceedings 20th EUPVSEC*, 2005.

[123] W. Beyer, J. Hüpkes, and H. Stiebig. Transparent conducting oxide films for thin film silicon photovoltaics. *Thin Solid Films*, 516(2-4):147–154, 2007.

[124] S. Mridha and D. Basak. Aluminium doped ZnO films: Electrical, optical and photoresponse studies. *Journal of Physics D: Applied Physics*, 40(22):6902–6907, 2007.

[125] Z. Qiao, C. Agashe, and D. Mergel. Dielectric modeling of transmittance spectra of thin ZnO:Al films. *Thin Solid Films*, 496(2):520–525, 2006.

[126] R. H. Franken. Transparent conducting oxide contacts and textures metal back reflectors for thin film silicon solar cells. *Thesis*, page 59, 2006.

[127] J. E. Cotter. Optical intensity of light in layers of silicon with rear diffuse reflectors. *Journal of Applied Physics*, 84(1):618–624, 1998.

[128] J. Müller, B. Rech, J. Springer, and M. Vaněček. TCO and light trapping in silicon thin film solar cells. *Solar Energy*, 77(6):917–930, 2004.

[129] O. Kluth, B. Rech, L. Houben, S. Wieder, G. Schöpe, C. Beneking, H. Wagner, A. Löffl, and H. W. Schock. Texture etched ZnO:Al coated glass substrates for silicon based thin film solar cells. *Thin Solid Films*, 351(1-2):247–253, 1999.

[130] J. K. Rath, Y. Liu, M. M. De Jong, J. De Wild, J. A. Schuttauf, M. Brinza, and R. E. I. Schropp. Transparent conducting oxide layers for thin film silicon solar cells. *Thin Solid Films*, 518(24 SUPPL.):129–135, 2010.

[131] O. Berger, D. Inns, and A. G. Aberle. Commercial white paint as back surface reflector for thin-film solar cells. *Solar Energy Materials and Solar Cells*, 91(13):1215–1221, 2007.

[132] H. Knauss, E.L. Salabas, M. Fecioru, H.D. Goldbach, J. Hötzel, S. Krull, O. Kluth, R. Kravets, P.A. Losio, J. Reinhardt, J. Sutterlüti, and T. Eisenhammer. Reduction of cell thickness for industrial micromorph tandem modules. *EUPVSEC Proceedings*, pages 3064 – 3067, 2010.

[133] H. Fritzsche. Development in understanding and controlling the Staebler-Wronski effect in a-Si:H. *Annual Review of Materials Science*, 31:47–79, 2001.

[134] A. Shalav, B. S. Richards, and M. A. Green. Luminescent layers for enhanced silicon solar cell performance: Up-conversion. *Solar Energy Materials and Solar Cells*, 91(9):829–842, 2007.

[135] A. Shalav, B. S. Richards, K. Krämer, and H. Güdel. Improvements of an up-conversion $\beta - NaYF_4:Er^{3+}$ phosphor/silicon solar cell system for an enhanced response in the near-infrared. In *Conference Record of the IEEE Photovoltaic Specialists Conference*, pages 114–117, 2005.

[136] M.P. M.P. Hehlen, M.L.F Philips, N.J. Cockroft, and H.U. Güdel. *Pergamon, New York*, 10:9458, 2001.

[137] H. Cotal, C. Fetzer, J. Boisvert, G. Kinsey, R. King, P. Hebert, H. Yoon, and N. Karam. III-V multijunction solar cells for concentrating photovoltaics. *Energy and Environmental Science*, 2(2):174–192, 2009.

[138] O. Kluth, B. Rech, L. Houben, S. Wieder, G. Schöpe, C. Beneking, H. Wagner, A. Löffl, and H. W. Schock. Texture etched ZnO:Al coated glass substrates for silicon based thin film solar cells. *Thin Solid Films*, 351(1-2):247–253, 1999.

Summary

In this thesis one of the many possible methods to increase the efficiency of solar cells is described. The method investigated is based on adapting the solar light in such a way that the solar cell can convert more light into electricity. The part of the solar spectrum that is adapted is the part that can not be absorbed by the solar cells, because the photon energy is too low and the light is transmitted through the solar cell. This conversion of light is done by so called upconversion, which means that lower energy photons are converted into higher energy photons that can be absorbed by the solar cell. Photon upconversion is a well investigated process and many upconverter materials are known. The upconverters used in this thesis are those based on lanthanide ions doped in crystalline hosts. Lanthanide ions have very specific absorption and emission lines, which means that by choosing an appropriate ion one can convert any arbitrary wavelength. Upconverters based on lanthanide ions were mainly investigated on a fundamental level and only applied to solar cells to a limited extent. Before the research described in this thesis started only two applications of upconverters onto solar cells were known. One of the most important aspects when one wants to apply upconverters onto solar cells is the light intensity necessary for efficient conversion. Because the upconversion process requires two photons to make a new, higher energy photon, the conversion process is non-linearly dependent on the light intensity. This is the main limitation for practical applications. Therefore, next to applying upconverters onto solar cells also more fundamental questions are addressed in this thesis, for instance, the question what determines efficient conversion.

After a general introduction in Chapter 1 and a description of experimental methods and techniques in Chapter 2, in chapter 3 the influence of the host material on the upconversion efficiency is investigated. The host material influences non-radiative decays, the absorption strength, the lifetime and the energy transfer rate between the lanthanide ions. By investigating two upconverter hosts with small differences, the hexagonal β-$NaYF_4$:Er^{3+}, Yb^{3+} and its less efficient cubic phase α-$NaYF_4$:Er^{3+}, Yb^{3+}, we have tried to investigate the origin of the difference in upconversion efficiency. For this, emission and absorption spectra are

measured under the same conditions and concentrations of the lanthanide ions. From absorption spectra is was shown that the absorption strength of the energy levels is approximately two times stronger in the β-phase and the upconverted emission was, as expected, overall larger in the hexagonal structure. To investigate the interaction between the ions, lifetime measurements were performed. These time resolved measurement, show first an increase in emission followed by a decay. From this, rise and decay times were extracted. The differences in the decay times of the different energy levels for the different crystal structures were insignificant. The rise times showed larger differences. The rise time is determined by the interaction between the ions. In contrast to what is expected from theory, the rise time was longer in the β-phase, which implies a lesser efficient interaction between the ions than in the α-phase. However, this longer rise time can also be attributed to energy migration between the sensitizer ions, before it reaches the activator ions. For this to happen a longer rise time will be measured, but also higher emission intensity because more ions participate in the upconversion process.

In the fourth chapter the influence of increasing the absorption strength on the upconverter efficiency is investigated. For this, another low phonon host material was characterized and coupling of an upconverter with a plasmon resonance is investigated. Upconversion in the host material Gd_2O_2S shows very efficient upconversion at relatively low light intensities. Although also saturation of the upconverted emission was measured. When saturation becomes visible, many intermediate transitions, broadening of the emission peaks and 3-photon upconversion is observed. For solar cell application, the locations of the peaks are not important as long as the upconverted emission is in the wavelength range were the solar cells absorbs. Thus for solar cell application Gd_2O_2S: Er^{3+}, Yb^{3+} is a promising upconverter. The other method to increase the absorption strength is by coupling the absorption with a plasmon resonance. For this, metal nanoparticles were made with a plasmon resonance at the same wavelength as where the upconverter absorbs. Gold nanorods were suitable particles for this. The gold nanorods were coated with a thin silica layer and mixed with $NaYF_4$ upconverter nanoparticles. A significant decrease in lifetime was measured at the absorption wavelength, which could indicate an increased absorption strength.

The second part of the research presented in this thesis is concerned with application of the upconverter onto solar cells. In this research the β-$NaYF_4$: Er^{3+}, Yb^{3+} and Gd_2O_2S: Er^{3+}, Yb^{3+} upconverters were applied onto amorphous silicon solar cells (a-Si:H). Before the upconverters could be applied, the solar cells had to be made bifacial; i.e., illumination from the backside should be possible. How this is done is described in the fifth chapter. The standard solar cells made at our laboratory have a metal back contact and are not suitable. Therefore the metal back contact was replaced by a transparent conductive oxide (TCO). The choice was ZnO:Al 0.5%, with low alumina concentration to minimize the free carrier absorption to keep a high transparency in the near infrared. The new solar cells show similar electrical parameters as those with metal back contact,

though a small increase in series resistance could not be avoided due to the lower conductivity of the TCO layer. The upconverter materials could be dropcasted on this back contact and a white back reflector made sure the light was directed back into the solar cell. It is known that a-Si:H has already a high absorption for sub band gap light due to deep defect states. Transitions involving these defect states may cause photogenerated free carriers that contribute to the current. It was tried to make solar cells with a lower density of defect states to decrease the absorption of the sub band gap light. This was done by changing the absorption layer thickness and the type of superstrate the solar cells were made on.

In the last chapter, the upconverters described in chapters 3 and 4 were combined with the solar cells described in chapter 5. At first, proof of principle experiments on solar cells with $NaYF_4$ upconverter were performed with laser light. I-V curves were measured and an increased response was determined in the upconverter solar cells. However, the response that was measured under laser light could not be contributed to the upconverter only. A part of the response is due to defect states. A large difference between the response due to defects or upconversion is the dependence on the light intensity and thus a way to distinguish the two contributions is by intensity dependent measurements. The EQE of the sub band gap response was nearly constant with increasing light intensity, while the upconverter response shows an increase of EQE with increasing light intensity. When the Gd_2O_2S upconverter was applied onto the solar cells different results were obtained. The response was much higher under laser light excitation and the sub band gap response was comparatively small. However, also saturation was measured in the solar cells and a maximum quantum efficiency of 0.1% was measured. Finally, to proof viability of the concept a set-up was made to concentrate simulated solar light. The use of concentrated light is not uncommon for solar cells and thus these experiments are closer to real life than laser light excitation. All wavelengths longer than 900 nm were concentrated, which means that the range of the spectrum was much broader than the part that is absorbed by the upconverter. As upconverter material again Gd_2O_2S was applied. Though a large part of the response is due to sub band gap defect absorption an increased response due to the upconverter was measured as well. This means that the upconversion efficiency is high enough to increase the response under concentration of (simulated) solar light and larger improvements can be expected for types of solar cells that have very low sub band gap absorption.

Nederlandse Samenvatting

Algemene inleiding

Energie van de zon kan een grote bijdrage leveren aan een CO_2 vrije energieproductie. Er is genoeg zonne-instraling om aan de wereldwijde energievraag te voldoen. Dit zonlicht kan op twee manieren omgezet worden in voor ons nuttige energie: warmte of elektriciteit. Een zonnecollector zet zonlicht om in warmte, zonnecellen zetten zonlicht direct om in elektrische stroom. Om een grote bijdrage van zonnestroom aan duurzame energie te kunnen realiseren moeten zonnecellen goedkoper en efficiënter worden. Zonnecellen kunnen goedkoper worden door makkelijk winbare, in de aardkorst ruim aanwezige materialen te gebruiken en door het productieproces te verbeteren. Zonnecellen efficiënter maken kan door de zonnecel zo aan te passen dat ze meer zonlicht kunnen absorberen of door het zonlicht zo aan te passen dat het geschikter is om geabsorbeerd te worden door de zonnecel. In dit proefschrift wordt beschreven hoe die laatste methode in zijn werk gaat. Hiervoor is het eerst nodig om te weten waarom zonnecellen niet al het zonlicht absorberen en hoe je het licht kan aanpassen.

Om te beginnen is het nodig te weten wat het zonlicht precies is. We weten dat zonlicht uit verschillende kleuren bestaat. Dit is weergegeven in de figuur op de volgende bladzijde. Het licht dat wij kunnen zien heeft een golflengte van 350 (violet) tot 750 nanometer (rood). Licht met kortere golflengtes wordt aangeduid als ultraviolet licht (UV) en licht met langere golflengtes als infrarood licht (IR). Bij elke golflengte hoort een bepaalde energie, die we de foton-energie noemen. Deze foton-energie in omgekeerd evenredig met de golflengte. Hoe langer de golflengte, hoe kleiner de bijbehorende foton-energie. Eén van de redenen waarom wij niet alle kleuren kunnen zien is omdat onze ogen er niet gevoelig voor zijn. De foton-energie is te klein om deze op te merken. Met zonnecellen werkt dat precies zo, fotonen met te weinig energie worden niet geabsorbeerd. Zonnecellen laten deze fotonen door, zoals glas zichtbaar licht doorlaat.

De zonnecellen die zijn gebruikt voor de experimenten beschreven in dit proefschrift zijn gemaakt van amorf silicium. Amorf silicium kan licht absorberen tot ongeveer 780 nm; voor langere golflengtes is dit materiaal transparant.

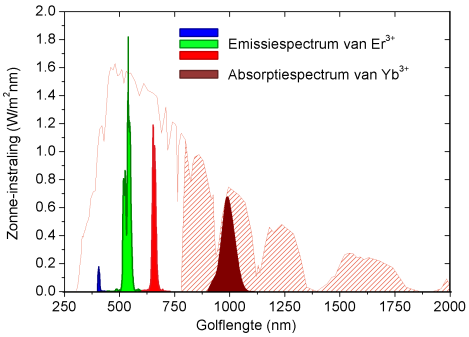

Waar deze grens ligt, is afhankelijk van het materiaal waar de zonnecel van gemaakt is. Zonnecellen worden gemaakt van zogenaamde **halfgeleiders**. Dit is een materiaal dat qua elektrische eigenschappen tussen een geleider (bijv. koper) en een isolator (bijv. glas) inzit. Een materiaal is een geleider als de elektronen vrij kunnen bewegen en een isolator als de elektronen bij een specifiek atoom horen en vastzitten op één plek. Elektrische stroom is immers niets anders dan beweging van vrije elektronen. In een geleider kunnen de elektronen vrij bewegen, in een isolator zitten de elektronen op een bepaalde plek, horen ze bij een atoom. Een halfgeleider is iets er tussenin. Elektronen kunnen losgemaakt worden van hun bijbehorende atoom na absorptie van een foton. Nadat een elektron is losgemaakt van het bijbehorende atoom, kan dit elektron vrij bewegen. Het elektron bevindt zich dan in de **geleidingsband**. Maar om de elektronen in de geleidingsband te kunnen brengen, moet de foton-energie wel groot genoeg zijn. Er moet een **bandafstand** overwonnen worden. Het is deze bandafstand die bepaalt tot welke golflengte een halfgeleider licht absorbeert. Fotonen met minder energie dan de bandafstand worden niet geabsorbeerd door het materiaal, maar doorgelaten. Een halfgeleider is transparant voor fotonen met een energie kleiner dan de bandafstand.

Hierdoor absorbeert amorf silicium slechts ongeveer 50% van de hoeveelheid energie die in het zonlicht zit. Dit is weergegeven in de figuur hierboven. Het witte deel wordt direct geabsorbeerd, het rood gestreepte deel wordt doorgelaten. Afhankelijk van de bandafstand van het materiaal kan dit variëren, materialen met een hoge bandafstand absorberen minder licht dan materialen met lage bandafstand. De stroom in een zonnecel met lage bandafstand is dus groter dan in zonnecellen met hoge bandafstand. Helaas gaat dit ten koste van de spanning, want de spanning die een zonnecel kan leveren is direct afhankelijk van de bandafstand. Het totale vermogen (stroom x spanning) dat een zonnecel kan leveren is dus direct afhankelijk van de bandafstand. Een ideale zonnecel heeft dus een hoge bandafstand (t.b.v. de spanning) én absorbeert langgolvig licht (t.b.v. de stroom). Helaas is dit niet mogelijk. Maar er zijn wel verschillende manieren om dit probleem aan te pakken.

Eén van de manieren om ook het langgolvig licht te absorberen én de hoge spanning te behouden is het veranderen van de golflengte van het licht dat niet geabsorbeerd wordt. Er zijn vele materialen beschikbaar die dit kunnen. De materialen gebruikt in dit proefschrift zijn materialen gebaseerd op lanthaniden. Lanthaniden zijn een groep elementen met dezelfde chemische eigenschappen, maar variërende optische eigenschappen. Er zijn 14 verschillende lanthaniden en daardoor is er een

breed scala aan mogelijkheden om licht te absorberen en van golflengte te veranderen. De lanthaniden kunnen in verschillende materialen geplaatst worden terwijl ze hun optische eigenschappen behouden. De materialen waarin de lanthaniden geplaatst worden, worden host materialen genoemd. Dit kunnen verschillende soorten glas zijn, maar ook keramische materialen of kristallen. In het host materiaal nemen de lanthanides meestal de vorm van het ion Ln^{3+} aan. In de figuur is weergegeven welke lanthaniden gebruikt zijn voor het onderzoek beschreven in dit proefschrift. Licht dat door Yb^{3+} (Ytterbium) wordt geabsorbeerd (de donker rode piek) kan met behulp van een andere ion, namelijk Er^{3+} (Erbium), worden omgezet naar kortere golflengtes (de gekleurde pieken).

Materialen die langere golflengtes naar kortere golflengtes omzetten, worden upconverters genoemd. Er is al veel bekend over de mechanismen achter upconversie met lanthaniden. Een belangrijke eigenschap van upconversie is dat er minimaal twee laag-energetische fotonen geabsorbeerd moeten worden om één hoog-energetisch foton uit te zenden. Dit maakt het upconversieproces afhankelijk van hoeveel licht er op valt. Hoe meer licht de upconverter kan absorberen, hoe meer licht in principe kan worden omgezet. Hoe efficiënt het licht bij verschillende intensiteit omgezet kan worden voor toepassing op zonnecellen is één van de belangrijkste eigenschappen. Daarom is er naast het toegepaste onderzoek in dit proefschrift ook fundamenteel onderzoek gedaan naar de vraag welke upconvertereigenschappen belangrijk zijn voor een efficiënte omzetting.

Samenvatting

Dit proefschrift beschrijft hoe upconversie van licht het rendement van zonnecellen kan verbeteren. Hoofdstuk 1 geeft een algemene introductie over upconverters en upconverter-zonnecellen. Het tweede hoofdstuk beschrijft de methoden en experimentele technieken die gebruikt zijn voor het onderzoek. In hoofdstukken 3 en 4 worden de upconverter materialen onderzocht. Er is onderzocht hoe het host materiaal het upconversieproces beïnvloedt en hoe de absorptiesterkte verbeterd kan worden. De host materialen bepalen hoe makkelijk de lanthanide de fotonen kan absorberen, hoe lang het duurt voordat het weer een foton uitzendt, hoe sterk de interactie is tussen de verschillende lanthaniden, van welk energieniveau een foton wordt uitgezonden en van de mate waarin fotonen wordt geabsorbeerd waarvan de energie in warmte wordt omgezet. Door twee upconverter host materialen te onderzoeken met kleine verschillen: hexagonaal β-$NaYF_4$: Er^{3+}, Yb^{3+} en de minder efficiënte kubische vorm α-$NaYF_4$: Er^{3+}, Yb^{3+}, is geprobeerd een oorzaak te vinden in de verschillen tussen het rendement van het upconversieproces. Emissie en absorptie metingen laten zien dat de lanthaniden twee keer beter de fotonen absorberen in de β structuur en dat de emissie intensiteit hoger is. Om de interactie tussen de lanthaniden te onderzoeken, zijn levensduur metingen gedaan. Deze tijds-opgeloste metingen van de emissie laten eerst een stijging in emissie zien gevolgd door een verval. Hieruit konden vervaltijden en opbouwtijden bepaald worden. Hoe lang de opbouw duurt, wordt bepaald door de interactie

tussen de verschillende ionen. In tegenstelling tot wat wordt verwacht uit de theorie, was de opbouwtijd langer in de β structuur dan die in de α structuur. Het hogere energieniveau wordt dus langzamer bereikt in de hexagonal structuur. Een verklaring hiervoor is dat er meer Yb ionen meedoen aan het upconversieproces. De energie wordt dan eerst overgedragen tussen verschillende Yb ionen, voordat het bij een Er ion komt. Hierdoor kan er een langere opbouwtijd en hoger emissie intensiteit gemeten worden. In de α structuur zou deze interactie minder zijn, omdat de absorptie lager is. Minder Yb ionen doen mee aan het upconversieproces en energie raakt verloren voordat het overgedragen kan worden aan een Er ion.

In het vierde hoofdstuk is de invloed van de absorptiesterkte op het upconversieproces onderzocht. Hiervoor was een ander host-materiaal beschikbaar, Gd_2O_2S, met sterkere covalente bindingen dan $NaYF_4$ waardoor de absorptiesterkte groter is dan in $NaYF_4$. Upconversie in het host-materiaal Gd_2O_2S is zeer efficiënt bij lage licht intensiteiten, < 1 W/cm^2. Bij hogere intensiteit verzadigde deze upconverter wat inhoudt dat de emissie niet hoger wordt als er meer licht op valt. Wanneer een upconverter verzadigt, is mede sterk afhankelijk van het host materiaal. De host materialen die onderzocht zijn, verzadigden bij zeer verschillende intensiteiten. Dit komt o.a. doordat de optimale concentratie van de ionen veel lager is in Gd_2O_2S. In hoofdstuk 3 is het host materiaal $NaYF_4$ beschreven. Dit is één van de meest efficiënte host materialen. Maar Gd_2O_2S bleek veel efficiënter te zijn bij de lichtintensiteiten die gebruikt zijn in de experimenten, maximale intensiteit van de laser was 3 W/cm^2. Dat de lichtintensiteit belangrijk is, blijkt uit het volgende voorbeeld. In $NaYF_4$ kan maximaal 50% van de geaborbeerde fotonen worden omgezet in hoog-energetische fotonen, terwijl dat in Gd_2O_2S slechts een paar procent is. Maar omdat de metingen bij lage lichtintensiteit zijn gedaan en de $NaYF_4$ ver van verzadigd was, werd de 50% bij lange na niet gehaald terwijl het maximum wel werd gehaald bij Gd_2O_2S . Daardoor werd een beter upconversierendement gemeten in Gd_2O_2S dan in $NaYF_4$. Doordat Gd_2O_2S zo efficiënt is bij lage intensiteit is deze een veelbelovend host materiaal voor upconverters voor zonnellen.

Hoe efficiënt de upconverter is bij een bepaalde lichtintensiteit is erg belangrijk voor toepassing met zonnecellen, omdat de intensiteit van zonlicht maar binnen zekere grenzen kan worden gevarieerd. Zonlicht kan geconcentreerd worden, maar er is een praktisch maximum aan concentratie. In de laatste twee hoofdstukken is beschreven hoe de upconverter en zonnecellen samengevoegd zijn en welke metingen zijn gedaan om het effect van de upconverter op de werking van de zonnecel te meten. De zonnecellen gebruikt in dit onderzoek zijn gemaakt van amorf silicium. Een amorf silicium zonnecel is één van de verschillende typen dunne film zonnecellen. Dit houdt in dat de laag die licht moet absorberen zeer dun is, minder dan 1 micrometer. Zonder verdere inzet van optische methoden is dit eigenlijk te dun om voldoende licht te absorberen. Daarom wordt aan de achterkant van de zonnecellen een reflector geplaatst. Licht dat de eerste keer niet geabsorbeerd wordt, wordt terug de zonnecel in gekaatst om nog een kans te krijgen om geabsorbeerd te worden. Ook wordt met behulp van ruwe oppervlakken licht opzettelijk

verstrooid, waardoor het een nog langere af te leggen weg in de halfgeleiderlaag heeft. In een upconverter zonnecel komt er nog een extra laag bij, namelijk de upconverterlaag. Deze bevindt zich aan de achterkant van de zonnecel, doch vóór de reflector. Het infrarode licht wordt immers niet geabsorbeerd en kan dus aan de achterkant van de zonnecel in de upconverterlaag veranderd worden van golflengte. Vervolgens wordt dit licht met een geschikte golflengte weer de zonnecel in gestuurd met behulp van de reflector. Op deze manier kan dus extra licht omgezet worden in stroom.

De metingen aan de upconverter-zonnecellen zijn gedaan op verschillende manieren met verschillende upconverters. In eerste instantie is een laser gebruikt, die licht uitzendt van 981 nm. Daarnaast is licht van een zonnesimulator geconcentreerd met behulp van lenzen. Er is gekeken naar de fotostroom, omdat daar een verhoging wordt verwacht. Omdat amorf silicium zelf van nature ook al een beetje infrarood licht absorbeert door defecten, werden telkens twee setjes zonnecellen gemaakt. Eén met upconverter en één zonder, maar verder precies hetzelfde. Door defecten kunnen fotonen met kleinere energie dan de bandafstand geabsorbeerd worden en zo toch nog een elektron in de geleidingsband brengen. Voor de zonnecellen met upconverters, zowel met $NaYF_4$ en Gd_2O_2S als host materiaal, is méér stroom gemeten dan in de zonnecellen zonder upconverters. Wanneer de intensiteit van het licht werd gevarieerd, werden de verschillen tussen de cellen met en zonder upconverter beter zichtbaar. De response in de zonnecellen met $NaYF_4$ upconverter bleef stijgen, terwijl met de Gd_2O_2S upconverter een maximale kwantum efficiëntie werd bereikt van 0.1%. Het maximum kwam door verzadiging van de upconverter en werd bereikt bij 0.6 W/cm^2. De fotostroom is echter wel hoger met de upconverter in Gd_2O_2S dan met de upconverter in $NaYF_4$. Dit blijkt ook uit de metingen aan de individuele upconverterlagen.

De Gd_2O_2S upconverter is gebruikt voor metingen met geconcentreerd licht uit de zonnesimulator. In dit experiment werd het langgolvige licht met golflengtes langer dan 900 nm tot 25 keer geconcentreerd. Dit houdt in dat er veel meer licht op de zonnecel valt dan kan worden geabsorbeerd door de upconverter, want Yb absorbeert slechts licht tussen de 920 en 1050 nm. Van de gemeten response zal een groot deel door de defecten komen. Met intensiteit metingen kon er duidelijk onderscheid gemaakt worden tussen de respons van de upconverter en die van de defecten. Dit houdt in dat het rendement van de upconverter hoog genoeg is om onder realistische concentraties van het zonlicht een effect te kunnen zien.

Met het onderzoek beschreven in dit proefschrift is aangetoond dat upconversie in principe het rendement van zonnecellen kan verbeteren. De hoeveelheid stroom die werd toegevoegd door upconversie van infrarood licht was echter relatief klein en verder onderzoek is nodig om upconversie daadwerkelijk praktisch toe te passen. Er zijn verschillende redenen waarom de stroomwinst klein is. Het belangrijkste is dat lanthaniden slechts een beperkt deel van het spectrum absorberen. Dit is ook terug te zien in de figuur. Er wordt alleen licht geabsorbeerd tussen de 900 en 1050 nm, terwijl al het licht vanaf 780 nm door de cel wordt doorgelaten. Als een upcon-

verter daadwerkelijk toegepast zou worden op zonnecellen is dit, naast verbetering van de gevoeligheid bij lage lichtintensiteit, één van de belangrijkste aspecten die verbeterd zou moeten worden. De laatste jaren wordt het onderzoek in deze richting geïntensiveerd; de intensiteit waarbij efficiënte upconversie plaatsvindt, wordt steeds belangrijker. Daarnaast worden er steeds meer materialen gevonden die een breder spectrum kunnen absorberen en omzetten naar geschiktere golflengtes. Dit biedt mogelijkheden tot verder onderzoek naar lichtconversie en toepassing daarvan in verschillende typen zonnecellen.

List of publications

This thesis is based on the following publications and conference proceedings:

- De Wild, J., Meijerink, A., Rath, J.K., Van Sark, W.G.J.H.M. & Schropp, R.E.I. 2011, "Upconverter solar cells: Materials and applications", *Energy and Environmental Science*, vol. 4, no. 12, pp. 4835-4848. **(chapter 1)**

- De Wild, J., Meijerink, A., Rath, J.K., Van Sark, W.G.J.H.M. & Schropp, R.E.I. 2010, "Towards upconversion for amorphous silicon solar cells", *Solar Energy Materials and Solar Cells*, vol. 94, no. 11, pp. 1919-1922. **(chapters 3 and 6)**

- De Wild, J., Rath, J.K., Meijerink, A., Van Sark, W.G.J.H.M. & Schropp, R.E.I. 2010, "Enhanced near-infrared response of a-Si:H solar cells with β-$NaYF_4$: Yb^{3+} (18%), Er^{3+} (2%) upconversion phosphors", *Solar Energy Materials and Solar Cells*, vol. 94, no. 12, pp. 2395-2398. **(chapters 3 and 6)**

- De Wild, J., Duindam, T., Rath, J.K., Meijerink, A., Van Sark, W.G.J.H.M. & Schropp, R.E.I. 2012, "Increased upconversion response in a-Si:H solar cells with broad band light " accepted in *IEEE Journal of Photovoltaics* **(chapters 4 and 6)**

- Rath, J.K., Liu, Y., De Jong, M.M., De Wild, J., Schuttauf, J.A., Brinza, M. & Schropp, R.E.I. 2010, "Transparent conducting oxide layers for thin film silicon solar cells", *Thin Solid Films*, vol. 518, no. 24 SUPPL., pp. e129-e135. **(chapter 5)**

- De Wild, J., Meijerink, A., Rath, J.K., Van Sark, W.G.J.H.M. & Schropp, R.E.I. 2009, "Cell concept for thin film a-Si:H solar cells including photon upconversions", *24th EUPVSEC Proceedings*, 10.4229/24thEUPVSEC2009-1CV.3.46., pp. 350 - 353. **(chapters 3, 5 and 6)**

- De Wild, J., Meijerink, A., Rath, J.K., Van Sark, W.G.J.H.M. & Schropp, R.E.I. 2010, "Improved Photon Upconversion in Amorphous Silicon Solar Cells", *25th EUPVSEC Proceedings*, 10.4229/25thEUPVSEC2010-1CO.8.1., pp. 255 - 259. **(chapters 4 and 6)**

Dankwoord

Dit proefschrift is uiteraard niet zonder de hulp van anderen tot stand gekomen. Ik wil hier graag de mensen bedanken die me daarbij direct of indirect hebben geholpen.

Ik ben 4 jaar geleden begonnen aan mijn promotieonderzoek dat is gedaan in twee vakgroepen: Physics of Devices en Condensed Matter and Interfaces. De meeste tijd heb ik doorgebracht in de groep Physics of Devices onder begeleiding van mijn promotor Ruud Schropp. Ruud, bedankt voor het in mij gestelde vertrouwen en dat je mij de kans hebt gegeven om aan het promotieonderzoek te beginnen. Bedankt voor de begeleiding de afgelopen jaren en de vrijheid die je me hebt gegeven om mijn onderzoek te doen.

Het deel van mij onderzoek dat is gedaan bij CMI, is gedaan onder begeleiding van mijn promotor Andries Meijerink. Andries, bedankt voor al je inbreng en suggesties op de artikelen en het proefschrift, maar ook voor je hulp tijdens de experimenten.

Wilfried van Sark en Jatin Rath, bedankt voor jullie inbreng, suggesties, ideeën, commentaar en nuttige discussies de afgelopen jaren.

Verder wil ik graag de leden van de leescommissie bedanken die de tijd hebben genomen om mijn proefschrift door te nemen. Bedankt, Jaap Dijkhuis, Daniel Vanmaekelbergh, John Kelly en Tom Gregorkiewick.

Gavin Conibeer, thank you for your interest in my research and for inviting me at the E-MRS conference in Nice. Marcel, bedankt voor je enthousiasme en discussies.

De experimenten beschreven in dit proefschrift konden niet gedaan worden zonder de hulp van mijn gewaardeerde collega's: Karine, Caspar, Bart, Martin en Arjen. Bedankt voor het maken van de zonnecellen, de feedback op mijn metingen, de werkende meetopstellingen, dus eigenlijk dat jullie het mogelijk hebben gemaakt dat ik mijn onderzoek kon doen. Hans Ligthart, dank je voor je hulp bij de experimenten in de CMI groep en Arjen van de Glind voor je intensieve hulp bij het maken van de gouden nanostaafjes.

Post-doc en mijn mede-promovendi van Device Physics: Henriette, Xin, Zachar,

Kees, Pim, Oumkeltoum, Yinghuang, Akshata, kamergenoot Lourens. Bedankt voor jullie gezelschap en discussies. Minne en Diederick, bedankt voor de geweldige tijd in Japan en niet te vergeten samen met een paar oud collega's Ruud, Jan Willem, Sylvester en Roberto voor de heerlijke lunches bij Tricolore. Isabel and Caterina, thank you, you became good friends. De afgelopen jaren heb ik ook nog studenten mogen begeleiden die bijdrage hebben geleverd aan mijn proefschrift: Jurgen, Carlijn, Thijs, Maria en Floor. Bedankt voor jullie inzet. De laatste paar maanden heb ik doorgebracht bij CMI, bedankt iedereen voor de gezelligheid en hulp en met name Dominika. It was really nice to share a room with you the last months. Als laatste wil ik Riny nog bedanken. Ik kon altijd even langskomen voor een praatje, ook over andere dingen dan tekenen en schilderen of werk. Dat was altijd fijn.

Ik kwam ook 4 jaar geleden als nieuweling in de stad Utrecht. In Utrecht heb ik zeer veel mensen leren kennen via couchsurfing. Het is een komen en gaan van vrienden en zou iedereen willen bedanken want CS heeft een grote bijdrage geleverd aan mijn tijd hier in Utrecht. Ik wil graag beginnen bij Liza en Sanne. Jullie stonden voor me klaar op de meest bizarre tijden en zijn goede vriendinnen gebleken. Jasper wil ik ook graag bedanken, voor de introductie in CS vlak voordat ik in Utrecht kwam wonen en de goede muzikale uitwisselingen. Dio, I would like to thank for all our evenings out, the ouzo experiences, creative evenings, short hollidays and certainly not at least the good conversations. Laura Buckles, thanks for trusting me, supporting me and good luck with your last mile. Bedankt andere vrienden van couchsurfing, Jorine, Linda, Julia en vele anderen. Er is altijd wat te doen met jullie!

Voordat ik in Utrecht kwam, heb ik eerst nog een blauwe maandag in Wageningen gestudeerd. Laura en Bas, jullie hebben me echt overal gevolgd en zijn me altijd blijven steunen. Bedankt daarvoor. Roel, mijn muzikale input, DJ collega en goed vriend. Bedankt voor je interesse in mijn onderzoek en dat je een goede vriend bent. Als laatste wil ik mijn vrienden uit Nijmegen bedanken. Bedankt Aurelie en Mylene, het is altijd leuk om weer samen te zijn en op naar het volgende weekendje in Brussel. Katrin, thank you, always great to hang out with you, where ever it will be. Marcel, Kars, Harm, bedankt voor alle jaren in Nijmegen, de lol, het bier, jullie muzikale uitspattingen, de vierdaagse feesten en niet te vergeten jullie vriendschap.

Als laatste wil ik mijn familie bedanken. Mijn ouders, mijn zussen, Maaike en Wendy, Erwin en Martin, mijn zwagers, maar ook de kleinsten Jens, Milan en Mirla. Ik hoop dat na het lezen van dit boekje, een beetje duidelijk is geworden waarmee ik bezig ben geweest de afgelopen 4 jaar. En bedankt voor al jullie steun en belangstelling door de jaren heen.

Curriculum Vitae

The author was born in Spijkenisse, the Netherlands on September 15, 1982. She obtained here secondary school diploma in 2000 from Angelus Merula in Spijkenisse. After 2 years in tempory jobs she started studying physics at Radboud University Nijmegen in 2002 and obtained her bachelor degree in 2006. She spent one semester studying abroad in Sweden. After her bachelor, she enrolled at Utrecht University and studied energy science. She did her thesis at the Energy Research Center of the Netherlands (ECN) on boron oxygen degradation in crystalline silicon. She received her MSc in September 2008.

From September 2008 she was employed as a PhD student at the Nanophotonics group Physics of Devices. Under the supervision of Ruud Schropp, Wilfried van Sark, Jatin Rath and Andries Meijerink she started a research project on enhancing the efficiency of solar cells by upconversion. The research was carried out in the group Physics of Devices where the solar cells were made and characterized and the group Condensed Matter and Interfaces under supervision of Andries Meijerink where the upconverter materials were made and characterized. Most of the results of this project are described in this thesis and are published in scientific papers and presented at international conferences. She was awarded a poster price for best poster at the 24th European Photovoltaic and Solar Energy Conference in Hamburg and invited speaker at the European Material Research Society in Nice in 2011.

In the course of the project, she also supervised 3 bachelor and 2 master students, assisted in teaching of various courses, was part of the organization of the DO (Debye Research) days and was involved in outreach activities to present solar energy to a broader audience.